

INDOOR LOCALIZATION USING MAGNETIC FIELDS

Kalyan Sasidhar Pathapati Subbu, BE, MS

Dissertation Prepared for the Degree of  
DOCTOR OF PHILOSOPHY

UNIVERSITY OF NORTH TEXAS

December 2011

APPROVED:

Ram Dantu, Major Professor  
Philip H. Sweany, Committee Member  
Paul Tarau, Committee Member  
Zouming Wang, Committee Member  
Barrett Bryant, Chair of the Department of  
Computer Science and Engineering  
Costas Tsatsoulis, Dean of the College of  
Engineering  
James Meernik, Acting Dean of the  
Toulouse Graduate School

UMI Number: 3529276

All rights reserved

INFORMATION TO ALL USERS

The quality of this reproduction is dependent upon the quality of the copy submitted.

In the unlikely event that the author did not send a complete manuscript and there are missing pages, these will be noted. Also, if material had to be removed, a note will indicate the deletion.



UMI 3529276

Published by ProQuest LLC (2012). Copyright in the Dissertation held by the Author.

Microform Edition © ProQuest LLC.

All rights reserved. This work is protected against unauthorized copying under Title 17, United States Code



ProQuest LLC.  
789 East Eisenhower Parkway  
P.O. Box 1346  
Ann Arbor, MI 48106 - 1346

Pathapati Subbu, Kalyan Sasidhar. Indoor Localization Using Magnetic Fields.

Doctor of Philosophy (Computer Science and Engineering), December 2011, 140 pp., 21 tables, 76 figures, references, 98 titles.

Indoor localization consists of locating oneself inside new buildings. GPS does not work indoors due to multipath reflection and signal blockage. WiFi based systems assume ubiquitous availability and infrastructure based systems require expensive installations, hence making indoor localization an open problem.

This dissertation consists of solving the problem of indoor localization by thoroughly exploiting the indoor ambient magnetic fields comprising mainly of disturbances termed as anomalies in the Earth's magnetic field caused by pillars, doors and elevators in hallways which are ferromagnetic in nature. By observing uniqueness in magnetic signatures collected from different campus buildings, the work presents the identification of landmarks and guideposts from these signatures and further develops magnetic maps of buildings - all of which can be used to locate and navigate people indoors. To understand the reason behind these anomalies, first a comparison between the measured and model generated Earth's magnetic field is made, verifying the presence of a constant field without any disturbances. Then by modeling the magnetic field behavior of different pillars such as steel reinforced concrete, solid steel, and other structures like doors and elevators, the interaction of the Earth's field with the ferromagnetic fields is described thereby explaining the causes of the uniqueness in the signatures that comprise these disturbances.

Next, by employing the dynamic time warping algorithm to account for time differences in signatures obtained from users walking at different speeds, an indoor

localization application capable of classifying locations using the magnetic signatures is developed solely on the smart phone. The application required users to walk short distances of 3-6 m anywhere in hallway to be located with accuracies of 80-99%. The classification framework was further validated with over 90% accuracies using model generated magnetic signatures representing hallways with different kinds of pillars, doors and elevators. All in all, this dissertation contributes the following: 1) provides a framework for understanding the presence of ambient magnetic fields indoors and utilizing them to solve the indoor localization problem; 2) develops an application that is independent of the user and the smart phones and 3) requires no other infrastructure since it is deployed on a device that encapsulates the sensing, computing and inferring functionalities, thereby making it a novel contribution to the mobile and pervasive computing domain.

Copyright 2011  
by  
Kalyan Sasidhar Pathapati Subbu

## ACKNOWLEDGMENTS

I wish to thank various individuals who have helped me throughout the course of this dissertation. First and foremost, I would like to thank my advisor Dr. Ram Dantu from the bottom of my heart, who has inspired me right from the day I started, constantly motivating me, providing direction, and invaluable suggestions required for this dissertation. It has been a pleasure to work and grab the ample opportunities given by Dr. Dantu to explore my research interests and improve my thinking, writing and communication skills. I would like to thank Dr. Philip H. Sweany, Dr. Paul Tarau, and Dr. Zouming Wang for serving on my dissertation committee. My acknowledgments to Dr. Duncan Weathers of the Physics department at UNT for his valuable suggestions and information. I take this opportunity to thank all my friends and labmates at the Network Security lab.

This dissertation would not have been possible without the unconditional love and support of my loving mother, father and brother. I would like to greatly thank and dedicate this work to my late maternal grandfather Sri K. Ranga Rao and uncle Dr. K. Chandrasekhar.

## CONTENTS

ACKNOWLEDGMENTS	iii
LIST OF TABLES	vii
LIST OF FIGURES	ix
CHAPTER 1. INTRODUCTION	1
1.1. Introduction	1
1.2. Motivation	2
1.3. Problem Definition	4
1.4. Road Map: Overview of Each Chapter Contents	4
1.5. Contributions	6
CHAPTER 2. ARCHITECTURE	9
2.1. High Level Architecture	9
2.2. Smartphone and Its Sensors	10
2.3. Preliminary Data Acquisition	13
2.4. Summary	16
CHAPTER 3. INDOOR TRACKING	17
3.1. Introduction	17
3.2. Related Work	18
3.3. Fusion Model	19
3.4. Sequential Estimation	22
3.5. Tracking Results	25
3.6. Summary	30
CHAPTER 4. AMBIENT SOUND BASED LOCALIZATION	31
4.1. Introduction	31
4.2. Related Work	32
4.3. Methodology	32

4.4. Classification	33
4.5. Results	34
4.6. Summary	36
<b>CHAPTER 5. MAGNETIC MAPS FOR INDOOR LOCALIZATION</b>	<b>37</b>
5.1. Introduction	38
5.2. Related Work	39
5.3. Experimental Setup	39
5.4. Landmarks and Guideposts	42
5.5. Magnetic Maps	45
5.6. Magnetic Field Behavior	46
5.7. Summary	52
<b>CHAPTER 6. FERROMAGNETISM</b>	<b>53</b>
6.1. Introduction	53
6.2. The Earth's Magnetic Field	59
6.3. Analytical Modeling of Magnetic Signatures	66
6.4. Pillars	67
6.5. Door Frames	75
6.6. Elevators	76
6.7. Summary	77
<b>CHAPTER 7. DYNAMIC TIME WARPING</b>	<b>78</b>
7.1. Introduction	78
7.2. Applicability to the Problem	79
7.3. Summary	81
<b>CHAPTER 8. COARSE INDOOR LOCALIZATION</b>	<b>82</b>
8.1. Data Collection and Classification Framework	82
8.2. Performance Evaluation	84
8.3. Summary	89

CHAPTER 9. FINE LOCALIZATION	90
9.1. Introduction	90
9.2. Challenges	91
9.3. Data Collection and Classification Framework	94
9.4. LocateMe Implementation	97
9.5. Results	98
9.6. Discussion	105
9.7. Related Work	106
9.8. Summary	109
CHAPTER 10. ROOM IDENTIFICATION	110
10.1. Related Work	110
10.2. Methodology	110
10.3. Summary	115
CHAPTER 11. SIMULATION BASED VALIDATION OF CLASSIFICATION	
FRAMEWORK	116
11.1. Generation of Magnetic Signatures	116
11.2. Results	121
11.3. Summary	125
CHAPTER 12. CONCLUSIONS	126
12.1. Summary of Contributions	126
12.2. Limitations	128
12.3. Potential Applications and Future Work	129
REFERENCES	131

## LIST OF TABLES

2.1 Significance of triaxial measurements.	10
2.2 Locations of experiments.	13
3.1 Tracking accuracy of particle filter for different turns.	28
4.1 Confusion matrix of acoustic environment classes.	36
5.1 Measurement uncertainty.	41
6.1 Magnetic field between pillars.	63
6.2 Dimensions of grid and rebars.	68
6.3 Scale factor.	72
8.1 Overall hallway accuracy(%).	87
8.2 Accuracy for entire building (%).	88
9.1 Data collection statistics showing the number of hallways ( $N_{hwys}$ ), number of fingerprint repetitions ( $F_r$ ) , average hallway length ( $HL_{avg}$ ) and total training file size ( $Tr_{fs}$ ) for each of the buildings.	95
9.2 Accuracy (A), Avg estimation error ( $\sigma_e$ (m)) and Avg localization distances ( $\delta_l$ (m)) for College of Engineering.	100
9.3 Accuracy (A), Avg estimation error ( $\sigma_e$ (m)) and Avg localization distances ( $\delta_l$ (m)) for University Union.	101
9.4 Smartphones and their specifications.	102
9.5 Avg estimation error( $\sigma_e$ (m)) and Avg localization distances ( $\delta_l$ (m))for different $\sigma_r$ using particle filters.	102
9.6 Performance - memory and power consumption on Nexus One.	105
10.1 Measurement statistics.	112

10.2 Correlation coefficients for different rooms.	112
10.3 Time warping distances between test and training signatures of labs.	115
11.1 Different pillars: Dimensions in cm.	120
11.2 Avg estimation error( $\sigma_e$ (m)) and Avg localization distances ( $\delta_l$ (m))for different length hallways.	125

## LIST OF FIGURES

1.1 Smartphone statistics: (a) Usage of non-voice data applications. (b) Smartphone share.	3
2.1 Modular level depiction of different components.	9
2.2 X represents the azimuth which is the angle in current reference to magnetic north. The units of measure are within 0-360 degrees imagining a complete rotation divided by 360 equal divisions.	12
2.3 Screenshot of G1 and Nexus One: The input to the software are the sensors that need to be activated, the time period of measurement and an optional filename.	12
2.4 Ambient sound from the recreation center.	14
2.5 Magnitude of acceleration data: The peaks are forces exerted on the X and Y axis during walking and the small blips indicate jerks caused in the Z axis while traveling in an elevator.	14
2.6 Integrated plot: The arrow shows the time instant at which the first turn was taken. The corresponding number of steps can be obtained from the accelerometer data at that time instant.	15
2.7 Magnetometer data of different objects: (a) standing near a pillar, (b) a small magnet.	15
3.1 Proposed data fusion model.	20
3.2 Parallel network showing accelerometer and compass data fusion process.	21
3.3 Particle filter fusion block.	25
3.4 Distance estimation plots: (a) estimated and measured distance without fusion, (b) estimated and measured distance after combining compass data.	26
3.5 Error statistics: (a) average error, (b) maximum error, (c) minimum error.	27
3.6 Trajectory estimation: (a) single turn, (a) four turns.	28

3.7 Compass data fluctuation from 200 degrees to around 140 degrees. The anomaly detected by the magnetometer shows a sudden increase in the magnetic field strength.	29
4.1 MFCCs extracted from audio sample.	33
4.2 Centroid comparison with test sample.	35
5.1 Picture illustrating the pillars on either side of the CSE corridor wing 2 on the second floor of the College of Engineering building.	40
5.2 CSE Corridor Wing 2 building layout with magnetic field intensity of each pillar. From this figure we can see the spacing between each pillar, the magnetic intensity of each pillar and also the landmarks created which are located at ends (P2 and P16) and also a significant pillar in the middle (P11).	42
5.3 Plot showing the variations in the magnetic field while walking past each pillar from one end of the Electrical Engineering corridor to the other.	43
5.4 Layout of new buildings: Reinforced cylindrical pillars are present throughout the building. Fig. 5.5 is labeled in the picture where measurements were taken on the second floor.	43
5.5 Magnetic field plot of the Biology building referenced in Fig. 5.4: Each peak represents a pillar that was passed on the second floor. These can be used in location identification as landmarks or guideposts for indoor navigation.	44
5.6 Magnetic field measurements in Chemistry building: Data obtained by a person walking from the main entrance to the back entrance of the building. Notice the number of samples did not affect the similar results. Total number of samples: Droid 371, Nexus One 166.	45
5.7 Guideposts: The first peak indicates a pillar that is 4m away from the CSE department. The next guidepost is found at a distance of 40m away which is	

comprised of high and low magnitudes in the signature. This helps to find the distance to reach a destination.

46

5.8 The plot shows the magnetic field strength variations of pillars (marked by P1R, P1L..) on either side of the corridor specified by its length and width in meters.

46

5.9 Hysteresis Loop: B represents the magnetic flux density while H signifies the magnetizing force. The point at which the magnetic force is zero while still having a positive magnetic flux is called the residual magnetism, represented by point b. The saturation point or point a, represents the alignment of all atoms in the material. This is also known as the highest magnetization point.

47

5.10 Eq. 11 diagram representing a structured pillar and its dimensions represented by the variables: length (a), width (b), height (h) and the distance (z) at which the field is being measured.

48

5.11 Magnetic field distribution of a pillar: Measured and theoretically generated using Eq.11. This plot shows a similar distribution over 2m which demonstrates Eq.11 as an acceptable theoretical model for the magnetic field distribution.

49

5.12 Magnetic field distributions for different times of a day: The variation is similar over any time period throughout the day.

50

5.13 Magnetic signatures over a period of nine months: The CSE corridor was analyzed using data from February, June and October of 2010. This shows the consistency of the signature over a long period of time.

50

5.14 Magnetic field signature containing electrical equipment: The vending machines produced a low field which is a result of opposing currents.

51

5.15 Types of pillars throughout the building: (a) solid (corner), (b) solid (middle), (c) solid (pair), (d) h-shape, and (e) solid (small).

52

6.1 Ferromagnetism: (a) Random orientation of atoms before being induced by external magnetic field. (b) Parallel alignment of atoms to each other after the application of external magnetic field.	54
6.2 Components of geomagnetic field vector.	59
6.3 The IGRF model showing the individual components of the Earth's magnetic field and their variations along with the inclination and declination. The latitude and longitude values are for the area of Denton, Texas.	61
6.4 Measured Earth's magnetic field at different locations: The field variation is around $3 \mu\text{T}$ , $4 \mu\text{T}$ , and $2 \mu\text{T}$ in (a), (b) and (c) respectively.	62
6.5 Comparison between generated and measured Earth's magnetic fields.	62
6.6 Interaction of dipoles of magnetic fields.	64
6.7 Experiment procedure: The arrows indicate the two way horizontal walking pattern from the center of the hallway towards the pillars.	65
6.8 Impact on Earth's field: For the first and last 10 secs, there is no major change in the Earth's magnetic field. As the distance towards the pillar decreased, the magnitude changed drastically to (a) a high value of $115 \mu\text{T}$ at one pillar, (b) a low value of $33 \mu\text{T}$ at another pillar, (c) the high and low magnetic disturbance caused by the two pillars are clearly indicated along with the Earth's field until 4.3 secs and then between 6.5-8.3 secs approximately.	66
6.9 Type of grids: (a) cylindrical grid, (b) rectangular grid.	68
6.10 Analytical and Measured magnetic field distributions of reinforced pillars: (a) Cylindrical grid size of 2.5x2.5 foot. (b) A typical cylindrical steel reinforced pillar. (c) Rectangular grid size of 2.5x2.5foot. (d) A rectangular steel reinforced pillar.	69
6.11 Magnetic field strength as a function of grid size: As the grid size increases, the distance between the dipoles increases, thereby reducing the resultant moment due to lesser dipole-dipole interaction. The resultant moment in turn reduces the magnetic field.	70

6.12 Magnetic field strength as a function of grid and rod size: The field strength increases as the rod diameter increases, and reduces as the grid size increases.	70
6.13 Magnetic field distribution of a solid steel structure: Analytical and Measured.	71
6.14 Pillar Width: (a) The analytical distribution of pillars of different widths follows a Gaussian distribution. (b) Analytical and Measured magnetic field distribution of a 0.3 m (1 foot) wide pillar.	73
6.15 Distance and Magnetic field relation for current carrying wires.	74
6.16 Signatures captured at two different vertical distances are similar showing that the measurement procedure is independent of heights.	74
6.17 Door identification: (a) The signature below the door, maps closely to three frames, one at the start and the other two at the start and end of the window section. (b) The door in (a) clearly identified by the dotted rectangle in the signature of the entire hallway. (c) The analytical implementation of the signature by considering each frame in the door as a ferromagnetic object.	75
6.18 Elevator signature: (a) A 2.5 foot wide elevator. (b) 4 foot freight elevator. (c) Analytical implementation for elevator width detection.	76
7.1 Signature variation along the time and magnitude axis: (a) Speed variations causing a shift in the signature collected from Subject 2. (b) Shorter signature with magnitude variations caused by faster speed of commuting in a wheelchair.	79
8.1 Hallways in two buildings: Chemistry (a) and (b), College of Engineering (c) and (d), with clearly visible steel pillars.	83
8.2 Magnetic maps: (a) The high intensities indicate high magnetic fields on one side of the hallway. (b) The peaks in the 1D signature support the high intensities in (a).	84
8.3 Correct classification: (a) Two subjects walking with different speeds in the same hallway obtaining similar signatures but with magnitude and time shifts. (b) DTW warps one signature with the other obtaining a close match.	85

8.4 Misclassification: (a) Dissimilar signatures before alignment. (b) Alignment of one signature with the other by DTW, resulting in a mismatch between the two signatures.	85
8.5 Classification of walking patterns: (a) Signatures showing a large time difference. (b) DTW warps the signature and obtains a close match.	86
8.6 Distances between CSE and other hallways in the COE building: As can be seen, for all subjects, the lowest distance was obtained between the stored and the test CSE hallways, i.e. the hallway in which a subject walked.	87
8.7 Resulting localization program on the phone presenting the matched hallway and the computational response time of the phone.	88
9.1 Variance of magnetic signatures: As can be seen, there is no major variation in the signatures that could render it ineffective for our solution.	91
9.2 Distance relation: Signatures measured at 2 feet have a reduced magnitude when compared to that from 0.5 feet but the patterns are retained.	92
9.3 Device placement: Signatures obtained by placing the smartphone in a holster, pocket, and holding in the hand.	93
9.4 Signatures captured using two devices are similar showing that the measurement procedure is independent of devices.	93
9.5 The paths AB, CD, EF and Mech, show the hallways where data collection and system evaluation were performed. Hallway in (c) corresponds to path CD in (a) and that in (d) corresponds to path EF in (b).	94
9.6 A test signature (below) and map (above) denoted by $T_e = \{te_1, te_2, \dots, te_n\}$ , and $M = \{m_1, m_2, \dots, m_m\}$ , respectively. Using a sliding window on $M$ , $T_e$ is compared with segments of the map, $\{M_a \dots M_m\}$ , $\{M_{a+1} \dots M_{m+1}\}$ corresponding to $W1$ and $W2$ , of width equal to $W_l$ , the window length in samples.	96

9.7 A short test signature and the maps in the database are normalized and fed to the DTW module which finds the best possible match between them. The localization distance and estimation error are computed from the matched signature.	97
9.8 User Interface: (a) splash screen (sensor frequency analysis), (b) home screen, (c) building selection, and (d) capture live data.	98
9.9 Alignment by DTW: Short test signatures (a) and (d) are compared with windowed segments from maps (b) and (e) to obtain correct matches as (c) and (f) respectively. (The correctly matched segments are marked by an ellipse in the maps. Finally, the distance walked is estimated by using the sample number at which the match was obtained).	99
9.10 Estimation errors for University Union as a function of window length or resolution.	100
9.11 A linear relationship between response times and window length for COE (a) and University Union (b) buildings.	103
9.12 The screen shows the classified hallway, position of the user in that hallway and from a nearby landmark. The response time of the algorithm is also shown.	104
10.1 Different classrooms: (a) classroom with computers, (b) classroom without computers, (c) room without PCs, (d) a research laboratory.	111
10.2 Research labs signature alignment: (a) original signature of F238 from two different subjects, (b) aligned signatures, (c) original signature of F237 from two different subjects, (d) aligned signatures (e) original signature of F238 and F237 from a single subject, (f) a mismatch of signatures.	113
10.3 Classroom signature alignment: (a) B140. (b) B192. (c) Improper match of B140 and B192. (d) Correct match of B140 signatures.	114
11.1 Magnetic field distribution in measured data: The magnitude is high near the first pillar. As the distance increases, the magnitude reduces and then increases when	

approaching the next pillar. The amplitude of the field at the two pillars depends  
on the magnetization intensity of each pillar.

122

11.2 Generated magnetic signatures: The highs and lows of magnetic fields that were  
observed in the measured signatures can be seen at each of the pillars.

123

11.3 DTW on synthetic signatures: (a) Training and test signatures. (b) Aligned  
signatures.

124

## CHAPTER 1

### INTRODUCTION

#### 1.1. Introduction

Imagine locating oneself inside buildings that are completely new. With some preexisting knowledge of the environment, humans may be able to locate themselves easily by building a mental map of the building. But if it is a first time visitor for whom the environment is completely unknown, how will he find his location?. Localization is the process of identifying a particular location inorder to navigate oneself from that location to different destinations. In an indoor scenario, this pertains to identifying the hallway the person is walking in, the distance walked in that hallway, and the room one is present in. Knowing this information prevents getting lost in a building and keeping track of one's location.

No GPS for indoors: With the advent of global position systems (GPS), outdoor localization and navigation have been facilitated. GPS technology in itself has a major problem in that it cannot function indoors due to multipath reflection and signal blockage from buildings resulting in signal attenuation. Due to this inherent problem of GPS, indoor localization system design has not received its share of attention.

WiFi based systems require ubiquitous availability of wireless connectivity, expensive installations, could suffer from signal fluctuation or degradation. Location-based services (LBS) [1] are offered by some cell phone networks to provide information to mobile phone subscribers about their current location. The service provider obtains the location from a GPS chip built into the phone, or using radiolocation and trilateration based on the signal-strength of the closest cell-phone towers. LBS services use a single base station to determine the location of a phone with maximal accuracy of about 100 m which is largely insufficient for indoor localization purposes.

The only positioning method that has indoor applications and allows autonomy is dead reckoning (DR). It is a process of determining one's position with respect to a known initial position using relative information about heading, speed and time. Such positioning is provided by an inertial navigation system (INS). Based on micro-electro-mechanical systems (MEMS) technology, these systems contain an inertial sensing unit comprising of an accelerometer, compass, barometer, and gyroscope, carried by the user [2]. A major problem with DR is the formation of accumulation errors in heading and acceleration that grow over time resulting in large position errors. Therefore, frequent calibration of DR sensors is required. Also continuously wearing additional sensor units may not be convenient for a common person. These kinds of sensors are known as wearable sensors. There has been a multitude of indoor localization and navigation systems developed using wearable sensors. Some of the existing mobile indoor localization/navigation systems developed have been surveyed in [3, 4]. I also review some of the seminal papers in the forthcoming chapters. Although, a plethora of systems have been developed that range from infrastructure based using WiFi, RFID, Bluetooth, Ultrasound to wearable sensors, there has not been a universally accepted solution.

## 1.2. Motivation

The primary motivation for this dissertation is the absence of a simple, infrastructure less and easy to use indoor localization system that satisfies the requirements of a user centered system which is one that should be applicable to any kind of user yet perform a common task of providing location information. For developing such a system, a device should be capable of encapsulating a) sensing and location estimation functionalities; and b) convenience, availability and usability requirements.

The mobile phone as a multimodal sensor node: The recent proliferation of intelligent multimedia based mobile phones has made the mobile computing research community rethink the application capabilities of these devices which are no longer constrained to just voice communication. Most of these phones are embedded with accelerometers, microphones and magnetic field sensors. These sensors are monolithic, do not depend on or interact with

each other differing from sensors in a sensor network that are distributed, dependent on or interact with each other. A variety of applications can be developed by exploiting these built-in sensors.

There has been a rapid growth in the usage of smartphones for purposes other than communication. A recent survey by Aaron Smit [5] shows the different applications or purposes for which mobile or smartphones are being used. Similarly, with various operating systems based smartphones being available in the market, it is worthwhile to see the most used smartphones in terms of the operating system. Both these statistics are depicted in Fig. 1.1.

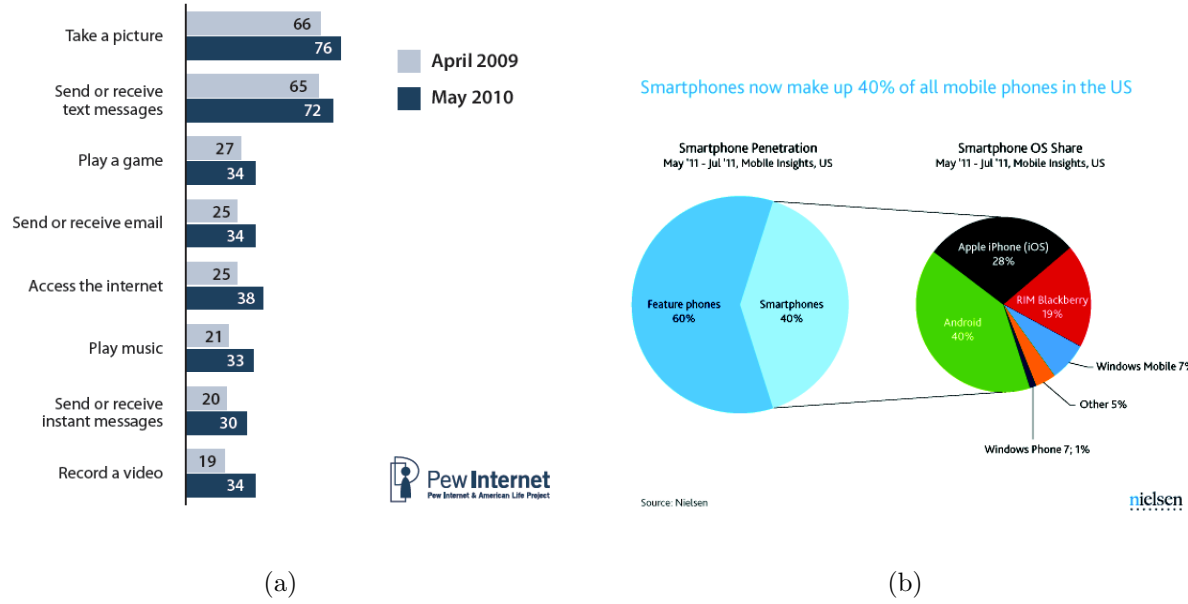


FIGURE 1.1. Smartphone statistics: (a) Usage of non-voice data applications.  
(b) Smartphone share.

From Figure 1.1, we can infer:

- There is a preference in using smartphones for a variety of non-voice applications.
- The growth of Android based smartphones has encouraged developers to write applications using the different built-in sensors. Some of the applications are tilt screen, metal detectors, voice recorders, etc to name a few.

- The survey also found 74% of Android smartphone and 79% percent of iPhone owners downloaded applications in the past 30 days.

The above statistics, in particular Fig. 1.1(b), clearly indicate the potential of Android based smartphones. The availability, ease of using such phones and the hunger for applications by consumers support my motivation for using Android based smartphones for the work developed in this dissertation which is primarily providing a solution to the indoor localization problem.

### 1.3. Problem Definition

This dissertation focuses on how to provide location information to individuals in different indoor environments using just a mobile phone. By utilizing the built-in sensors, the system is expected to work as follows: When a person whose location is unknown, walks a certain distance in that location for instance a hallway, the localization system should be able identify his location and estimate the distance traversed in that hallway. This involves, collection of ambient sensor information and classification of the location based on the sensed information. Based on these requirements, some of the challenges involved in this work are: 1) enabling the sensors to continuously sense the data; 2) incorporating algorithms to process the data and perform accurate classification; and 3) developing and implementing a real time location estimation system entirely on the mobile phone.

### 1.4. Road Map: Overview of Each Chapter Contents

This dissertation discusses methods for sensing multi-modal data using the built-in sensors of a smartphone and utilizing that data for indoor tracking and localization applications. The content in this dissertation is organized into 12 chapters.

- Chapter 1 (Introduction) In this chapter, I give an overview of indoor localization and some of the existing systems. I describe the motivation behind this dissertation, the problem definition and outline the contributions.
- Chapter 2 (Architecture): In this chapter, I describe the smartphone and the characteristics of each of the built-in sensor used in this work followed by an architecture

consisting of different modules. I then discuss a general data collection methodology followed for collecting different ambient information.

- Chapter 3 (Indoor tracking) In this chapter, I present a stochastic filter based indoor tracking application to estimate the distance walked by a person and the turns taken by fusing the accelerometer and the compass data. I discuss the problems that limit the functionalities of these sensors.
- Chapter 4 (Ambient Sound Based Localization): This chapter uses the audio sensor of a mobile phone to collect different background sounds and classify the sounds using a vector quantization and nearest neighbor technique. In other words, I describe a simple sound based context aware application. The remaining chapters form the crux of this dissertation.
- Chapter 5 (Magnetic Maps for Indoor Localization): In this chapter, I first describe a data collection technique using the magnetic field sensor as a magnetometer to collect the magnetic signatures or anomalies due to ferromagnetic objects in different hallways. I present the research findings which include identification of landmarks and guideposts from the magnetic signatures and the development of 3D magnetic maps. The chapter also validates the measured data through theoretical analysis.
- Chapter 6 (Ferromagnetism): In this chapter, I discuss the ferromagnetism phenomenon. This is a very integral part of this dissertation since it provides a detailed analytical discussion on the causes of ambient magnetic fields measured in Chapter 5.
- Chapter 7 (Dynamic Time Warping): In this chapter, I provide an introduction to the classification technique employed and its applicability to this work. I also provide a justification for the use of this technique by comparing its advantages with another classification technique namely the hidden markov model.
- Chapter 8 (Coarse Localization): This chapter builds upon the findings from Chapter 5. I discuss the applicability of ambient magnetic signatures of different hallways

for indoor localization. By employing the dynamic time warping classification framework, I present an application that can differentiate signatures and identify a person as being present in a particular hallway.

- Chapter 9 (Fine Localization): This work is an extension of the previous chapter. I present an application developed on the smartphone that performs localization using the windowed dynamic time warping on short test signatures obtained by walking short distances in the hallway. The estimation errors, localization distances or distance required to walk in a certain hallway are computed thereby presenting an application that requires the user to only walk a few meters in a hallway to find his position.
- Chapter 10 (Room Identification): In this chapter, using the same concept of classification, I show the feasibility of differentiating and identifying different classrooms, laboratories etc based on their magnetic signatures.
- Chapter 11 (Simulation Based Validation of Classification Framework): This chapter utilizes the theoretical analysis presented in Chapter 6 to simulate magnetic signatures of different hallways and validate the classification framework on these signatures.
- Chapter 12 (Conclusions): In this chapter, I conclude this dissertation by summarizing the contributions and highlighting some limitations of the work.

## 1.5. Contributions

This dissertation mainly targets the usage of smartphones for indoor localization. By leveraging the built-in sensors to sense the ambient environment, I use different sensor information as solutions for indoor localization. I list some of the contributions of the each chapter in this work:

- **Chapter 2**
  - (1) Providing an understanding of the characteristics of built-in sensors
  - (2) Evaluating the sensing capability of sensors

- **Chapter 3**
  - (1) Combining the accelerometer and compass data in a sensor fusion model
  - (2) Detecting turns from compass data with low errors even in the presence of magnetic interferences
- **Chapter 4**
  - (1) Proposing a data collection methodology using the built-in microphone
  - (2) Providing a classification framework for contextual awareness based on ambient sound
- **Chapter 5**
  - (1) Showcasing the feasibility of identifying landmarks and guideposts from magnetic signatures
  - (2) Developing magnetic maps of buildings for navigational purposes
  - (3) Uncertainty treatment of magnetic field sensor data to test for data accuracy
  - (4) Theoretically analyzing the magnetic field distribution behavior of pillars
- **Chapter 6**
  - (1) Theoretical analysis for causes of magnetic signatures
  - (2) Analytical implementation explaining
    - (a) Impact of ferromagnetic structures on the Earth's magnetic field
    - (b) Interaction of Earth's magnetic field and the ferromagnetic field components
    - (c) The difference between magnetic behavior of steel reinforced concrete and solid pillars
    - (d) Identifying door and elevator width from signatures
- **Chapter 8**
  - (1) Novel usage of the dynamic time warping technique in providing a solution to indoor localization
  - (2) Fingerprinting different hallways using their magnetic signatures

(3) Validating the classification system over a variety of users and their ways of indoor commuting

(4) Evaluating the system in 26 and 15 hallways of two different buildings and obtaining accuracies of 92.6%, and 91.1% respectively

- **Chapter 9**

(1) Extending the coarse localization work to provide finer localization

(2) Evaluating the smartphone based application across 10 hallways in two different buildings yielding classification accuracies between 81-99%, localization distances of less than 6.5m and estimation errors of less than 4m

- **Chapter 10**

(1) Extending the hallway classification process to different rooms

(2) Developing an application that can differentiate rooms based on their magnetic signatures

- **Chapter 11**

(1) Presenting a simulation framework for generating magnetic signatures of different hypothetical hallways

(2) Validating the proposed time warping based classification framework over different kinds of magnetic signatures

## CHAPTER 2

### ARCHITECTURE

In this chapter, I present the overall architecture followed for developing localization applications using the different built-in sensors of a mobile phone. Then, I describe the characteristics of the individual sensors. Following this, I present the preliminary data collection results.

#### 2.1. High Level Architecture

The high level architecture is depicted in Fig. 2.1. Each of the modules and their functionalities are briefly explained below.

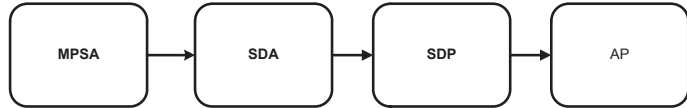


FIGURE 2.1. Modular level depiction of different components.

- Mobile Phone Sensor Activation (MPSA): This module activates the sensors to start listening/sensing the activity or the environment. This activation happens when the user starts to perform the experiments. The user interface prompts for entering the duration of the recording.
- Sensor data acquisition (SDA): Once the program activates the sensors, they start recording the different sensor data and writing into a file capable of being read by MATLAB or Excel.
- Sensor data preprocessing (SDP): This block preprocesses the data by implementing a Butterworth filter. Depending on the sampling rates of the sensor data, the amount of smoothening required is varied.

- Application (AP): This module comprises of the application that uses the data from the appropriate sensor to perform indoor localization. For instance, the indoor tracking using accelerometer and orientation sensor data; the indoor localization using magnetic field data; and context awareness using ambient sound data from the microphone.

## 2.2. Smartphone and Its Sensors

### 2.2.1. Hardware

The mobile phone used in the early phases of research was the G1 from Google running the Android 1.1 operating system, 32 bit Qualcomm MSM7201A (528MHz CPU clock), 256MiB ROM, and 192 MB RAM. With the exponential improvement of technology including the processors, storage space, software etc, Google released Nexus One by HTC in 2010. The smartphone had Android 2.1 operating system running, with a 1 GHz Qualcomm QSD 8250 Snapdragon ARM and 512 MB of storage space. A three axis accelerometer, a microphone, and a three axis magnetic field sensor are embedded in these phones.

In general, the normal phone orientation used for all the measurements has the phone situated with its X axis parallel to the direction of travel, the Y axis horizontally perpendicular, and the Z axis vertical. As Table 2.1 shows, the two horizontal axes are X and Y. In this context, our desired orientation is a quantifiable placement of the phone relative to the direction of travel. Below, I list each of the sensors.

TABLE 2.1. Significance of triaxial measurements.

Axis	Direction	Typical Walking
X	Left/Right	Taking turns
Y	Front/Rear	Walking straight
Z	Up/Down	Upstairs or Downstairs

- Microphone: This sensor had a 16 bit nominal quantization and sampling frequency 44.1KHz.

- Accelerometer: This is a BMA three axis accelerometer. There is a mass in the sensor that has finger-like protrusions. During an acceleration, the distance between these protrusions changes, which changes the capacitance between the protrusions as well. This changing capacitance is measured and converted to a signal and calibrated to a specific acceleration. Table 2.1 lists the significance of the tri-axial accelerometer. Basically, the sensor measures the force applied on each of the axis.
- Magnetic field sensor: This is a three axis Asahi-Kasei 8973 [6] Hall effect sensor that measures the magnetic field and outputs its measurement in units of  $\mu\text{T}$  in all the three orthogonal directions.

Hall effect is a phenomena that results when magnetic fields cause the deflection of electrons traveling through a plate. This deflection causes more electrons to gather on one side of the plate than the other, which creates a small potential difference. The sensor actually measures this potential difference, and converts this voltage to the corresponding field magnetic strength required to produce that amount of deflection in the electrons.

- Orientation sensor: The magnetic field sensor is also used as an orientation sensor by the compass providing the phone's angular orientations. The direction the phone is facing is called its azimuth which is computed using the magnetic field data as

$$(1) \quad \text{azimuth} = \arctan(y/x)$$

Figure 2.2 shows how the azimuth is recorded by the orientation sensor.

### 2.2.2. Software

Fig. 2.3 shows the application software on both the G1 and Nexus One smartphones.

Application software was written to activate each of the sensors and their respective Application Programming Interfaces (APIs). For instance, to capture sounds using the microphone, a class was implemented as part of the Android platform called *android.media.MediaRecorder* [7]. The steps are described below:

- (1) Create a new instance of *android.media.MediaRecorder*;

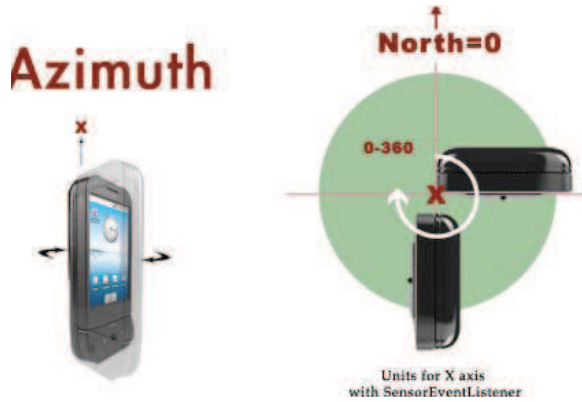


FIGURE 2.2. X represents the azimuth which is the angle in current reference to magnetic north. The units of measure are within 0-360 degrees imagining a complete rotation divided by 360 equal divisions.



FIGURE 2.3. Screenshot of G1 and Nexus One: The input to the software are the sensors that need to be activated, the time period of measurement and an optional filename.

- (2) Create a file path where the data will be saved;
- (3) Use `MediaRecorder.set AudioSource()` to set the audio source to `MediaRecorder.AudioSource.MIC`;
- (4) Use `MediaRecorder.setOutputFormat()` to set output file format. The popular format in mobile devices is 3GPP;

- (5) Use `MediaRecorder.setAudioEncoder()` to set the audio encoder. The default audio encoder/decoder provided in android is AMR-NB which samples at 8kHz with various data rate from 4.75 to 12.2 kbps;
- (6) Call `start()` to start audio capture, and call `stop()` to stop
- (7) When the recording task is done, `release()` needs to be called to release the resources allocated on the `MediaRecorder` instance.

To use the accelerometer and magnetometer, similar steps were followed but the respective sensor managers were enabled to start listening to the sensors and store the data.

### 2.3. Preliminary Data Acquisition

Initial work was done on the accelerometer and the orientation sensor to analyze their sensitivity in detecting walking patterns and turns respectively. Table 2.2 summarizes the locations, type of activity and number of measurements taken at each location.

TABLE 2.2. Locations of experiments.

Location	Type of Walking Activity	Number of Measurements
Student Lounge	Four short turns	25
Computer Science Corridor	Four long turns	15
Elevator	Traveling floors	20
General Access Building	Three turns	13

#### 2.3.1. Microphone

The basic use of microphone is to record voice or audio data. Using this simple functionality, I recorded audio in different backgrounds. Figure 2.4 shows raw audio data captured at the recreational center.

#### 2.3.2. Accelerometer

The accelerometer records the force exerted on the phone while walking. For every step taken, a peak appeared in each of the axes. The total magnitude was computed as  $\sqrt{x^2 + y^2 + z^2}$ .

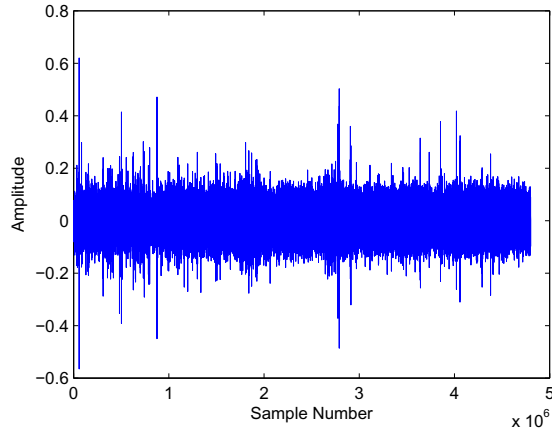


FIGURE 2.4. Ambient sound from the recreation center.

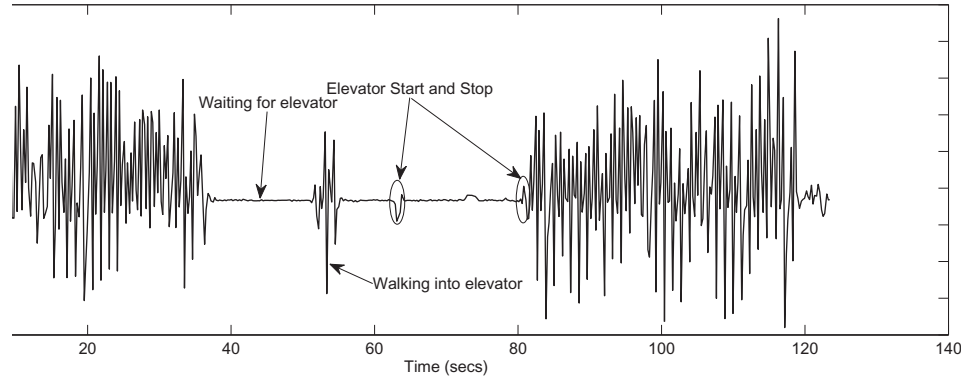


FIGURE 2.5. Magnitude of acceleration data: The peaks are forces exerted on the X and Y axis during walking and the small blips indicate jerks caused in the Z axis while traveling in an elevator.

### 2.3.3. Orientation sensor as a compass

The compass in general is used for finding the direction of travel. For every turn taken, the azimuth in degrees was recorded. The experiment as mentioned earlier was repeated to see the sensitivity and consistency of the sensor in recording the correct azimuth. This was important to utilize the sensor along with the accelerometer in computing the distance walked and also the direction. Fig. 2.6 depicts the integrated plot of accelerometer and compass data.

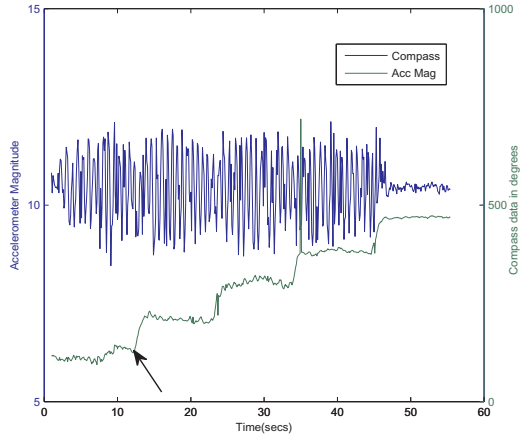


FIGURE 2.6. Integrated plot: The arrow shows the time instant at which the first turn was taken. The corresponding number of steps can be obtained from the accelerometer data at that time instant.

#### 2.3.4. Orientation Sensor as a Magnetometer

The orientation sensor was used to collect the magnetic fields rather than the azimuth. In other words, the magnitude of the magnetic fields were collected instead of the directional data obtained when using the compass. The sensor was sensitive to magnetic fluctuations indoors especially near pillars and metallic objects. Figure 2.7 illustrates the fields collected at different locations.

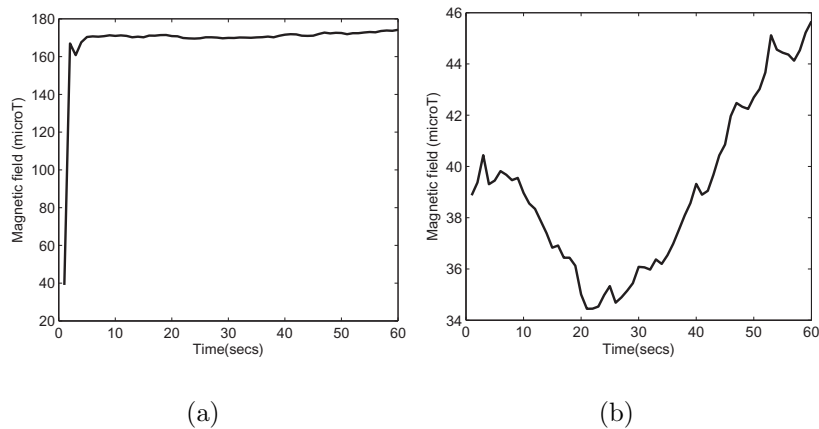


FIGURE 2.7. Magnetometer data of different objects: (a) standing near a pillar, (b) a small magnet.

## 2.4. Summary

In this chapter, I presented an overall architecture or the sequence of modules. I then briefly described the characteristics of the individual embedded sensors. Using the preliminary data collected, I provided an understanding of what and how the sensors sense different phenomena. The data sensed by each of the sensors are utilized in developing applications explained in the forthcoming chapters.

## CHAPTER 3

### INDOOR TRACKING

Most of the existing solutions for localization include tracking a user's whereabouts using multiple sensors. In this chapter, I describe an indoor tracking system developed using the accelerometer and the orientation sensor built-in Google's G1 mobile phone. In particular, I use a stochastic filter to combine the data from the two sensors and estimate the distance walked and the turns taken. I show the advantages of using the fusion technique and also the problems of the sensors that limit the functionalities of the tracking system.

#### 3.1. Introduction

As mentioned in the Introduction of this dissertation, localization is the task of identifying the position of a person. The position could be the coordinates or distance from a known point at that particular location. Tracking on the other hand is continuously obtaining the motion information of the person or object. In other words, obtaining the trajectory of path traversed over a period of time. This requires sensors to continuously sense the information about the environment and also the activity performed by the human. This work attempts to combine information from the accelerometer and orientation sensor to track the trajectory of a user. The goal is to see if 1) existing stochastic techniques used by the robotics and wearable sensor community for tracking can be applied to data from mobile phone sensors; and 2) a user can be located using the tracking application.

Combining the sensor data collected from multiple sensors involves incorporation of multi sensor fusion techniques. Multisensor data fusion [8, 9] is the amalgamation of outputs from multiple sensors to infer something beneficial. The principal motivation is to improve the quality of information output. Applications include missile surveillance, target detection, military units identification, robot localization and tracking, automated control of industrial

manufacturing systems and medical diagnosis. The fusion process can take place at different levels namely raw data level, feature level or decision level [10]. Some of the existing fusion techniques are Bayesian filtering consisting of kalman and particle filtering. Both have their own advantages and disadvantages [14]. Particle filtering is the commonly employed technique for tracking purposes due to its multimodal, nonlinear model acceptance capability [11, 12, 13, 14, 15].

Section 3.2 reviews the work in the literature. In Section 3.3, I present a simple fusion model for combining the sensor information, followed by Section 3.4 with a description of the stochastic estimation algorithm in estimating the distance and direction. In Section 3.5, I discuss the distance and direction estimation results using the algorithm. In Section 3.6, I conclude by highlighting the work in this chapter along with some drawbacks and a prelude to the next chapter.

### 3.2. Related Work

Brezmes et al. [16] propose an activity monitoring using accelerometers. Quentin and Bertrand [2] developed a personal navigation module for indoor and outdoor scenarios using a GPS receiver, digital magnetic compass, accelerometer and barometer. Alan et al. [17] developed an indoor way finding functional interface for cognitively impaired people by using an iPaq to direct people indoors by providing messages and alerts in the form of audio, text and images. This work involved uploading images of the selected paths, communicating with a remote server, a separate location and navigation wizard. The People Sensor [18], an electronic mobility aid designed for the visually impaired consists of pyroelectric and ultrasound sensors for locating and differentiating human and non-human sounds. Ojeda [19] introduced a dead reckoning based navigation system using an inertial measurement unit (IMU) connected to the boot of a person to collect sensor data. Kai [11] developed a continuous location and direction estimation model with compass and GPS using human walking models and particle filters.

Ross and Blasch [20] proposed a wearable orientation device prototype, which provides directional information based on the user's starting point and the direction of movement.

The heading was measured by a digital compass attached to the user's head or body. Oliver et al. [12] developed a pedestrian navigation system using a foot mounted inertial sensor and a building map in a particle filter framework. Krach [14] developed a tracking algorithm using a cascaded model of Kalman and particle filtering for processing different types of sensor data. Dieter et al.'s. [15] work on Bayesian filtering for location estimation clearly explains the concept of particle filtering with examples of detecting a robot's location by sensor fusion of infrared proximity badges and ultrasonic time-of-flight tags. Hightower [21] discussed the practical performance capabilities of particle filters for location estimation on devices ranging from high-end servers to handhelds. They compare the accuracy of particle filters with some deterministic position estimation algorithms. location based services (LBS), or location-aware services aim at providing information/services relevant to the current location and context of a mobile user [22]. Some of the indoor localization systems are the Active Badge Location System [23], RADAR [24], Cricket [25] and Cricket Compass [26]. A substantial review of these localization systems is provided in [27].

The above reviewed related work mostly consists of body worn sensors and their electronics monitored by servers, PCs and laptops carried in backpacks. These sensors are custom made into wearable units which could be expensive for large scale production. The practical feasibility of these units for navigation purposes is questionable due to convenience issues. On the other hand, I show that it is possible to perform tracking using the same sensor but the major difference being their presence in mobile handsets that are convenient to use.

### 3.3. Fusion Model

The proposed fusion model shown in Fig. 3.1 applies the Level 1 Processing level of the JDL model [8]. JDL stands for Joint Directors of Laboratories. They introduced a data fusion model which comprises of the following levels of processing and combining the data.

- Sources of information
- Source preprocessing

- Transforms sensor data into a consistent set of units and coordinates – Data Alignment module
- Assigns data to be used by statistical estimation techniques – Position/Kinematic estimation module

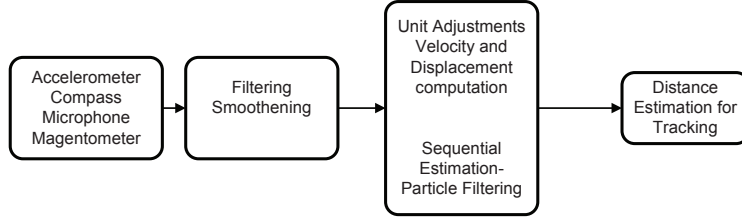


FIGURE 3.1. Proposed data fusion model.

This level combines the azimuth, position for every time instant, to obtain estimates of position or distance for tracking purposes. The correspondence to the JDL model is briefly explained below.

- The accelerometer and compass sensors correspond to the sources of information specified in the JDL model. This can also be attributed to raw data level fusion where the raw accelerometer and compass data are used in the particle filter fusion model that is explained in Section 3.4.2.
- Data preprocessing which includes filtering and smoothening can be attributed to the source preprocessing module.
- Strapdown navigation algorithms which are used to process the vector of acceleration correspond to data alignment process in the fusion model.
- Sequential estimation using particle filters corresponds to the Position or Kinematic estimation process in the JDL model.

### 3.3.1. Fusion Architecture

Since this works makes use of two sensors which are to be processed separately first, I chose a parallel network. The raw accelerometer data denoted by  $\sigma_X$ ,  $\sigma_Y$ ,  $\sigma_Z$  is sent to one fusion cell to compute the magnitude, velocity and position or distance information and the

heading data denoted by  $\phi$  is processed/filtered by another fusion cell. The requirement is to collect information from all these sensors and process them in a final fusion cell. This is why I opted for the centralized network architecture where processed information from both the sensors is fused at the final fusion center. Fig. 3.2 shows the architecture.

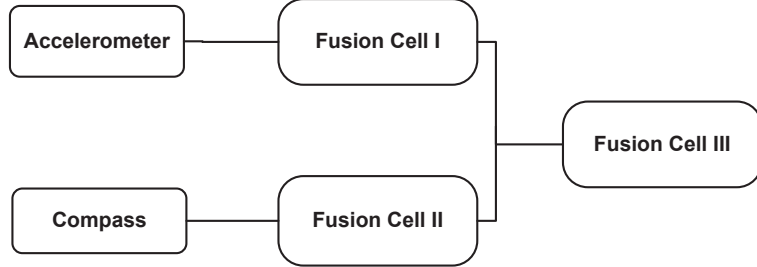


FIGURE 3.2. Parallel network showing accelerometer and compass data fusion process.

### 3.3.2. Data Processing

3.3.2.1. Accelerometer data. The acceleration recorded using the accelerometer was filtered using a Butterworth filter. The velocity and distance traveled were obtained from denoised data. The X and Y coordinates were in turn calculated from the obtained distance using Euclidean distance formula. Let  $a_i$ ,  $v_i$  and  $d_i$  be the acceleration, velocity and distance traveled at  $i_{th}$  time instant respectively.  $\Delta t$  be the sampling interval. Approximately 10 samples were recorded for every second. The velocity was computed by

$$(2) \quad v_i = v_{i-1} + \frac{(a_{i-1} + a_i)}{2} \Delta t$$

and the relative displacement was computed by

$$(3) \quad d_i = d_i - d_{i-1} = v_i \Delta t = v_{i-1} \Delta t + \frac{(a_{i-1} + a_i)}{2} \Delta t^2$$

3.3.2.2. Azimuth data. The azimuth was calculated from the magnetic field sensor as explained in Section 2.2 of Chapter 2. The directional data from the compass was smoothed but also transformed to a consistent value when there was a sudden drop to  $0^\circ$  or sudden increase to  $360^\circ$ . To compensate this situation, depending on the reading,  $360^\circ$  was either added or subtracted to bring back to a uniform scale. For instance if the heading or direction

values were 330, 335, 340, 323, 345, 359, 0, based on the previous values it can be inferred that the heading range was between 330 – 350 thereby adding 360° to the last value.

### 3.4. Sequential Estimation

Bayesian approach is traditionally used for obtaining an optimal solution to a state estimate since it computes the posterior probability density using all the available information including the set of measurements [28]. In cases where an estimate is required for every time instant, the Bayesian approach may not be suitable. Recursive filters can be used to process the measurements sequentially as they are obtained at every time instant. This method is advantageous in that the set of measurements need not be stored for computation. The state of a system or rather its probability density function is estimated for the next time instant based on the previous measurement. This forms the prediction stage. Then the estimated value is compared with the original measurement that is obtained in the time instant for which the prediction was made. This forms the update stage which uses the Bayes theorem.

#### 3.4.1. Particle Filtering

Particle filters are probability based approximation algorithms that belong to the family of sequential monte carlo methods [29]. As explained in [15], for estimating a quantity, Bayes filters maintain a probability distribution for the quantity estimate at time  $k$  referred to as the belief  $Bel(s_k)$ . A set of  $N_s$  particles is used to represent the posterior density or belief given by Eq 4.

$$(4) \quad p(s_k|Z_k) \approx \sum_{j=1}^{N_s} \pi_k^j \lambda(s_k - s_k^j)$$

where each particle with index  $j$  has a state  $s_k^j$  and a weight  $\pi_k^j$ . The sum over all particles weights is one. The particles are drawn according to the proposal density,  $q(s_k|s_k^j, Z_k)$ , such that their respective weight is calculated using Eq 5.

$$(5) \quad \pi_k^j \propto \pi_{k-1}^j \frac{p(Z_k|s_k^j)p(Z_k|s_{k-1}^j)}{q(s_k^j|s_{k-1}^j, Z_k)}$$

Using a procedure called sequential importance sampling with resampling (SISR) [28], the weights of each sample are updated with each new sensor measurement. In this context, SISR involves predicting each samples motion using a state model, weighting all samples by the sensors likelihood model for the current measurement, and resampling by choosing a new set of samples according to the weights of the prior samples. The weights are updated based on the measurements using Eq 6.

A particle filter can fuse measurements taken by heterogeneous sensors. For every additional sensor employed, a new likelihood model must be created characterizing the sensor. Likelihood is defined as the conditional probability  $P(Z|s)$ , the probability of position  $s$  of the moving human subject relative to the sensor given measurement  $Z$  taken by the sensor. For multiple sensors, the measurement likelihoods can be multiplied in the weight update process.

$$(6) \quad \pi_k^j = \pi_{k-1}^j p(Z_k | s_k^j)$$

### 3.4.2. Particle filter analytical model

The models explained here were adopted from [13].

- State model:
  - Walking in a straight line: Here, the position of the person is tracked in terms of the distance traveled. This forms the state model  $s_k$  which consists of  $d_k$  as the distance given by Eq. 7

$$(7) \quad s_k = (d_k)$$

where  $d_k = (d_{k-1} + \nu)$  indicates that the present distance traveled depends upon the distance covered in the previous time instant added by noise  $\nu$  called process noise.

- Walking with a single turn: Here, the trajectory walked by the person is tracked in terms of the distance traveled. This forms the state model  $s_k$  which consists

of  $d_k$  as the distance given by Eq 8

$$(8) \quad s_k = \begin{bmatrix} x_k \\ y_k \end{bmatrix}$$

where  $x_k = (x_k - 1) + \nu$  and  $y_k = (y_k - 1) + \nu$  indicate that the present  $x$  and  $y$  coordinates of the trajectory walked depend upon the coordinates in the previous time instant added by noise  $\nu$  called Process noise.

- Measurement model: The set of measurements denoted by  $Z_k$  are obtained from the sensors and they represent the state of the system added with noise  $n_\delta$  given by Eq 9.

$$(9) \quad Z_k = h(s_k, n_\delta)$$

- Particle filter propagation: The initial set of particles are assumed to be Gaussian distributed around the initial state value which is considered as zero indicating the initial distance traveled. The measurement likelihood is calculated using the Gaussian kernel function as given in Eq 10.

$$(10) \quad p(Z_k | s_k^j) = \frac{1}{\sigma_\nu \sqrt{2\pi}} e^{-\frac{(Z_k - s_k^j)^2}{2\sigma_\nu^2}}$$

And finally the weights are updated based on the measurements using Eq 6. The fusion model using the particle filter is shown in Fig. 3.3. The measurements from the sensors are used in the particle filter program [30]. The accelerometer data is double integrated to obtain the distance value for every time instant. Then both the heading and the distance values are incorporated into the measurement model. The state model, the particles and their weights are all initialized. As measurements are obtained for every time instant, the estimation occurs in the prediction phase and the correction in the update phase. Based on these measurements, the weights are adjusted and the particles are resampled.

Algorithm 1 runs at every time step  $t$ . Steps (i) and (ii) update the sensor measurements respectively. According to the probability distribution, namely distribution of weights, at the previous time  $t - 1$ , Steps (iii) and (iv) draw one sample from the set of previous samples.

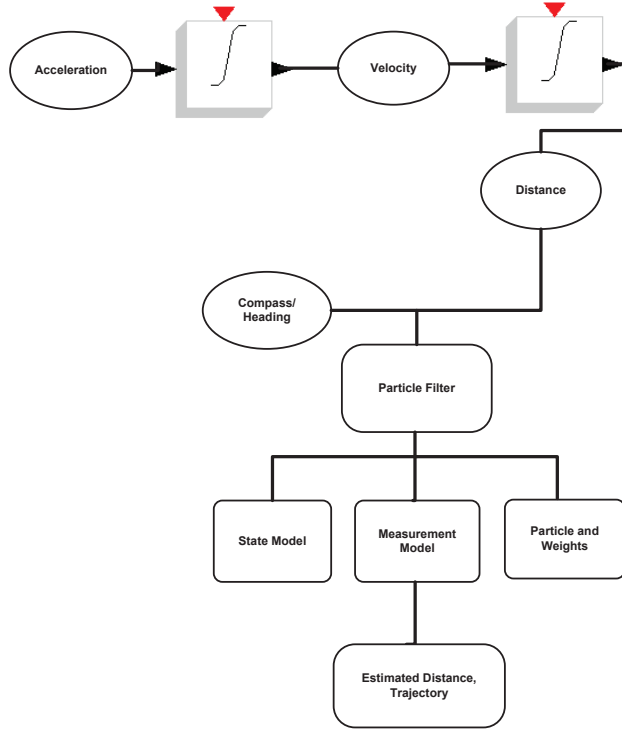


FIGURE 3.3. Particle filter fusion block.

Hence, samples with higher weights will be drawn more frequently. Steps (v) and (vi) add additional noise to the samples to settle the inherent sample impoverishment problem of SIR particle filter. Step (vii) updates the weights based on the likelihood of the measurements.

### 3.5. Tracking Results

#### 3.5.1. Distance Estimation

The essence of estimating the distance traveled is basically to compute the remaining distance to the destination and navigate the person. The estimation accuracy of the system is a very important factor here. Simple walking experiments for a distance of 11m (manually measured) were performed. The recorded acceleration was double integrated to obtain the velocity and distance as explained in Section 3.3.2.1. I evaluated the performance of the particle filter with fused (accelerometer and compass) and single sensor (accelerometer) information. A comparison of the measured and estimated distance is shown in Fig. 3.4.

---

**Algorithm 1** Particle filter algorithm

---

```

1: for k=1:2 do
2:   (i) Update measurement  $Acc_k$  for accelerometer data
3:   (ii) Update measurement  $Com_k$  for compass data
4: end for
5: for i=1:N do
6:   (1) (iii) Draw sample  $Acc_{t-1}^i$  where  $p(Acc_{t-1}^i) = Acc_{t-1}^i, w_{t-1j=1\dots N}^i$ 
7:   (2) (iv) Draw sample  $Com_{t-1}^i$  where  $p(Com_{t-1}^i) = Com_{t-1}^i, w_{t-1j=1\dots N}^i$ 
8:   (3) (v)  $Acc_{t-1}^i = Acc_{t-1}^i + \delta$ 
9:   (4) (vi)  $Com_{t-1}^i = Com_{t-1}^i + \delta$ 
10:  (5) (vii) Update weights using  $\pi_k^j = \pi_{k-1}^j p(Acc_k | s_k^j) \cdot p(Com_k | s_k^j)$ 
11: end for
12: for i=1:N do
13:   (viii) Normalize weight by  $w_t^i = \frac{w_t^i}{\sum_{i=1}^n (w_t^i)}$ 
14: end for

```

---

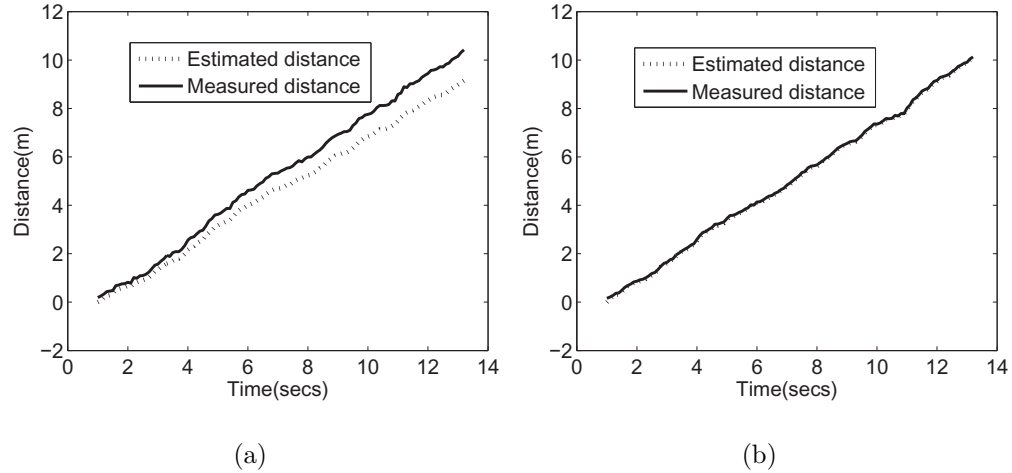


FIGURE 3.4. Distance estimation plots: (a) estimated and measured distance without fusion, (b) estimated and measured distance after combining compass data.

### 3.5.2. Error Statistics Comparison

For the distance estimation, I computed the error between the estimated and measured distance. Different particle sizes were used to evaluate the particle filter performance over fused and single sensor information. The minimum, maximum and average error were calculated for both cases and depicted in Fig. 3.5.

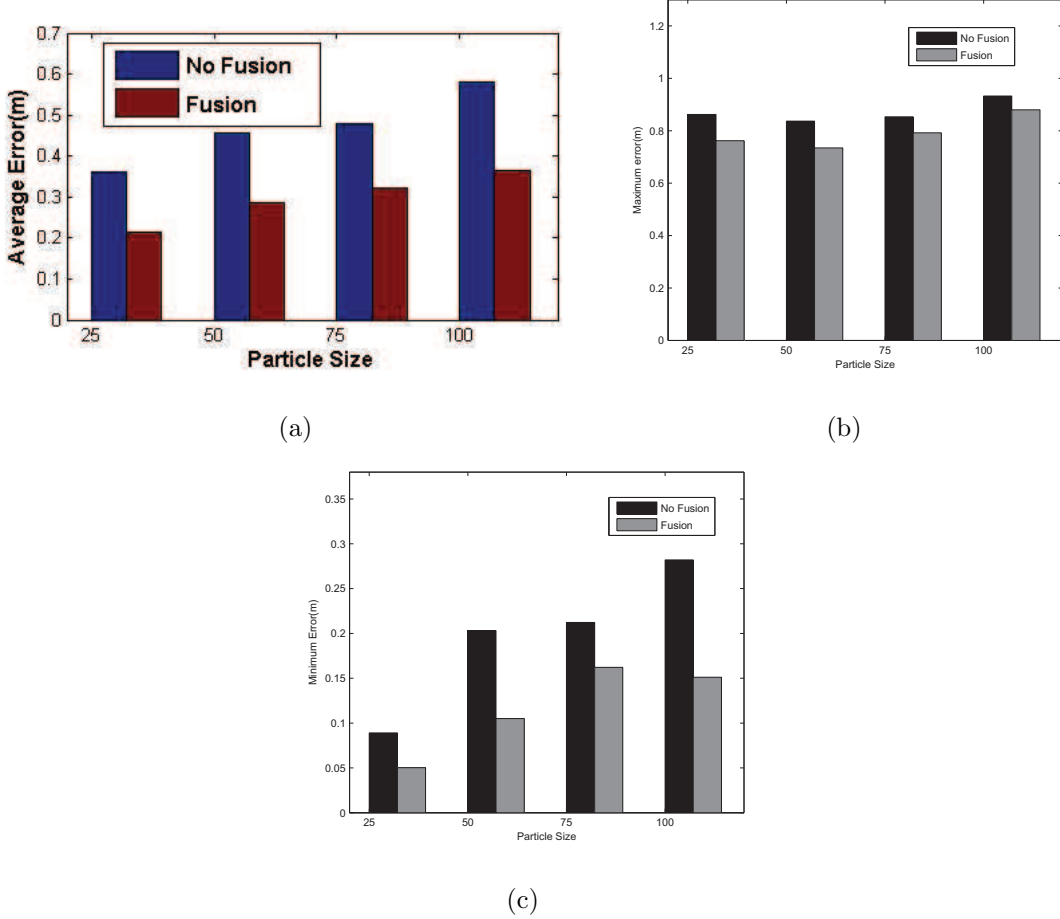


FIGURE 3.5. Error statistics: (a) average error, (b) maximum error, (c) minimum error.

### 3.5.3. Trajectory Estimation

Estimating the trajectory is another important factor in the tracking system. Detecting a correct turn requires monitoring the distance walked and also the angle of turn taken. The experiment consisted of making single, two and four turns. For a single turn, the

subject walked in a straight line for 14m, made a right turn and then walked for another 18m, thereby covering a total distance of 32m. For four turns the subject walked different distances, but approximately covering a total distance of 35-38m. Fig. 3.6 shows the particle filter performance for one and four turns.

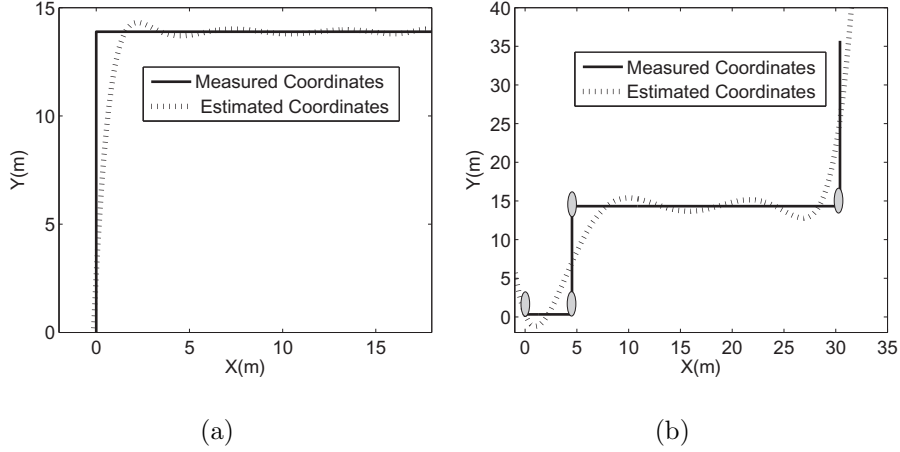


FIGURE 3.6. Trajectory estimation: (a) single turn, (a) four turns.

### 3.5.4. Tracking Accuracy

As mentioned earlier, accurately estimating the trajectory walked is very essential. The average error between estimated and measured coordinates was computed from which the accuracy of the particle filter was obtained. These are tabulated in Table 3.1.

TABLE 3.1. Tracking accuracy of particle filter for different turns.

$N_T$	Loc	$N_R$	$A_E$ (m)	A(%)
1	W6	30	1.14	86
	W1	25	0.97	83
	W2	26	0.88	82
	AnS1	34	1.15	85
	L1	35	1.13	87
2	W2	25	1.28	72
	W3	35	1.22	78
	EE	28	1.27	73
	W4	31	1.29	81
	W5	32	2.24	76
4	F1	28	1.31	79
	W2	35	1.32	78
	W3	28	1.37	73
	W4	31	1.31	83
	W5	32	1.29	82

where  $N_T$  denotes number of turns and  $N_R$ , number of repetitions. The locations are denoted as W1-W6 different wings on the Computer Science and Engineering department, EE Electrical Engineering, AS Arts and Science department, L1 is the library wing and F1 is floor 1 near the Dean's office lounge. As we can see, the accuracy is low for certain locations and turns. This is due to the magnetic anomalies that cause the compass to fluctuate. In other words, wrong heading values were recorded by the compass. This information when used in the particle filter could result in low trajectory estimation since the particle weights are updated according to the measurements.

Magnetic anomalies are sudden variations in ambient magnetic fields that affect the compass in the phone thereby resulting in sudden change in the azimuth values recorded by the compass. For instance, at some spots along corridors I was able to identify this fluctuation in the compass. Although the phone was pointed towards the South, the compass showed it as North. Once the phone was moved from that point, the compass realigned itself pointing to the true North. Fig. 3.7 depicts this case of magnetic anomaly identified along the corridor.

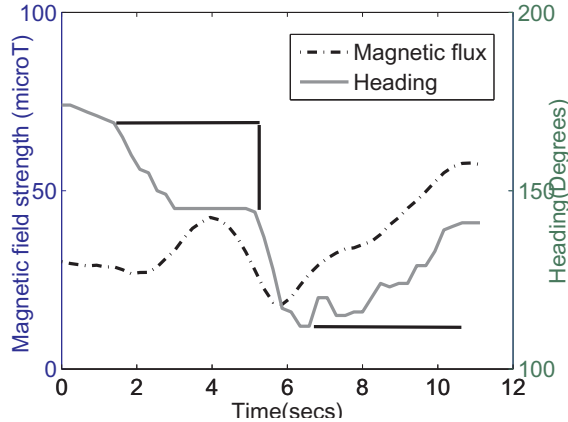


FIGURE 3.7. Compass data fluctuation from 200 degrees to around 140 degrees. The anomaly detected by the magnetometer shows a sudden increase in the magnetic field strength.

These anomalies were present in different areas of the buildings. Trying to compensate for such anomalies is a cumbersome task.

### 3.6. Summary

The goal in this work was to see if traditional stochastic filtering algorithms could be applied to multi-modal sensor data from a mobile phone. I described a simple indoor tracking system which worked with combined data from the accelerometer and orientation sensor of a mobile phone. By employing the particle filter fusion technique, I combined the data and estimated the distance traveled and the turns taken. The idea was to see if continuously tracking a user could help in easily obtaining indoor location information. Although encouraging results were obtained, the effect of magnetic interferences or anomalies on the compass data hindered the tracking system. Also, tracking involves continuously obtaining sensor information which could be a burden on the memory requirements and processing capabilities of the mobile phone. These are the major limitations of the work in this chapter.

To overcome these drawbacks, I looked into performing indoor localization by inferring the context or location using different ambient information available in the environment. The next chapter explains how I used a microphone to capture various environmental noises or sounds and performed location or context identification.

## CHAPTER 4

### AMBIENT SOUND BASED LOCALIZATION

This dissertation is about providing solutions for identifying locations using the built-in sensors. First, to start with, this chapter attempts to identify the context using the simplest built-in sensor - the microphone. The idea is to differentiate between different contexts/location such as being in an office, a conference room or traveling in a car or bus using background sounds. By employing traditional clustering techniques, I show that it is possible to identify the context.

#### 4.1. Introduction

Audio data possesses distinguishing features which can be used to separate classes of audio such as silence, pure speech, impure (noisy) speech, environmental and music. These features can be considered as elements of an n-dimensional vector. Environmental cues can be utilized to automatically present dynamic information to users relevant to their current context. Background sounds in offices, classrooms, streets and vehicles can be a rich source for modeling user context. Furthermore, the information obtained can be used to assist activity and location detection, based on the results of which the mobile devices can respond intellectually such as disruption prevention in the meetings, emergency dial, etc.

The remainder of this chapter is organized as follows: Section 4.2 provides an overview of related work. Section 4.3 presents the data collection and preprocessing and the feature extraction methodology. Section 4.4 discusses the classification algorithm. Section 4.5 presents the experimental set up and the results obtained for the classification phase. Finally, Section 4.6 concludes.

---

The content in this chapter is reproduced from Kalyan Subbu, Ning Xu, and Ram Dantu, “iKnow Where You Are,” International Conference on Computational Science and Engineering, 2009, vol. 4, pp. 469-474, with permission from IEEE.

## 4.2. Related Work

Peltonen et al. [31] performed auditory scene recognition of 26 different acoustic environments of which 17 scenes were classified with an accuracy of 68.4% using a feature vector consisting of multiple features. The recognition accuracy proved to be approximately 18 times better than the random guess rate. Work done by Sawhney [32] in environmental noise classification showed that the nearest neighbor classification technique proved to be robust. Ma et al. [33] used a 11-state HMM classifier and obtained accuracy of the individual scenes ranging from 75% to 100%. However, the noise classifier designed in this system is not capable of recognizing multiple and simultaneously occurring environmental noises. Clarkson [34] looked at obtaining environmental context through audio for applications and user interfaces. Work in nomadic computing [35] categorized system into sound scenes and sound objects. Results showed that their system detected 9/10 of the scene transitions.

## 4.3. Methodology

### 4.3.1. Data Collection and Preprocessing

Audio samples were collected by using the application software on the phone explained in Section 2.2.2. After data collection, the analog signals were digitized by sampling them. The recordings were segmented into 30 m secs or 256 samples of duration audio files and each sample was labeled according to the environment where they were recorded for analysis. Then the original audio document was divided into frames and Hamming windowing technique was used on each individual frame so as to minimize the signal discontinuities at the beginning and end of each frame. After this, the windowed frame was converted from time domain to frequency domain using Fast Fourier Transform.

### 4.3.2. Feature Extraction

The purpose of this step is to extract useful discriminative information from the time-domain waveform which will result in a compact set of feature vectors. Mel frequency cepstral coefficients (MFCCs) are the most commonly used acoustic features since they take the human perception sensitivity with respect to frequencies into consideration. The mel filter

banks are a set of triangular band pass filters obtained by mapping the normal frequency values over the mel scale. Fig. 4.1 shows the MFCC features extracted from a particular environmental sound.

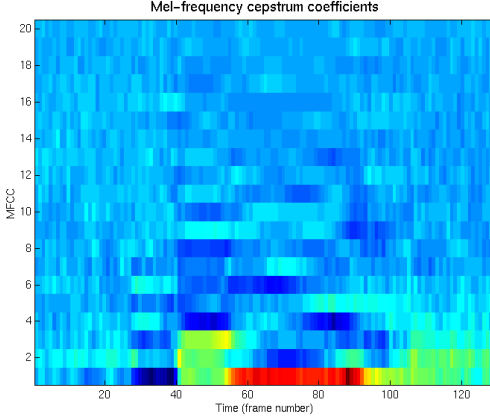


FIGURE 4.1. MFCCs extracted from audio sample.

## 4.4. Classification

### 4.4.1. Classification model

The vector quantization (VQ) method [36] was used as a classification algorithm due to its ease of implementation and accuracy. We assume that  $x = [x_1, x_2, x_3, \dots]^T$  is an N-dimensional vector whose components  $\{x_k, 1 \leq k \leq N\}$  are real-valued, continuous-amplitude random variables. The vector  $x$  is mapped onto another real-valued, discrete-amplitude, N dimensional vector  $y$ . The expression  $y = q(x)$  where  $q(\bullet)$  is the quantization operator indicates that  $y$  is the quantized value of  $x$ . Typically,  $y$  takes on one value from the finite set of values  $Y$  referred to as the reconstruction codebook, or simply the codebook and is given by  $Y = \{y_i, 1 \leq i \leq L\}$  where  $L$  is the size of the codebook. The vectors  $y_i$  are the set of code vectors given by  $y_i = [y_{i1}, y_{i2}, \dots]^T$ . To design a codebook the N-dimensional space of the random vector  $x$  is partitioned into  $L$  regions or cells  $\{C_i, 1 \leq i \leq L\}$  and a vector  $y_i$  is associated with each cell  $C_i$ . The quantizer assigns the code vector  $y_i$  if  $x \in C_i$ .

The well-known LBG vector quantization algorithm [37] for clustering a set of L training vectors into a set of M codebook vectors has been used for clustering the training samples and classifying the test samples with the trained ones. Algorithm (2) lists the pseudocode.

---

**Algorithm 2** LBG Vector Quantization algorithm.

---

```

1: Design a 1-vector codebook  $y_i = \{y_{i1}, y_{i2}, \dots\}$ 
2: Split codebook according to the rule:
   •  $y_n^+ = y_n(1+\epsilon)$ 
   •  $y_n^- = y_n(1-\epsilon)$ 
3:  $m = 2 * m$ 
4: Cluster vector using Nearest-Neighbor Search
5: Find and update centroids
6: Compute distortion  $D$ 
7: if  $\frac{D' - D}{D} < \epsilon$  then
8:   if  $m < M$  then
9:     Goto Step 2
10:  else
11:    Stop
12:  end if
13: else
14:   $D' = D$ 
15:  Goto Step 4
16: end if

```

---

#### 4.5. Results

For the classification phase, I chose different acoustic environments viz., bus, lab, office, lecture, home, urban driving in a car and walking in a street. Thirty recordings of each category were collected during different days and time of a day. Throughout the entire process of recording samples, the phone was held by the user. The duration of the recording

lasted for about 10 minutes but I used only 10 secs of audio for analysis. I then equally divided the number of training and test samples among the recordings obtained.

Then, using the VQ classification method, I compared a group of known test samples from bus, lab, gym, class, car with unknown test samples from a street and a room with the television on. Fig. 4.2 compares the new samples to the centroids of four different classes and finally clusters or classifies them to their respective classes of audio.

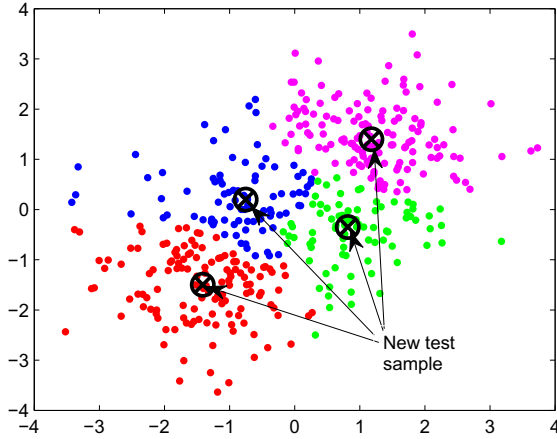


FIGURE 4.2. Centroid comparison with test sample.

To compute the recognition rate of the clustering algorithm, I used fifteen test samples of same type of audio for classification. The number of times it was correctly classified over the total number of test samples was used for calculating the recognition rate. The overall recognition rate was an average of the individual recognition rates of each audio scene. Table 4.1 shows the confusion matrix and the recognition rates of the individual samples.

We can see from the table that out of the 15 test samples of bus used for classification, all were correctly classified giving a 100% recognition rate. The same procedure was applied to calculate the recognition rate for the other audio samples. An overall recognition rate of 91% was obtained for the 5 classes of audio defined in this work.

TABLE 4.1. Confusion matrix of acoustic environment classes.

Scene	Bus	Lab	Gym	Class	Car	Percentage
Bus	15	0	0	0	0	100
Lab	0	14	0	1	0	93.3
Gym	0	0	15	0	0	100
Class	0	3	0	12	0	80
Car	2	0	0	0	13	86.6

#### 4.6. Summary

In this chapter, I exploited the built-in microphone to capture background sound and achieved presence detection in environments like bus, lab, office, car, etc. The vector quantization method of audio classification yielded recognition rates ranging from 86% to 100% for individual classes and 91% overall. The drawback in this work is a misclassification occurs if the background noise from two different hallways sounds similar. In other words, the algorithm fails to discriminate the locations.

Since accurately identifying the location is very important, I proceeded onto researching the possibility of exploiting any other physical quantity present in the environment and that which can be captured using the available built-in sensors. The presence of magnetic fields that caused disturbances in the compass explained in Chapter 3 provided a pathway to delve into the idea of utilizing ambient magnetic fields as a source of providing localization. In the next chapter, I present work that deals with collecting indoor magnetic fields and some interesting possibilities using the data.

## CHAPTER 5

### MAGNETIC MAPS FOR INDOOR LOCALIZATION

In Chapter 3, I showed that magnetic field fluctuations and anomalies inside buildings affect the compass which is one of the simplest navigation devices. Alternative navigation requires landmark identification so those landmarks can be used as guideposts in assisting individuals. This chapter discuss a methodology for collecting magnetic signatures and identifying landmarks, guideposts and creating magnetic maps of a building using the signatures. The magnetic field behavior is also demonstrated and compared with theoretical distributions of the magnetic fields.

Specifically, I look at answering the following research questions: 1) Is the proposed data collection procedure repeatable, implementable and independent of the user performing? 2) Can the ambient magnetic fields inside a building be utilized for indoor localization? 3) Are there long term variations in the magnetic field that can hinder the effectiveness of magnetic fields for localization?

An introduction to magnetic fields is provided in Section 5.1. This is followed by a description of the data collection procedure and statistical treatment of the data in Section 5.3. In Section 5.4, I explain the concept of identifying landmarks and guideposts. The creation of magnetic maps is described in Section 5.5. A theoretical analysis of the magnetic field distribution is provided in Section 5.6. Finally, I conclude the chapter in Section 5.7

---

The content in this chapter is reproduced from Gozick, B., Subbu, Kalyan Pathapati., Dantu, R., Maeshiro, T. , "Magnetic Maps for Indoor Navigation," Instrumentation and Measurement, IEEE Transactions on , vol.60, no.12, pp.3883-3891, Dec. 2011, with permission from IEEE.

## 5.1. Introduction

Magnetic field variations inside buildings are found in iron, cobalt or nickel and also occur from steel structures, electric power systems and electronic appliances. If these variations or anomalies are identified, they provide a unique fingerprint or profile for places inside buildings where they exist [38]. For instance, a specific corridor could be characterized by its magnetic field intensity profile or an office room can be profiled to help in the future for identifying the office you are presently in. Pillars and other structures that show high magnetic field values along these corridors could very well be identified as landmarks and used as guideposts for navigation. Developing magnetic maps [39] of buildings can educate the general public, employees, and even maintenance workers about the levels of magnetic flux in the surroundings. Once understood, these maps can help in the development of a building by providing a set structure or layout. The number of landmarks and their separating distances can then be implemented throughout the building to provide an easy analysis when integrating the building with indoor navigation.

Magnetic fields in general are caused by electrical installations [40], appliances and heavy duty machinery. There are two different types of magnetic fields namely static and dynamic. Dynamic magnetic fields are those that fluctuate dynamically from an electrical device such as a CRT or LCD screen. Static fields, which are generally larger, are seen in big machinery devices used in construction materials or medical applications like MRI or X-ray machines [41]. The IEEE Standard C95.6 prescribes the maximum permissible exposure (MPE) levels for a magnetic field or magnetic flux density. The MPE is expressed as a function of frequency of the field and the limit is more restrictive for one's head than for the rest of the body. For the head, the MPE for magnetic flux density is 353 mT at DC and 680 mT at 3kHz [42]. Since most of our appliances and devices operate somewhere around the 60Hz range, a limited exposure to magnetic field should fall somewhere below the MPE standards. For reference, the average magnetic field induced by the earth [43] in North America is about 50  $\mu$ T.

## 5.2. Related Work

Utilizing the magnetic field information inside buildings for localization and navigation purposes is an interesting aspect to be studied. Analyses have been done on the effect of short term exposure to these extraneous fields [42], but how can these residual fields be used for our advantage? Some work has been done using magnetic fields for indoor robot localization [38, 39, 44, 45]. Some work has been done on navigating the visually impaired; an area in which our techniques can be applied. Hashimoto et al. [46] also helps with indoor navigation for the visually impaired by applying an accelerometer to measure distance, and a gyroscope and magnetometer to approximate the direction. Ando and Graziani [47] developed a multi-sensor strategy and smart signal processing to identify structures or objects, communicating this information with the user. Hunaiti et al. [48] incorporated communication links into a new navigational technique.

## 5.3. Experimental Setup

### 5.3.1. Measurement System

The measurement system consists of the Motorola Droid and Nexus One smartphones from Google with a built-in AK8973 orientation sensor. The three axis sensor from Asahi Kasei consists of Si monolithic Hall geomagnetic sensor [6] detecting geomagnetism in the X-axis, Y-axis, and Z-axis. There is a signal conditioning circuit for processing this sensed magnetic field, a DAC for compensating the offset magnetic field, an ADC and an I<sup>2</sup>C interface for finally reading the digital data. The *I*<sup>2</sup>C known as Inter-IC is an interface designed for easy communication between peripherals residing on a same IC. The APIs specific to this sensor are enabled to read the data from the specified registers in the *I*<sup>2</sup>C.

An application was written in Java that runs on the phone to activate the sensors and record their readings. The magnetic field was measured in the x, y and z directions and the magnitude was calculated. These magnetic fields formed by stationary railings, walls, doorways and electrical equipment may be inside a building. By using all these objects,

we create a generalized signature for each part of a building that can be used for future navigation.

### 5.3.2. Methodology

The goal of this work is to a) develop magnetic maps using the data collected, and b) identify landmarks along corridors and use them as guideposts. Initial experiments were performed at the College of Engineering building and later expanded to buildings on the main campus. Daily walking patterns of people which include walking through a building entrance, down the hall and into a classroom, or entering into a lab and walking to a station were imitated. These patterns can help us focus on parts of the building that are heavily traveled for location identification. The College of Engineering building has seven long corridors with 14-18 pillars on either side. A picture of a corridor on the second floor is shown in Fig. 5.1



FIGURE 5.1. Picture illustrating the pillars on either side of the CSE corridor wing 2 on the second floor of the College of Engineering building.

Two kinds of experiments were performed along selected corridors with the phone's y-axis parallel to the North. In the first experiment, we collected the field strengths by standing near and around each pillar for duration of 15 secs. The idea was to analyze the static field strength levels at each pillar. In the second experiment, we walked past each pillar recording the values at and in between each pillar. Each pillar represented in Fig. 5.1 is evenly spaced 4.75m apart.

### 5.3.3. Measurement Uncertainty

Any measurement is bound to have uncertainty due to the instrument used or the quantity being measured. Typically uncertainty tests are performed to find the range of values for the variation of the measured quantity, in other words the margin of variation. In this work, since the magnetic field due to pillars and objects along corridors was measured repeatedly, it was necessary to understand the variation of the data obtained over these repeated measurements. Type A uncertainty test was performed to study this variation. Type A uncertainty test is a method for evaluating the uncertainty by statistically analyzing a series of observations [49] using  $U = \frac{s}{\sqrt{n}}$ , where  $s$  is the standard deviation and  $n$  is the number of measurements.

I chose 50 measurements of each of the seven pillars, an elevator and a vending machine present along the Computer Science and Engineering (CSE) for the uncertainty computation. Table 5.1 lists the interval levels at 95% confidence limits.

TABLE 5.1. Measurement uncertainty.

Pillar Number	Range of field strength ( $\mu$ T)
P2	$148.74 < 150 < 151.26$
P7	$21.10 < 22 < 22.90$
P4	$49.77 < 50.31 < 50.86$
P13	$43.4 < 45 < 46.66$
P10	$63 < 65 < 67$
P9	$30.19 < 31 < 31.81$
P3	$53.48 < 56 < 58.52$
Vending Machine	$61.5 < 63 < 65$
Elevator	$93.5 < 95.4 < 97.5$

Table 5.1 proves that the proposed measurement technique is repeatable and the magnetic fields emitted from these objects are fairly static.

## 5.4. Landmarks and Guideposts

### 5.4.1. Landmarks

Trying to locate a specific exit, staircase, office or classroom inside a building is a difficult task to achieve for the blind in a normal environment and even for sighted people in dark conditions during blackouts. There are many invisible landmarks that could be identified and used effectively. From the magnetic signatures, we found that some of the pillars emit a very high magnetic field while some emit low fields. The occurrences of these magnitudes in the signature could be landmarked and mapped out or used in series to figure out a specific location inside the building providing coarse navigation. For instance, specifying that landmark one, two and three along a corridor are identified as the first, fourth and the sixth pillars in the signature for CSE Corridor Wing 2 shown in Fig. 5.2.



FIGURE 5.2. CSE Corridor Wing 2 building layout with magnetic field intensity of each pillar. From this figure we can see the spacing between each pillar, the magnetic intensity of each pillar and also the landmarks created which are located at ends (P2 and P16) and also a significant pillar in the middle (P11).

Fig. 5.3 demonstrates the magnetic fields found in the Electrical Engineering corridor. Each spike recognizes a new pillar.

To coincide with the extensive measurements taken at the College of Engineering, more measurements were taken at the Biology, Chemistry, Environmental Science, General Academic, and Physics buildings. The technique explained in Section 5.3.2 was followed for these experiments in order to signify that the technique for magnetic mapping can be applied for buildings with different layouts.

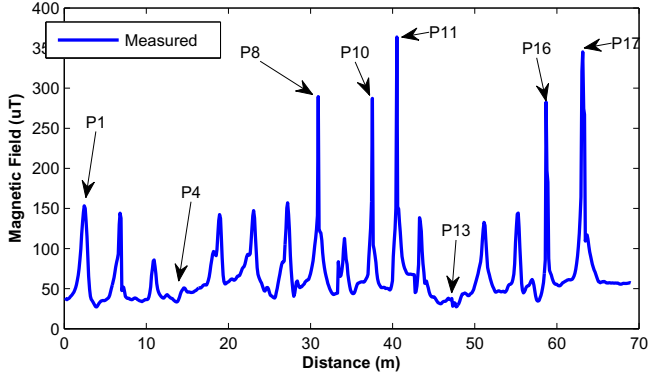


FIGURE 5.3. Plot showing the variations in the magnetic field while walking past each pillar from one end of the Electrical Engineering corridor to the other.



FIGURE 5.4. Layout of new buildings: Reinforced cylindrical pillars are present throughout the building. Fig. 5.5 is labeled in the picture where measurements were taken on the second floor.

Analysis showed that older buildings such as the General Academic and Physics building which are constructed mostly of brick, did not have a strong affect on the magnetic field sensors. The measurements taken did not fluctuate enough to obtain a visual magnetic profile. The newer buildings on campus though had an opposing analysis. The Biology, Chemistry and Environmental Science buildings, which are all fairly new, have big support structures that are positioned throughout each building. These structures are most likely

comprised of reinforced steel which can explain the existence of magnetic fields that is seen in classrooms and hallways. Fig. 5.4 illustrates these structures that can be used as landmarks and Fig. 5.5 represents these landmarks (visually depicted by four peaks). These peaks convey the pillars seen on the second floor in Fig. 5.4.

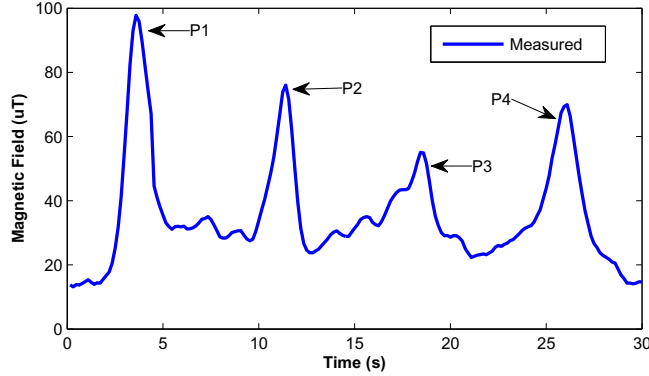


FIGURE 5.5. Magnetic field plot of the Biology building referenced in Fig. 5.4: Each peak represents a pillar that was passed on the second floor. These can be used in location identification as landmarks or guideposts for indoor navigation.

To study the effect of sampling rate on both the mobile phone and the results, two different people used two different phones at different sampling rates. Apart from slight magnitude differences seen in Fig. 5.6, the patterns obtained were relatively the same for different sampling rates. It is necessary to choose a sampling rate that is efficient in creating magnetic signatures while optimizing the integrity of the phone. Since our application uses only a mobile phone, conservation of both processor usage and power consumption is imperative to not hinder the phone from accomplishing its main purpose.

#### 5.4.2. Guideposts

Outdoor navigation is easy with the help of GPS that provides easily identifiable landmarks. Indoor navigation, particularly for the blind, can be arduous if there are only pillars and not many landmarks. Moreover, GPS does not work with precision indoors since it is affected by attenuation. Guideposts are specific points of interest that can be used for fine navigation. For example, at any point in time and space within a building, a signature

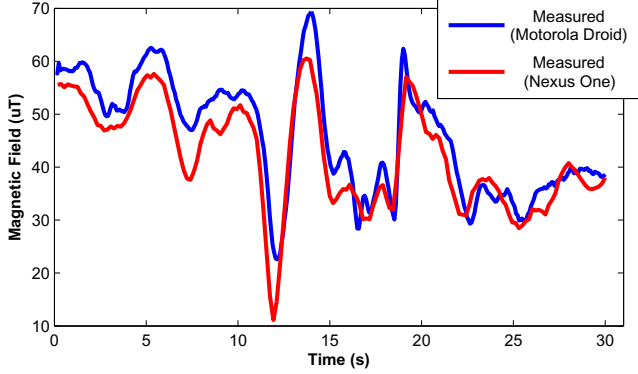


FIGURE 5.6. Magnetic field measurements in Chemistry building: Data obtained by a person walking from the main entrance to the back entrance of the building. Notice the number of samples did not affect the similar results. Total number of samples: Droid 371, Nexus One 166.

comprising of pillar 7 and its surroundings could be landmarked and recognized as 5m from the present location or next to room 230.

If the distance between each landmark is known, it becomes easy to quantify guideposts. Most buildings have a uniform structural layout that can be utilized in this way providing some kind of organized navigational information. In all the corridors, the pillars are equally spaced approximately 4m apart. Fig. 5.7 explains this concept in detail. In the tested corridor, elevators, which are stationed between two pillars, had no influence on the field produced by neighboring pillars and therefore did not hinder in finding guideposts.

## 5.5. Magnetic Maps

After characterizing pillars with their unique magnetic magnitudes and identifying landmarks as a signature comprising of one or more pillars, a map of that uniqueness was developed as shown in Fig. 5.8. This magnetic map illustrates the magnetic intensity of the CSE hallway in the College of Engineering building. The magnetic field was recorded in front of each pillar and between each pillar on both sides of the corridor. The magnetic field was also recorded in the middle of the corridor to complete a grid formation. This can be seen in Fig. 5.1 which illustrates the pillars on both sides of a corridor. The data was further used to interpolate the magnetic field readings along other points on the corridor to obtain

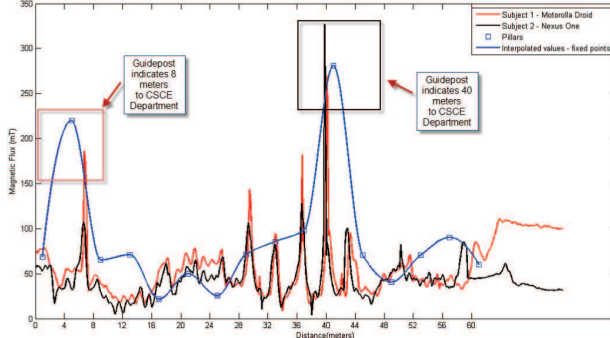


FIGURE 5.7. Guideposts: The first peak indicates a pillar that is 4m away from the CSE department. The next guidepost is found at a distance of 40m away which is comprised of high and low magnitudes in the signature. This helps to find the distance to reach a destination.

a magnetic map of a corridor. Darker reds represent a greater field presence where darker blues signify a weaker field.

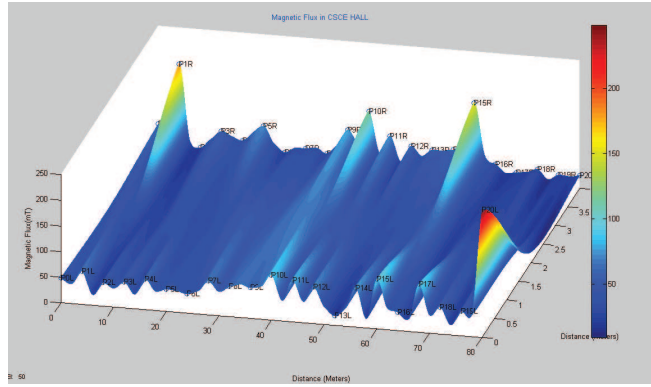


FIGURE 5.8. The plot shows the magnetic field strength variations of pillars (marked by P1R, P1L..) on either side of the corridor specified by its length and width in meters.

## 5.6. Magnetic Field Behavior

### 5.6.1. Theoretical Calculations

The retentivity of the material is the point at which some magnetic field remains in the material after the magnetizing force has been removed. The ability to retain such a force is the basis of ferromagnetism and the foundation of this research. This point is below

maximum saturation and can be seen in the hysteresis loop shown in Fig. 5.9 as point b or the Residual Magnetism ( $B_r$ ) [50]. At saturation (point a), the magnetic force ( $H$ ) along with the magnetization of the material would be aiding to the total magnetic field of the ferromagnetic material. Since no external field is present, we use an equation that is based on Asahi-Kasei simulations that will be used in comparison to the measured data taken by the Android based smartphones.

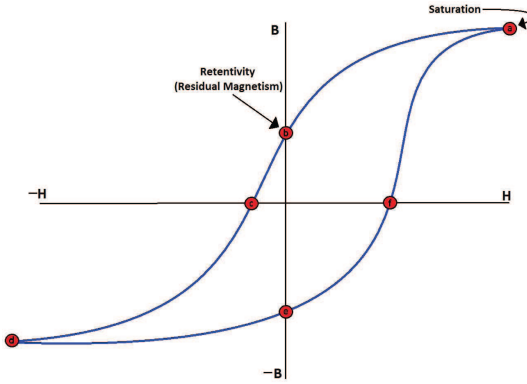


FIGURE 5.9. Hysteresis Loop: B represents the magnetic flux density while H signifies the magnetizing force. The point at which the magnetic force is zero while still having a positive magnetic flux is called the residual magnetism, represented by point b. The saturation point or point a, represents the alignment of all atoms in the material. This is also known as the highest magnetization point.

Magnetic fields are naturally produced by ferromagnetic materials and are also induced by a steady or variable electrical current. We do not assume that current flows through the pillars and based on the experiments performed, the variation in the magnetic field near pillars can be attributed to the density of ferromagnetic material in each pillar making it an arduous task to exactly model these variations. The ferromagnetic pillars used here can be categorized as steel. Understanding how these materials interact when induced by an external magnetic field and then maintaining that field through retention is difficult to model precisely without an exact analysis of the magnetic moment and volume of the material at an atomic level.

For this study, we use a function that is based on residual magnetism, the dimensions of the material and the distance at which it is being measured. This function is used by many magnet and magnetic sensor manufacturers, specifically Asahi-Kasei [51]. This function is also used in many simulation techniques and has been shown to be suitable for use as a model of the ferromagnetic material present in the pillars [52]. It is given by

$$(11) \quad B = \frac{Br}{pi} \left[ \tan^{-1} \left( \frac{ab}{2z\sqrt{4z + a^2 + b^2}} \right) - \tan^{-1} \left( \frac{ab}{2(z+h)\sqrt{4(z+h) + a^2 + b^2}} \right) \right]$$

The dimensions are shown in Fig. 5.10.

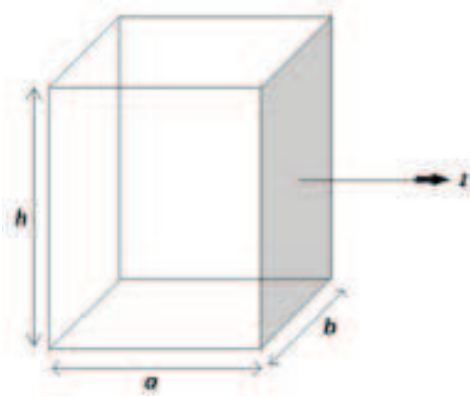


FIGURE 5.10. Eq. 11 diagram representing a structured pillar and its dimensions represented by the variables: length (a), width (b), height (h) and the distance (z) at which the field is being measured.

The expression is useful for modeling magnetic intensity distributions with respect to distance which is exactly what is needed for comparison with the tested pillars. The length, width, height, residual magnetic field at the surface, and distance from the magnetic surface are all taken into account to calculate the approximate magnetic field along the material's surface. The residual magnetic field is dependent on the material in question and because it is not affected by the shape of the material, is often used in simulation. Fig. 5.11 graphically compares the measured distribution of a pillar and the theoretical data using Eq. 11. The dimensions of each pillar are approximately 20cm by 20cm by 500cm and were measured at a constant distance from an initial 2.5cm from the pillar to a distance 213cm away from the pillar.

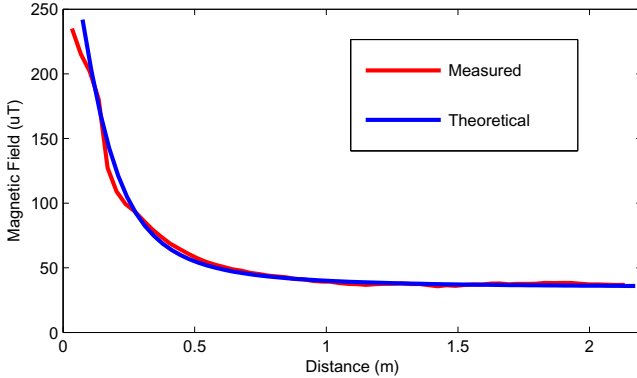


FIGURE 5.11. Magnetic field distribution of a pillar: Measured and theoretically generated using Eq.11. This plot shows a similar distribution over 2m which demonstrates Eq.11 as an acceptable theoretical model for the magnetic field distribution.

### 5.6.2. Distributions

Steel has a high retentivity so the material produces a magnetic field without an external source present. This remanent field makes it applicable for our proposal of creating magnetic maps for indoor navigation using android smartphones as measurement devices as steel is present in a majority of modern buildings. The measured magnetic field distribution of all the pillars follows the same path relative to its initial strength. This is dependent on the material's atomic magnetic moment density which is theoretically different for each individual pillar. This also creates the idea that each pillar is independent from one another as they produce different intensity levels. Surface distribution is not uniform as large distances along a pillar's surface were measured and demonstrated a change in field strengths. This, does not affect our hypothesis as field strengths remain constant where measured and this separating distance needs to be greater than 1m to see a significant change in intensity. The pillars were tested to obtain a consistency in field strength at different times of the day. Figure 5.12 illustrates the data obtained which shows a constant field throughout the day. Consistency in measurements is significant as it is a requirement in the classification of a pillar as a landmark. We also wanted to analyze long term fluctuations in the magnetic field data. Over the course of the experiment we gathered extensive amounts of data. To verify the

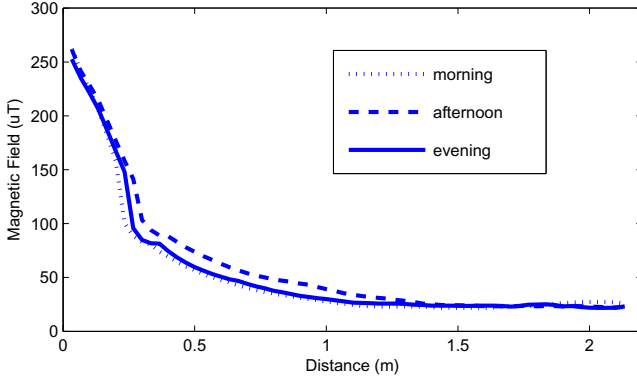


FIGURE 5.12. Magnetic field distributions for different times of a day: The variation is similar over any time period throughout the day.

sustainability of a corridor signature, we analyzed the CSE corridor data for three different months over a nine month period. Figure 5.13 represents this analysis which concluded that each corridor maintains a particular signature solidifying its use in creating a coarse localization tool. There are minor variations in the data that can be attributed to different walking speeds and patterns of humans.

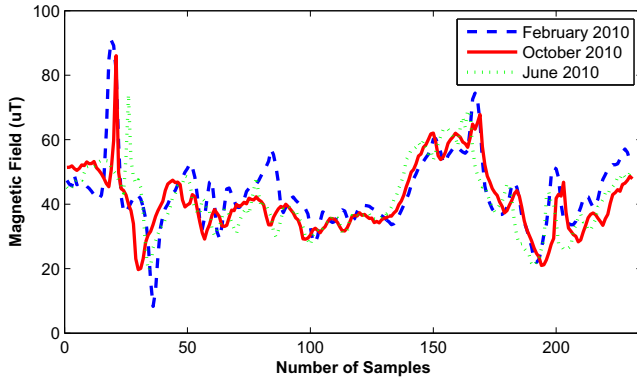


FIGURE 5.13. Magnetic signatures over a period of nine months: The CSE corridor was analyzed using data from February, June and October of 2010. This shows the consistency of the signature over a long period of time.

Since our technique needs to be flexible to be applied to all kinds of buildings, we take into account all the objects present to create a complete signature of an area. Fig. 5.14 represents a situation when electrical equipment is present during a measurement process. It illustrates a hallway containing multiple pillars and two vending machines.

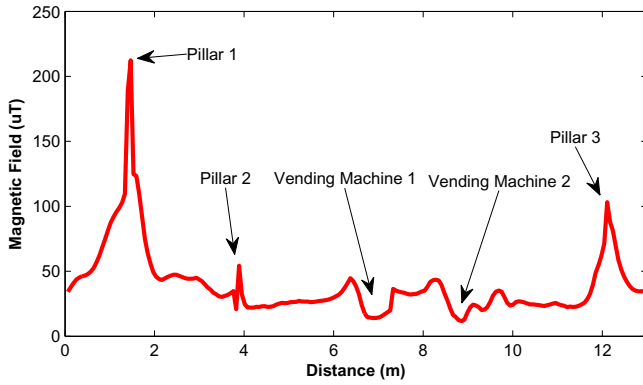


FIGURE 5.14. Magnetic field signature containing electrical equipment: The vending machines produced a low field which is a result of opposing currents.

As seen, the pillars emit a high magnetic field which can be used as landmarks whereas the vending machines emit a low magnetic field, a property of opposing current. With this characteristic, we do not classify them as a landmark. The data sets recorded were taken throughout the building which consists of two floors. The magnetic field produced by a pillar on the first floor is independent of that of the same pillar on the second floor as they tend to emit varying intensity levels. This can be due to the density of iron atoms throughout the material as it is more magnetized around one area of the pillar than another. This density characteristic helps with localization as the absence of a relationship between floor pillars actually aids to differentiate which floor you are on.

Not only are there numerous pillars throughout the building, but there are also different types of pillars with different dimensions that results in a maximum magnitude. It is also significant to note that the location of the many pillars seems to be important. Very high magnetic field producing solid pillars are observed to be positioned around corners of each corridor, H-Shaped pillars are stationed around office and lab areas, and small solid pillars are located around restroom facilities. These different pillars are illustrated in Fig. 5.15. The location of each type of pillar can be a factor in locating which part of the building you are in as the intensity for each type is different.



FIGURE 5.15. Types of pillars throughout the building: (a) solid (corner), (b) solid (middle), (c) solid (pair), (d) h-shape, and (e) solid (small).

## 5.7. Summary

This chapter showed a method for capturing indoor magnetic fields that affect the compass and utilizing them constructively to identify landmarks and guideposts essential for indoor localization. By collecting data using the mobile phone's built-in magnetic field sensor, I presented the idea of finding landmarks, guideposts and creating magnetic maps of buildings. The extensive measurements proved the stability of magnetic field data over long periods of time and repeatability of the data collection technique. These measurements also strengthen the hypothesis that with the exemption of older buildings, a magnetic map can be developed for every building using a smart phone so as to become an affective indoor navigational tool.

The next chapter provides detailed information on the occurrence of these magnetic fields and the reason for them being termed as anomalies.

## CHAPTER 6

### FERROMAGNETISM

In this section, I discuss the ferromagnetism phenomenon. The magnetic anomalies explained in the previous chapter are caused by the presence of ferromagnetic materials. These materials disturb the Earth's magnetic field. Rather than developing compensating mechanisms for the compass to counteract these anomalies, I captured the anomalies using the orientation sensor as a magnetometer, i.e collecting the magnetic fields indoors that include these anomalies. So, to start with, I explain the Weiss molecular theory and the Ising model which form the atomic level understanding of ferromagnetism in Section 6.1.1 and explain the relation between magnetization of a ferromagnet and temperature in Section 6.1.2.

Next, I introduce the basics of the Earth's magnetic field in Section 6.2 and validate the measured value of the magnetic field at different locations using an analytical model in Section 6.2.2. In Section 6.2.3, I explain the disturbances caused by ferromagnetic objects in the Earth's magnetic field both conceptually and mathematically.

The magnetic signatures measured in different buildings consisted of fields caused by steel reinforced concrete and solid steel pillars. I explain the differences between the signatures from both kinds of pillars through the implementation of an analytical model in Section 6.3.

#### 6.1. Introduction

Ferromagnetic materials are a class of magnetic materials that form permanent magnets and have many practical applications. Ferromagnetic materials exhibit long range ordering

---

The content in this chapter with the exception of Section 6.1, Section 6.1.1 and Section 6.1.2 are reproduced from Kalyan Pathapati Subbu, Brandon Gozick and Ram Dantu, "LocateMe: Magnetic Fields Based Indoor Localization Using Smartphones," ACM Transactions on Intelligent Systems and Technology (under review), with permission from ACM.

phenomenon at the atomic level which cause the unpaired electron spins to line up parallel to each other in a region called a domain. The domains are randomly oriented with respect to one another in the absence of external field. So although each domain has some net magnetization, there is no total magnetic field observed in the bulk of the sample. When an external magnetic field is applied, the domains already in the direction of the applied field grow at the expense of their neighbors as shown below.

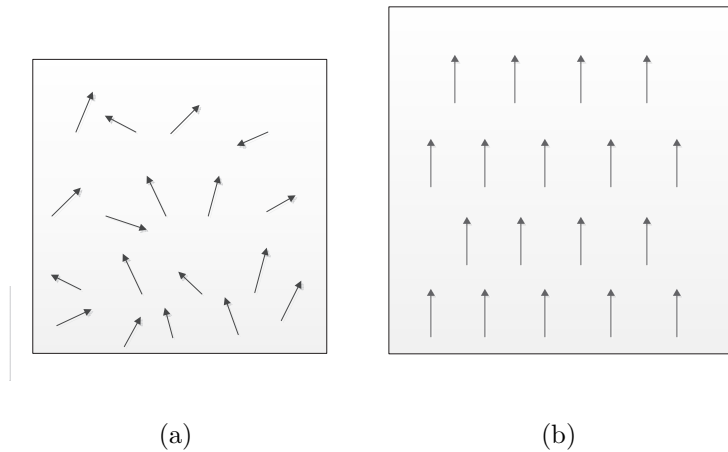


FIGURE 6.1. Ferromagnetism: (a) Random orientation of atoms before being induced by external magnetic field. (b) Parallel alignment of atoms to each other after the application of external magnetic field.

The spins are all in one direction and a net macroscopic magnetization is observed. The most important property of ferromagnetism is that it retains the magnetism even after the external field has been removed. At temperatures higher than the so called critical temperature or Curie's temperature, a ferromagnetic material undergoes second order phase transition into a paramagnetic material. The domains now have enough thermal energy to be randomly oriented again.

#### 6.1.1. Weiss Molecular Theory

Exchange interactions are interactions between two or more identical particles. In ferromagnetic materials, these interactions are spin-spin interactions for exchange interactions

tend to align neighboring spins. These interactions thus create small regions that are magnetized, now observed as magnetic domains. Exchange interactions are quantum mechanical effects, thus they are not results of any forces. They are the results of wave functions of indistinguishable particles, such as two electrons, being open to exchange symmetry. This states that no physical quantity will change after the exchanging of two identical particles. The spins of the two particles might also be identical, if the wave functions of the particles are symmetrical to each other; if the wave functions are anti-symmetrical, the spins of the electrons become opposite. If the electrons are parallel in position and spin, then they are magnetized, this is the cause of ferromagnetism in iron. I revisit the theory explained in [53]. According to this theory, the intensity of molecular field is directly proportional to the magnetization,

$$H_W = \gamma M$$

where  $\gamma$  is the molecular field constant. The total field acting on the material is

$$H_{tot} = H + H_W$$

The susceptibility  $\chi = \frac{M}{H}$ . Therefore,

$$\frac{M}{H + \gamma M} = \frac{C}{T}$$

or

$$M = \frac{CH}{T - C\gamma}$$

Therefore,

$$\chi = \frac{M}{H} = \frac{C}{T - \theta}$$

A positive value of  $\theta$  indicates that the molecular field acts in the same direction of the applied magnetic field which tends to make the magnetic moments align parallel to one another. This is the how the material becomes ferromagnetic.

### 6.1.2. The Ising Model

Ferromagnetism arises when a collection of atomic spins align such that their associated magnetic moments all point in the same direction, yielding a net magnetic moment which is macroscopic in size. The simplest theoretical description of ferromagnetism is called the Ising model. Below, I revisit the mathematics of the Ising model as explained in [54, 55].

Consider  $N$  atoms in the presence of a  $z$ -directed magnetic field of strength  $H$ . Suppose that all atoms are identical spin-1/2 systems. It follows that either  $s_i = +1$  (spin up) or  $s_i = -1$  (spin down), where  $s_i$  is (twice) the  $z$ -component of the  $i$ th atomic spin. The total energy of the system is written:

$$(12) \quad E = -J \sum s_i s_j - \mu H \sum_{i=1,N} s_i$$

The first term on the right-hand side of Equation 12 shows that the overall energy is lowered when neighboring atomic spins are aligned. This effect is mostly due to the Pauli exclusion principle which states that no two electrons can occupy the same quantum state. So two electrons on neighboring atoms which have parallel spins (i.e., occupy the same orbital state) cannot come close together in space. No such restriction applies if the electrons have anti-parallel spins. Different spatial separations imply different electrostatic interaction energies, and the exchange energy,  $J$ , measures this difference. Note that since the exchange energy is electrostatic in origin, it can be quite large: i.e.,  $J \sim 1\text{eV}$ . This is far larger than the energy associated with the direct magnetic interaction between neighboring atomic spins, which is only about  $10^{-4}\text{eV}$ .

The Ising model is analyzed using a simplified model called Mean Field Approximation (MPA). According to MPA, the energy of the  $i$ th atom is given by

$$(13) \quad e_i = -\frac{J}{2} \sum_{k=1,z} s_k s_i - \mu H s_i$$

where the sum is over the  $z$  nearest neighbors of atom  $i$ . The factor  $1/2$  is to ensure that each pair of neighboring atoms are not accounted twice when summed to obtain the total

energy,

$$(14) \quad E = \sum_{i=1,N} e_i,$$

We can write

$$(15) \quad e_i = -\mu H_{\text{eff}} s_i,$$

where

$$(16) \quad H_{\text{eff}} = H + \frac{J}{2\mu} \sum_{k=1,z} s_k.$$

Here,  $H_{\text{eff}}$  is the effective magnetic field, which is made up of two components: the external field,  $H$ , and the internal field generated by neighboring atoms. Considering a single atom in a magnetic field  $H_m$  and thermal equilibrium at temperature  $T$ . According to the well-known Boltzmann distribution, the mean spin of the atom is

$$(17) \quad \bar{s} = \frac{e^{+\beta\mu H_m} - e^{-\beta\mu H_m}}{e^{+\beta\mu H_m} + e^{-\beta\mu H_m}}$$

where  $\beta = 1/kT$ , and  $k$  is the Boltzmann constant. The above expression follows because the energy of the “spin up” state ( $s = +1$ ) is  $-\mu H_m$ , whereas the energy of the “spin down” state ( $s = -1$ ) is  $+\mu H_m$ . Hence,

$$(18) \quad \bar{s} = \tanh(\beta\mu H_m)$$

The assumption that all atoms have identical spins: i.e.,  $s_i = \bar{s}$ , is known as the mean field approximation. Further,

$$(19) \quad H_{\text{eff}} = H + \frac{z J \bar{s}}{2\mu}$$

Finally, Equations 18 and 19 are combined(identifying  $H_m$  and  $H_{\text{eff}}$ ) to obtain

$$(20) \quad \bar{s} = \tanh \{\beta\mu H + \beta z J \bar{s}/2\}$$

The critical temperature is defined as,

$$(21) \quad T_c = \frac{z J}{2 k},$$

and the critical magnetic field,

$$(22) \quad H_c = \frac{k T_c}{\mu} = \frac{z J}{2 \mu}$$

Equation 20 reduces to

$$(23) \quad \bar{s} = \tanh \left\{ \frac{T_c}{T} \left( \frac{H}{H_c} + \bar{s} \right) \right\}$$

Since the above equation is complicated to solve analytically, an iteration scheme is used as shown below,

$$(24) \quad \bar{s}_{i+1} = \tanh \left\{ \frac{T_c}{T} \left( \frac{H}{H_c} + \bar{s}_i \right) \right\}$$

The above formula is iterated until  $\bar{s}_{i+1} \rightarrow \bar{s}_i$ . The net magnetization is given by,

$$(25) \quad M = \mu \sum_{i=1,N} s_i = \mu N \bar{s}$$

The above equation shows that atomic spins result in a high kinetic energy which results in a magnetic field that creates magnetic moment by aligning these existing spins.

The net energy is given by,

$$(26) \quad E = \sum_{i=1,N} e_i = -N k T_c \left( \frac{H}{H_c} + \bar{s} \right) \bar{s}$$

and the heat capacity,

$$(27) \quad C = \frac{dE}{dT}$$

The Ising model and its implementation give an idea about the property of a ferromagnetic material, that is achieving a net magnetization and then losing it after a certain threshold.

## 6.2. The Earth's Magnetic Field

The Earth acts like a great spherical magnet, surrounded by a magnetic field [52, 56]. This magnetic field changes both with time and location and resembles the field generated by a tilted dipole magnet whose axis is offset from the axis of the Earth's rotation by approximately  $11^\circ$ . In other words, the location of the North and South geographic poles and the North and South magnetic poles are not same. At any point and time, the Earth's magnetic field can be characterized by a direction and intensity both of which can be measured.

The parameters that describe the direction of the magnetic field are declination (D) and inclination (I). D and I are measured in units of degrees, positive east for D and positive down for I. The intensity of the total field (F) is described by the horizontal (H), vertical (Z), and the north (X) and east (Y) components of the horizontal intensity. The Earth's magnetic field intensity is approximately between  $40\text{-}65 \mu\text{T}$ . Magnetic declination is the angle between magnetic North and true North. D is considered positive when the angle measured is east of true North and negative when West. Magnetic inclination is the angle between the horizontal plane and the total field vector, measured positive into Earth.

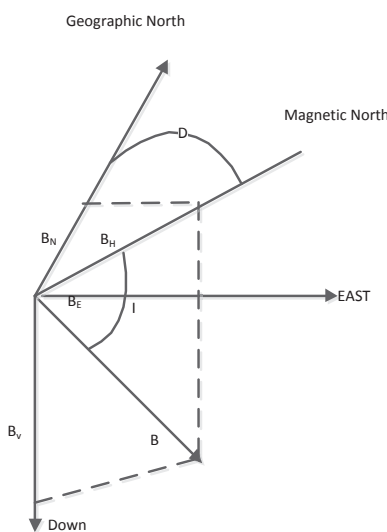


FIGURE 6.2. Components of geomagnetic field vector.

The intensity of horizontal component is given by

$$(28) \quad H = \sqrt{B_X^2 + B_Y^2}$$

The total intensity is given by

$$(29) \quad T = \sqrt{B_X^2 + B_Y^2 + B_Z^2}$$

The inclination I is given by

$$(30) \quad I = \arctan\left(\frac{B_Z}{\sqrt{B_X^2 + B_Y^2}}\right)$$

and the declination D is given by

$$(31) \quad D = \arcsin\left(\frac{B_Y}{\sqrt{B_X^2 + B_Y^2}}\right)$$

### 6.2.1. Generation Of Earth's Magnetic Field

The Earth's magnetic field is generated using the IGRF-International Geomagnetic Reference Field model [57] released by International Association of Geomagnetism and Aeronomy (IAGA). The IGRF is essentially a set of Gaussian coefficients,  $g_n^m$  and  $h_n^m$ , that are used in a spherical harmonic model. The model includes both the coefficients for the epoch year and secular variation variables, which track the change of these coefficients in nano T per year. These secular variation coefficients are used to extrapolate the Gaussian coefficients. Typically the IGRF consists of 120 coefficients, with 80 secular variation coefficients. The spherical harmonic model that is followed by the IGRF model is given by

$$(32) \quad V(r, \theta, \phi) = a \sum_{n=1}^k \left(\frac{a}{r}\right)^{n+1} \sum_{m=0}^n (g_n^m \cos m\phi + h_n^m \sin m\phi) P_n^m(\theta)$$

Where  $a$  is the reference radius of the Earth ( $a = 6371.2\text{km}$ ),  $r$  is the radius in kilometers,  $\theta$ , and  $\phi$  are the geocentric coordinates, the co-latitude and longitude respectively. The coefficients  $g_n^m$  and  $h_n^m$  are Gaussian coefficients put forth by the IAGA for the IGRF, and  $P_n^m(\theta)$  represents the Schmidt quasi-normalized associated Legendre functions of degree n

and order  $m$ . Legendre polynomials are a set of orthogonal polynomials that also satisfy the zero mean condition.

### 6.2.2. Model Validation

The IGRF model has been made available as a freely available software package. The Earth's magnetic field at a particular location can be obtained by entering the model, date, altitude, latitude, and longitude values. These values are used in the spherical harmonic model and finally the components of Earth's magnetic field, the inclination and declination and the change of each of these components over a year are calculated. A screenshot of the software is shown in Fig. 6.3.

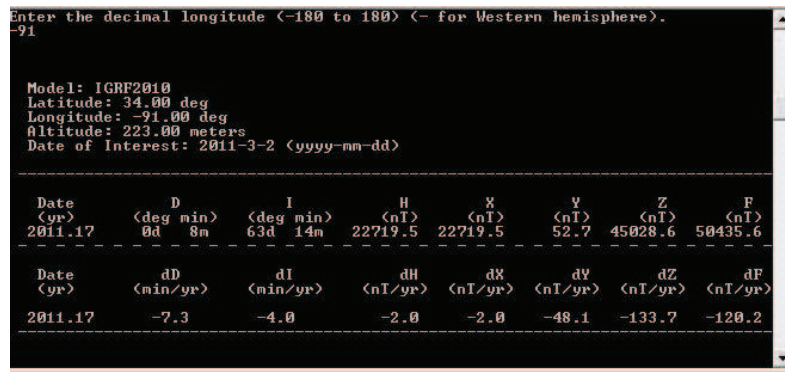


FIGURE 6.3. The IGRF model showing the individual components of the Earth's magnetic field and their variations along with the inclination and declination. The latitude and longitude values are for the area of Denton, Texas.

To verify if the Earth's magnetic field captured using the magnetometer in the mobile phone varied between the specified range of  $40\text{-}60\mu\text{T}$ , the magnetic field was collected three different locations outdoors and the individual components of the magnetic field are plotted in Fig. 6.4.

As can be seen, the Earth's magnetic field at the three locations is different but varies between the range specified. To show the closeness between the measured values and those obtained from the model, I visually compare the values and show them in Fig. 6.5.

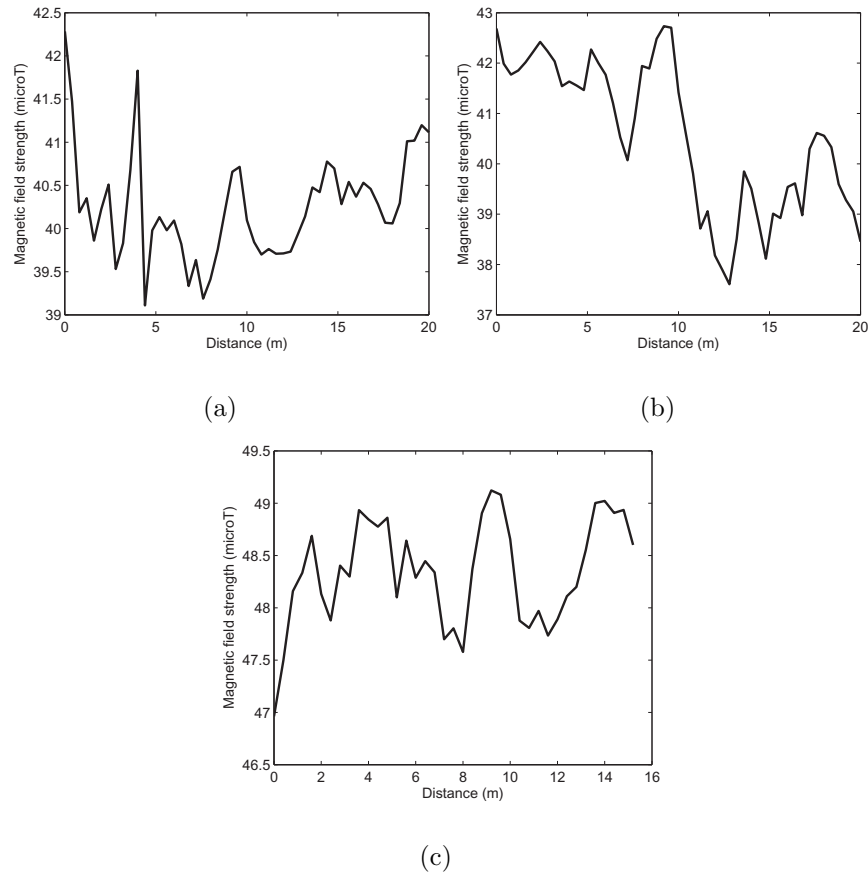


FIGURE 6.4. Measured Earth's magnetic field at different locations: The field variation is around  $3 \mu\text{T}$ ,  $4 \mu\text{T}$ , and  $2 \mu\text{T}$  in (a), (b) and (c) respectively.

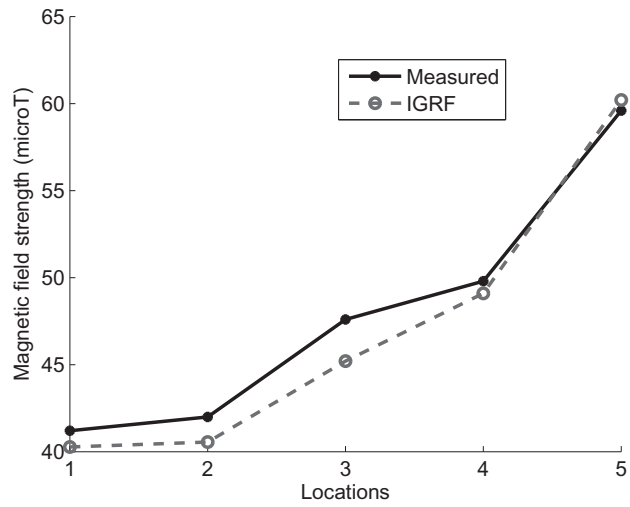


FIGURE 6.5. Comparison between generated and measured Earth's magnetic fields.

A strong correlation of 99.5 was obtained from above data. This validated the IGRF model. By analyzing the measured data in different hallways, the region between two pillars recorded values between  $40\text{-}60\mu\text{T}$ . The pillars were separated by a distance of 4.75 m. Therefore, the magnetic fields from one pillar did not affect the fields of another pillar. Using a dataset of 100 readings for each corridor, a statistical analysis was performed to analyze the magnitude of magnetic fields between pillars. Table 6.1 shows the magnetic field values present between pillars without any interferences.

TABLE 6.1. Magnetic field between pillars.

Building	# Hallways	# Measurements	EMF
DP	22	100	$48.74 < 50 < 51.26$
Union	8	100	$51.10 < 52 < 52.90$
LSc	9	100	$49.77 < 51.31 < 52.86$
EESAT	10	100	$53.4 < 55 < 56.66$
Chem	11	100	$43 < 45 < 47$

From the table we can see that without the presence of any interference, the magnetic field present was that of the Earth with 95% confidence intervals. The magnitude of this field varied between  $40\text{-}60\mu\text{T}$  which is the range of the Earth's field and this was verified by using the IGRF model explained above. Contrast to this, in indoor environments, the Earth's magnetic field is disturbed by ferromagnetic property of steel reinforced concrete pillars, door frames, and elevators. The next section explains the impact of these structures on the Earth's magnetic field.

#### 6.2.3. Impact of Ferromagnetic structures on the Earth's magnetic field

The Earth's magnetic field as mentioned earlier is affected by magnetic disturbances from different ferromagnetic structures which have their own magnetization. The magnetic fields from these structures can be termed as magnetic anomalies. In simple terms, this can be described as follows: Consider the Earth's magnetic field to be a set of parallel lines. On

interaction with a magnetic object, these lines tend to get attracted towards the object, this converges the magnetic field lines depending on the strength of the object.

Since the Earth is also considered as a dipole, the interaction between the Earth's magnetic field and the magnetic anomalies can be described and modeled as a dipole-dipole interaction [58]. The effect of these structures increases as the distance to the observation point decreases. In other words, the impact of the disturbance becomes stronger. To observe this phenomenon, the measurement procedure involved a user walk along a hallway passing different pillars. Assuming the position of the user to be the observation point, as the user moves, we can say that the magnetic dipole of the Earth also moves. As the distance between the user (observation point) and the pillar decreases, there is an interaction of the two dipoles which results in the individual components of both the Earth's magnetic field and the pillar undergo magnitude changes which leads to a change in the orientation of the total magnetic field vector. This change in the magnetic field vector is called the ANOMALY. Let us assume that the Earth's magnetic field is  $F_e$  and that of the pillar is  $F_p$  where the

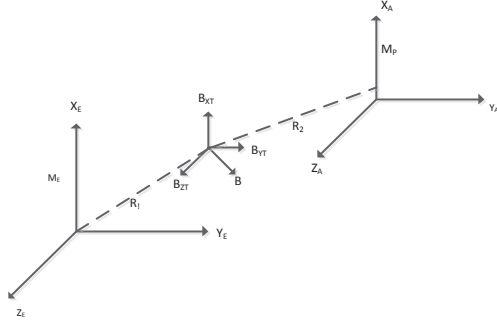


FIGURE 6.6. Interaction of dipoles of magnetic fields.

individual components are denoted as  $X_E$ ,  $Y_e$  and  $Z_e$  and  $X_p$ ,  $Y_p$  and  $Z_p$  respectively.

$$\begin{aligned}\vec{F}_T &= \vec{F}_e + \vec{F}_p \\ &= \vec{X}_e + \vec{Y}_e + \vec{Z}_e + \vec{X}_p + \vec{Y}_p + \vec{Z}_p\end{aligned}$$

The individual components of both the Earth's magnetic field and the ferromagnetic field are sometimes in opposite directions and this results in a negative magnitude. They can be denoted as

$$\begin{aligned}
 &= \vec{X}_e + (-\vec{X}_p) + \vec{Y}_e + (-\vec{Y}_p) + \vec{Z}_e + (-\vec{Z}_p) \\
 (33) \quad \vec{F}_T &= \vec{X}_T + \vec{Y}_T + \vec{Z}_T
 \end{aligned}$$

where  $X_T$ ,  $Y_T$  and  $Z_T$  are the magnetic field values obtained after the vector components add up. The resultant magnitude is obtained by

$$F_T = \sqrt{X_T^2 + Y_T^2 + Z_T^2}$$

This is basically a vector addition of the individual components of both the fields. An experiment was performed at the College of Engineering where the user walked from the center of the hallway sideways to the pillar, recorded the measurement for a duration of approximately 5-6 secs and then walked away from the pillar back to the center. Two different pillars were chosen as shown in Fig. 6.7.



FIGURE 6.7. Experiment procedure: The arrows indicate the two way horizontal walking pattern from the center of the hallway towards the pillars.

Figs. 6.8(a) and 6.8(b) clearly depict the effect of two pillars on the Earth's magnetic field. Now, these disturbances can be seen in the magnetic signature of the same hallway shown in Fig. 6.8(c), obtained by walking down the hallway past these pillars.

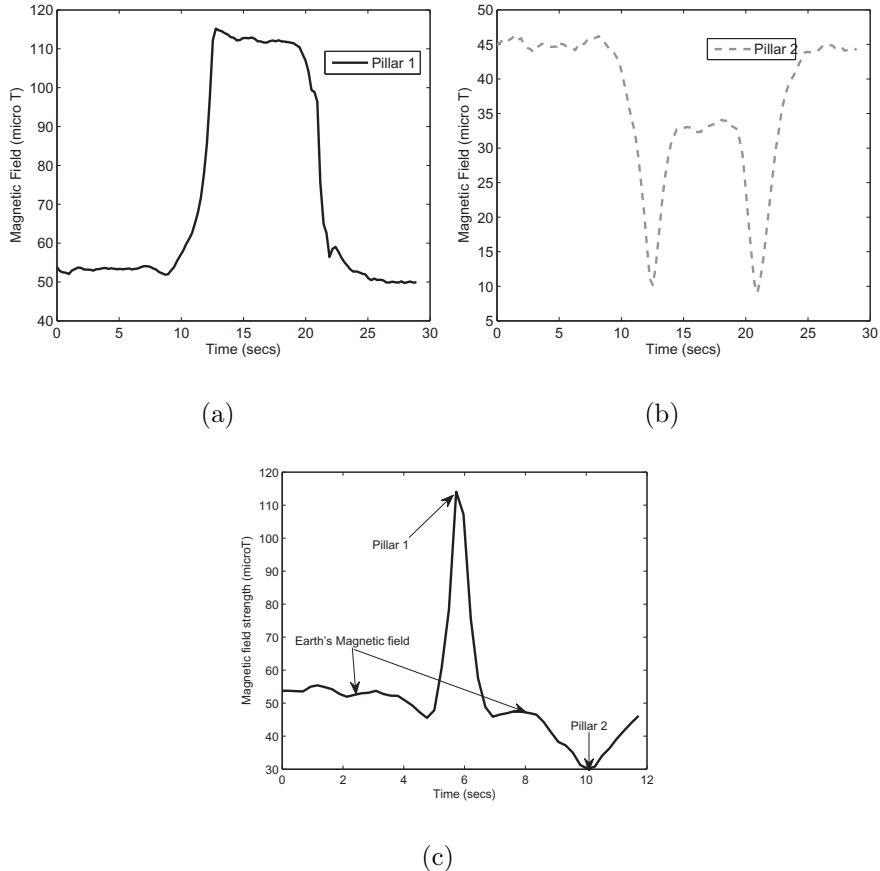


FIGURE 6.8. Impact on Earth's field: For the first and last 10 secs, there is no major change in the Earth's magnetic field. As the distance towards the pillar decreased, the magnitude changed drastically to (a) a high value of  $115 \mu\text{T}$  at one pillar, (b) a low value of  $33 \mu\text{T}$  at another pillar, (c) the high and low magnetic disturbance caused by the two pillars are clearly indicated along with the Earth's field until 4.3 secs and then between 6.5-8.3 secs approximately.

### 6.3. Analytical Modeling of Magnetic Signatures

It was observed that the magnitudes in the collected signatures varied between  $35 - 115 \mu\text{T}$  and  $100 - 220 \mu\text{T}$  in buildings that consisted of solid steel and steel reinforced concrete pillars respectively. In other words, the disturbances from steel reinforced concrete pillars seemed to be stronger than solid steel pillars. To quantitatively understand this observation,

I implemented an analytical model to generate magnetic field distributions of these pillars and compared them with the measured data.

The other motive behind the analytical modeling was to understand the different components of a magnetic signature since in a typical hallway, there are pillars, elevators and doors that are made of ferromagnetic materials such as steel or iron which cause disturbances in the Earth's magnetic field as explained in Section 6.2.3. This section discusses the disturbance due to each of the components on the Earth's magnetic field.

#### 6.4. Pillars

Since a ferromagnetic object generates its own magnetic field, it can be approximated as a dipole. The point dipole model [59] given by Equation 34 can be adopted.

$$(34) \quad B(\vec{m}, \vec{r}) = \frac{\mu}{4 * pi} \left[ 3 \frac{(\vec{m} \cdot \vec{r}) \vec{r}}{|\vec{r}|^5} - \frac{\vec{m}}{|\vec{r}|^3} \right]$$

where  $\mu$  is permeability of free space,  $\vec{m}$  denotes the magnetic moment, which is the average field strength at any particular point, also known as saturation magnetization and  $\vec{r}$  is the distance between the dipole and the observation point. The resultant moment arising due to the interaction of multiple dipoles is given by

$$(35) \quad M_{total} = \sqrt{m1^2 + m2^2 + m1 \cdot m2 \cos \phi}$$

with  $\phi$  being the angle between the dipoles and  $m1$  and  $m2$  the magnetic moments of the two interacting dipoles. By substituting  $M_{total}$  in Equation 34, the magnetic field can be obtained. The next section provides a discussion on the implementation of the dipole model for steel reinforced concrete pillars of different kinds and dimensions.

##### 6.4.1. Steel Reinforced Concrete

Typically, steel reinforced concrete pillars are constructed by first forming a grid like structure of steel rods or rebars tied together [60, 61]. The rods are equally spaced to form either a cylindrical grid for a cylindrical pillar or a rectangular grid for a rectangular pillar. Figure 6.9 shows these grids.

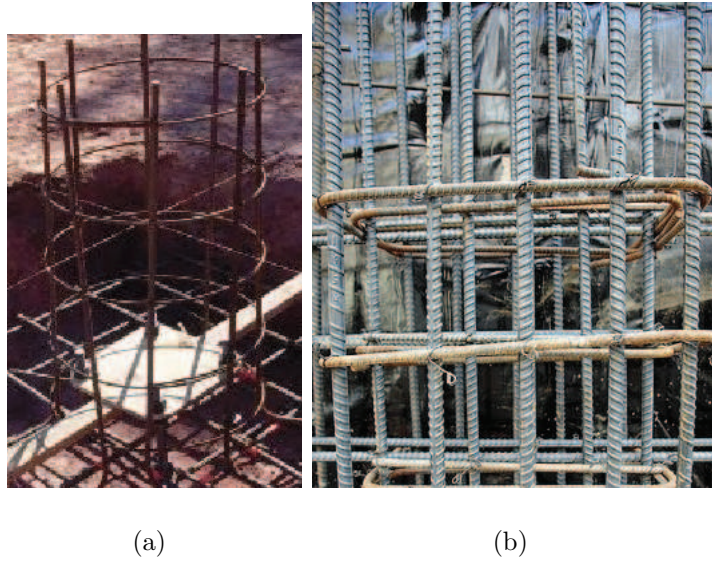


FIGURE 6.9. Type of grids: (a) cylindrical grid, (b) rectangular grid.

So, a grid can be considered as a set of four dipoles. This causes dipole-dipole interaction, the strength of which is proportional to several factors:

- (1) The magnitudes of the individual interacting dipoles
- (2) The distance separating the interacting dipoles
- (3) The orientation of the dipoles relative to one another

By calculating the combined or coupled dipole moment due to parallel and perpendicular dipoles using Equation 35, the resulting magnetic field distribution of a particular grid size was computed using Equation 34. For both steel reinforced and solid columns, I used the dimensions provided in Table 6.2.

TABLE 6.2. Dimensions of grid and rebars.

Grid Size (feet)	1x1	1.5x1.5	2x2	2.5x2.5	3x3	3.5x3.5	4x4
Rebar Diameter (inches)	0.3	0.3	0.3	0.5	0.5	0.8	1.2
Solid Size(feet)	0.3,1	0.5,1.5	0.8,2	1,2.5	1.2,3	1.5,3.5	1.8,4

Using Eqs. 35 and 34, the magnetic field distribution of different sized pillars was obtained. The implementation was performed by assuming a person walk past the pillars. This

should cause the magnitude to increase and drop as the distance to the pillars increases. Figure 6.10 shows the analytical and measured magnetic field distributions of cylindrical and rectangular grids.

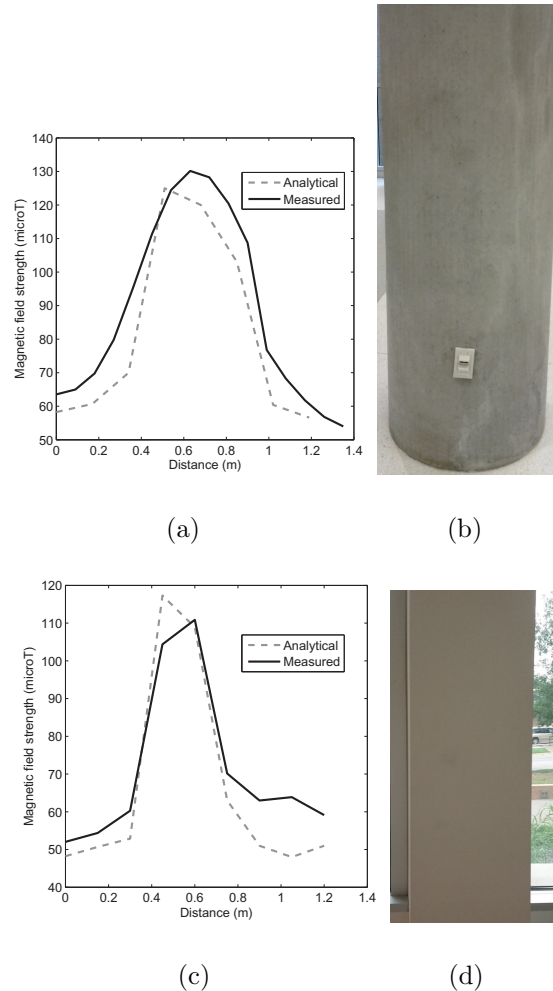


FIGURE 6.10. Analytical and Measured magnetic field distributions of reinforced pillars: (a) Cylindrical grid size of 2.5x2.5 foot. (b) A typical cylindrical steel reinforced pillar. (c) Rectangular grid size of 2.5x2.5foot. (d) A rectangular steel reinforced pillar.

This was the kind of magnetic behavior observed in buildings consisting of cylindrical and rectangular reinforced concrete pillars. Fig. 6.11 shows how varying the grid size or the vertical distance between the steel rods varied the magnetic fields.

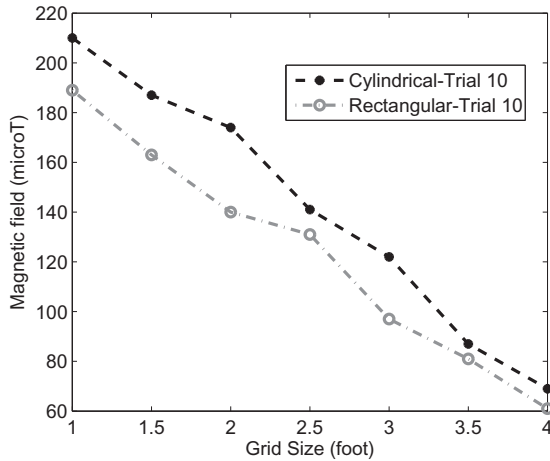


FIGURE 6.11. Magnetic field strength as a function of grid size: As the grid size increases, the distance between the dipoles increases, thereby reducing the resultant moment due to lesser dipole-dipole interaction. The resultant moment in turn reduces the magnetic field.

Sensitivity analysis was performed using the model by varying the vertical spacing in the grid for different rod sizes and keeping the horizontal spacing between the rods as a constant value of 1.5 inches. In other words, the variation in the magnetic field strength for each grid size with different sized rods was analyzed. Fig. 6.12 depicts this relation.

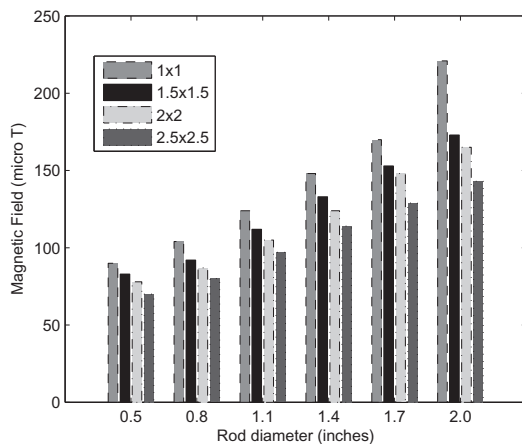


FIGURE 6.12. Magnetic field strength as a function of grid and rod size: The field strength increases as the rod diameter increases, and reduces as the grid size increases.

From Fig. 6.12, the following observations can be made:

- (1) The magnitude of the field increased as the rod size increased.
- (2) For a single rod size, the magnitude reduced as the grid size increased. This can be justified by the fact that as the grid size increased, the vertical distance between two dipoles/rods increased, thereby reducing the overall magnetic moment due to reduced dipole-dipole interaction.

By performing sensitivity analysis on the model, the variation of magnetic field strength was observed for different configurations of rod and grid sizes. An average reduction of 24% in the magnitude was obtained for each rod size as the grid size increased.

#### 6.4.2. Solid Steel

Now, using the same model, each pillar at the College of Engineering was approximated as a single dipole since it was a solid steel object. The simulation process was simply to calculate the magnetic field of a dipole at a certain distance. Fig. 6.13 below illustrates the analytical and measured distributions.

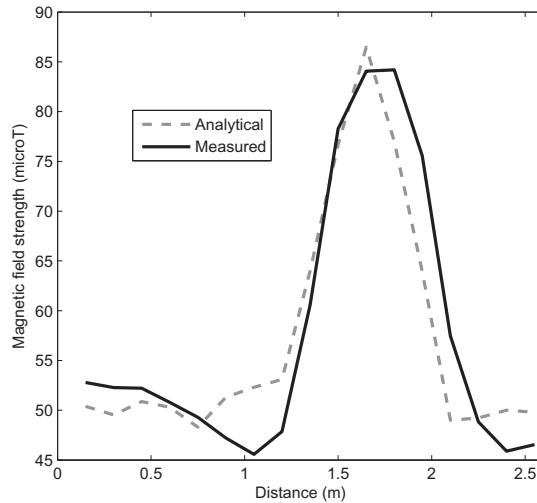


FIGURE 6.13. Magnetic field distribution of a solid steel structure: Analytical and Measured.

Now, a scale factor was computed between the magnitudes of the steel reinforced concrete and solid columns. Table 6.3 lists the factor.

TABLE 6.3. Scale factor.

Grid Size (feet)	1x1	1.5x1.5	2x2	2.5x2.5	3x3	3.5x3.5	4x4
$\alpha_1$	1.27	1.35	1.47	1.6	1.63	1.66	1.7
$\alpha_2$	1.12	1.2	1.21	1.4	1.5	1.8	1.9

The scale factor gives an indication as to how many times is the magnitude of the steel reinforced column bigger than the solid column. From the results it can be confirmed that steel reinforced concrete structures have higher magnitudes than solid pillars. I summarize the reasons for this behavior

- Reinforced structures have many steel rods as compared to a solid metal. Increasing the number of rods in the dipole model, increased the resultant magnetic field due to the coupled magnetic moment.
- The bigger the size of the rods inside the grid, stronger the magnetic field.
- As the vertical spacing in a grid increased, the magnetic field decreased due to the increased distance between dipoles reducing the dipole-dipole interaction.

#### 6.4.3. Pillar Width detection

As mentioned earlier, pillars are steel reinforced or a lump of solid steel. They can also be differentiated by their size. Specifically, some pillars are wider than others. It was observed that the magnetic field distribution width (the rise and drop of the magnetic field strength) varied according to the width of the pillar. Fig. 6.14(a) shows approximately how the distribution would look for different pillar widths and Fig. 6.14(b) depicts the measured and analytical distribution of a pillar nearly 1 foot wide present in the Chemistry building hallway at the main campus.

#### 6.4.4. Magnetic field due to current in a pillar

It is a known fact that magnetic fields are also caused by currents. Since it is not clear if the built-in magnetic field sensor is capturing these current caused magnetic fields, nevertheless it is imperative to consider these fields in the simulation analysis. Moreover,

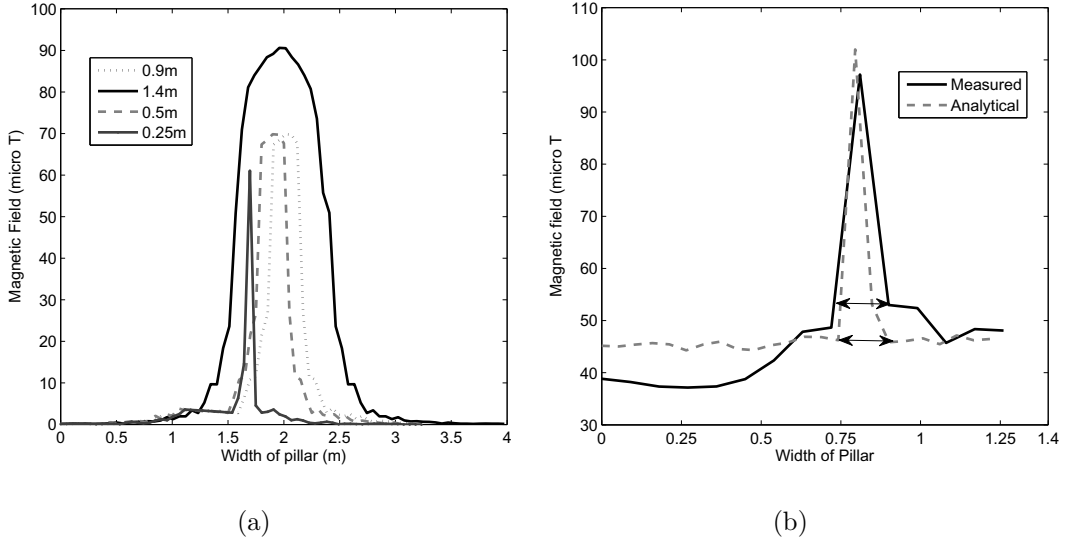


FIGURE 6.14. Pillar Width: (a) The analytical distribution of pillars of different widths follows a Gaussian distribution. (b) Analytical and Measured magnetic field distribution of a 0.3 m (1 foot) wide pillar.

some pillars may have wires carrying current passing through them. Magnetic fields caused by current carrying wires can be easily computed using the standard Ampere's law given by

$$(36) \quad B = \frac{\mu_o I}{2 * pi * r}$$

where  $I$  is the current flowing and  $r$  is the distance from which the magnetic field is measured. The magnetic field lines around a long wire which carries an electric current form concentric circles around the wire. The magnitude of these fields reduce as a function of distance as can be seen in Equation 36. With this relation, I assumed 5 parallel wires carrying current of 100A in the opposite direction and calculated the magnetic fields at distances of 0.5-2m. The wires were assumed to be spaced at 0.05m. The above formula can be extended to multiple current carrying wires placed at certain distances apart. Fig. 6.15 illustrates the inverse relation between distance and current causing magnetic fields. Based on this analysis, we can see that the magnetic field caused by these current carrying wires inside the pillar do not show any impact. In other words, the value of the magnetic field was not high enough for the magnetometer to capture.

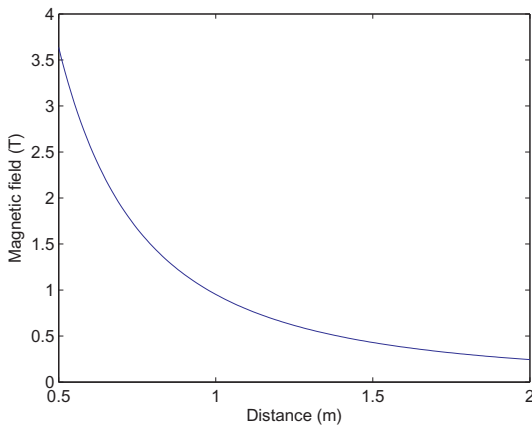


FIGURE 6.15. Distance and Magnetic field relation for current carrying wires.

#### 6.4.5. Magnetic field variation along a single pillar

Another observation from the measured data was that in a single pillar, there were variations in the magnetic field at different heights. We measured the data at heights of 2 and 3 feet. The idea behind measuring the field at different heights was to confirm if the magnetic signature based localization application can be used by people when holding the phone at different heights.

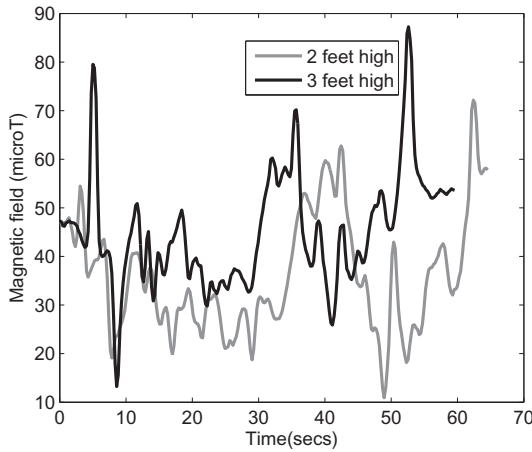


FIGURE 6.16. Signatures captured at two different vertical distances are similar showing that the measurement procedure is independent of heights.

## 6.5. Door Frames

Here I present an interesting finding of identifying door widths using their magnetic signatures.

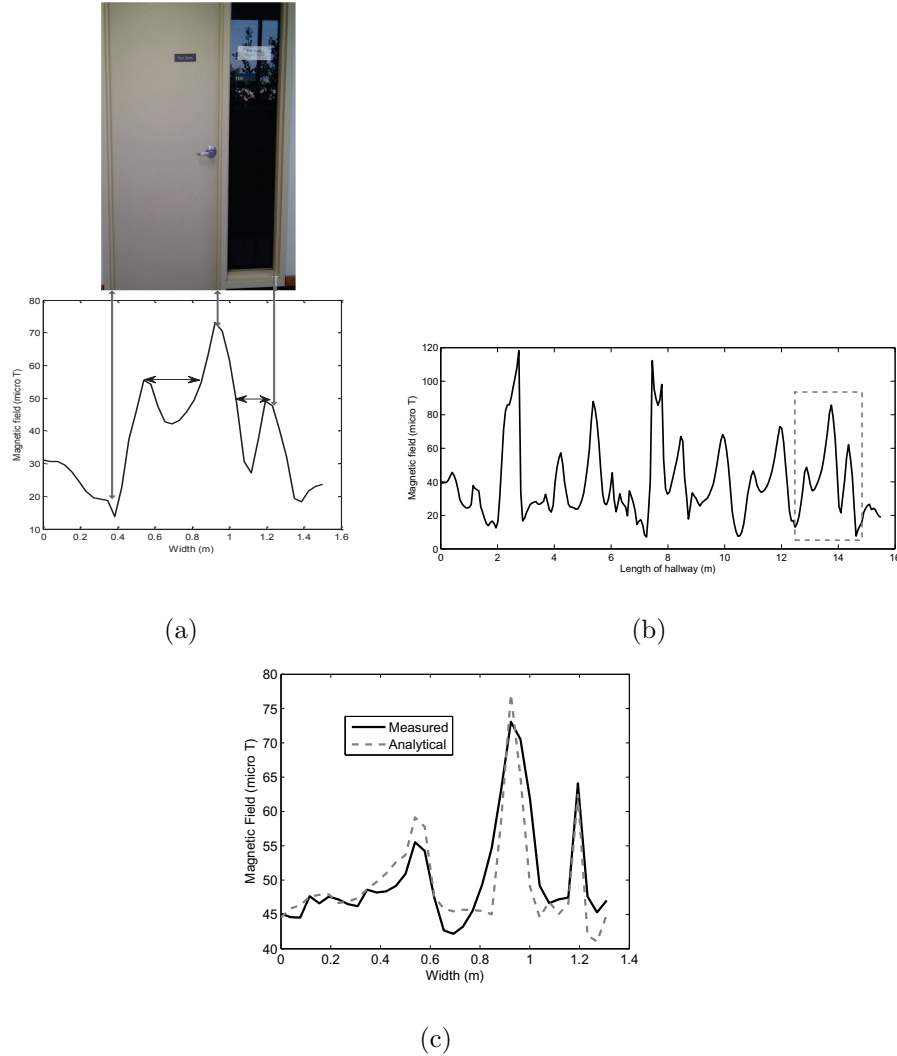


FIGURE 6.17. Door identification: (a) The signature below the door, maps closely to three frames, one at the start and the other two at the start and end of the window section. (b) The door in (a) clearly identified by the dotted rectangle in the signature of the entire hallway. (c) The analytical implementation of the signature by considering each frame in the door as a ferromagnetic object.

## 6.6. Elevators

Elevators are also ferromagnetic structures with a similar design as doors, consisting of an elevator door and metal frames/casing at the start and end. The College of Engineering had different sized elevators in terms of their width. Figs. 6.18 show two different elevators and the signature obtained by walking past them. (Note that the x axis scale is in meters for convenience)

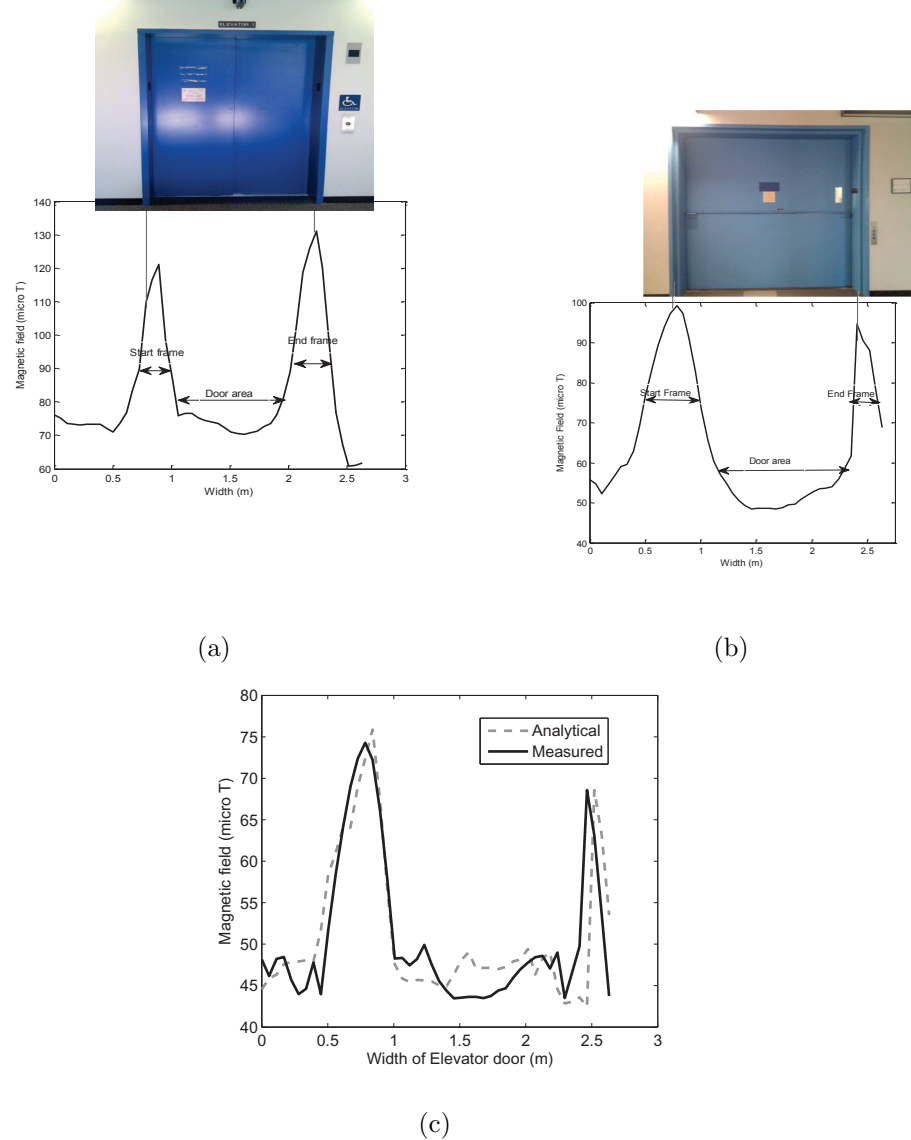


FIGURE 6.18. Elevator signature: (a) A 2.5 foot wide elevator. (b) 4 foot freight elevator. (c) Analytical implementation for elevator width detection.

The peaks at the start and end frames separated by a width gave the signature a unique pattern. This enabled to approximate the frames as thin ferromagnetic structures and use the analytical model to generate signature of an elevator and also detect the width of the elevator door as shown in Fig. 18(c). This concludes the discussion on the different sources of disturbances found in a magnetic signature.

## 6.7. Summary

The main idea behind this chapter was to provide a thorough understanding of why the magnetic signatures were unique. Specifically, providing answers to questions 1) What is the ferromagnetism? 2) What is the value of Earth's magnetic field indoors and outdoors? 3) How is the Earth's magnetic field affected by ferromagnetic structures? and 4) Why is the magnetic field at some pillars high and some pillars low resulting in a unique signature for every hallway?

Through conceptual and mathematical analysis by implementation of a model, I was able to answer each of the questions in a way that the underlying phenomenon and its effect which is ferromagnetism, can be easily understood in the context of this research that is magnetic signature based localization. To summarize, I accomplished the following in this chapter:

- (1) Validation of Earth's magnetic field using a theoretical model with measured data.
- (2) Quantify the impact of ferromagnetic structures on the Earth's magnetic field through vector addition of field components.
- (3) Calculate the magnetic fields of steel reinforced grids of different sizes for both cylindrical and rectangular columns.
- (4) Prove the hypothesis that steel reinforced concrete structures have greater magnitudes than solid steel pillars.
- (5) Analytical and experimental detection of pillar, door and elevator widths.

## CHAPTER 7

### DYNAMIC TIME WARPING

#### 7.1. Introduction

Dynamic Time Warping (DTW) is a well known technique for aligning two time series sequences of similar patterns but with deviations in the x or y axes. It has its applications in speech processing [62], sensor data classification [63], data mining [64, 65], and in analyzing the walking stability of people [66]. The technique in DTW is to compress or stretch the time axis of one (or both) sequences to achieve a better alignment. In general, consider two signatures,  $T = \{t_1, t_2, \dots, t_A\}$  and  $S = \{s_1, s_2, \dots, s_B\}$  of different lengths. The goal is to find the best match between the two signatures by some alignment  $w$ , the optimal warping path. The warping path is given by  $w = w(1), w(2), \dots, w(n)$ , where  $w_n = [i(n), j(n)]$  is the set of matched samples, where  $i$  and  $j$  corresponding to the time axes of two sequences respectively. The objective of the warping function is to minimize the overall cost function given by

$$(37) \quad D = \sum_{n=1}^N \delta(w(n))$$

where  $\delta(w(n))$  is the squared distance between the sample points given by

$$(38) \quad \delta(w(n)) = (i(n) - j(n))^2$$

The warping path must satisfy the following constraints:

- **Monotonicity:** The warping path must progress in the forward direction, i.e  $i(n) \geq i(n-1)$  and  $j(n) \geq j(n-1)$ , where  $w(n-1) = [i(n-1), j(n-1)]$  and  $w(n) = [i(n), j(n)]$ .
- **Boundary:** The function must always start at  $w(1) = (1, 1)$  and end at  $w(n) = (A, B)$

- The function must not skip any points, i.e  $i(n) - i(n-1) \leq 1$  and  $j(n) - j(n-1) \leq 1$

To generate a warping path, a cost matrix is constructed. This matrix represents the minimum cost required to reach a particular point  $(i, j)$  from  $(1, 1)$ . This minimization problem is usually solved using the dynamic programming approach, whereby a cumulative or accumulated distance  $\gamma(i, j)$  is computed as the sum of  $\delta(w(n))$ , the distance obtained from the current set of points and the minimum of the cumulative distances of the adjacent elements or neighbors. This is given by

$$(39) \quad \gamma(p, q) = \delta(w(n)) + \min[\gamma(p-1, q), \gamma(p-1, q-1), \gamma(p, q-1)]$$

## 7.2. Applicability to the Problem

The problem being tackled here is how to identify a location using magnetic fields?. The magnetic signatures collected can be categorized as time series data. We observed that when people walk along the same hallway, the signatures followed a similar pattern but with variations in the time axis due to different walking speeds or changes in magnitude that are related to distance from the source (walls or pillars) as shown in Fig. 7.1.

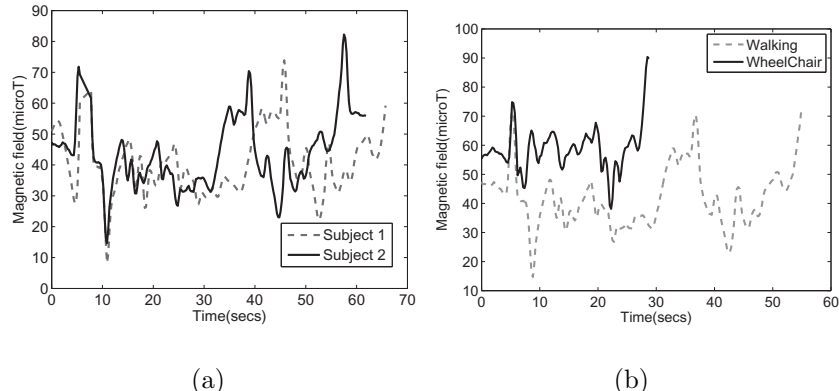


FIGURE 7.1. Signature variation along the time and magnitude axis: (a) Speed variations causing a shift in the signature collected from Subject 2. (b) Shorter signature with magnitude variations caused by faster speed of commuting in a wheelchair.

In Fig. 7.1(a), one signature leads the other and in Fig. 7.1(b), one signature is a stretched version of the other. So to match such signatures, an algorithm that can perform some form of alignment is in need. Dynamic time warping was chosen due to its alignment capability of such signals.

The idea behind applying the time warping technique is to match signatures obtained by people with different walking speeds to the correct signature in the database thereby facilitating accurate localization. This is extremely important for the application to be practically usable.

### 7.2.1. Advantages over HMM

A Markov model describes a system as a set of discrete states and transition probabilities of moving from any one state to any other state of the model. A hidden Markov model (HMM) is a statistical model in which the system being modeled is assumed to be a Markov process with unknown parameters.

HMM's basic principal is to perceive the characteristics by a random process [2]. Dynamic time warping (DTW) is an uncomplicated and effective algorithm, which is based on the ideology of the dynamic warping.

- HMM needs more data for training and repeated calculations, while DTW does not perform excessive calculations in the training phase.
- Each HMM model represents a signal by its states. Incorrect number of states will result in misclassification of the signals.
- DTW consumes less time in both the training and classification phases whereas HMM takes up more time due to a number of states to be computed. As the signals grow longer, the number of states will increase thereby increasing the computation time.
- Most importantly, DTW aligns similar looking signals that are shifted whereas HMM does not.

### 7.3. Summary

In this chapter, I explained the working of the dynamic time warping algorithm and its applicability to the problem being addressed here. Applying the advantages of this simple algorithm, in the next two chapters I show how to perform localization using the magnetic signatures obtained from different users walking along the same hallway.

## CHAPTER 8

### COARSE INDOOR LOCALIZATION

In this chapter, I present the classification of magnetic signatures collected from different hallways by employing the dynamic time warping technique explained in Chapter 7. The motive behind this approach is to account for the time variations in the magnetic signatures due to differences in the commuting speeds of sighted people, visually impaired people, and also persons with disabilities using wheelchairs. By tackling these factors, and combining the advantages of a smartphone, I present a novel classification system for indoor localization that was evaluated across 26 and 15 hallways of two different buildings resulting in accuracies of 92.6%, and 91.1% respectively.

#### 8.1. Data Collection and Classification Framework

##### 8.1.1. Data collection

The magnetic field data was collected along 26 hallways in the College of Engineering (COE) building and 15 hallways in the Chemistry building (CE). The hallway lengths varied between 20m-78m. The experiments were performed only on one side of a hallway by walking past the walls so that the ferromagnetic fields from pillars that are clearly visible or constructed inside walls) can also be measured in conjunction with the Earth's magnetic field. This method of collecting data is similar to *walltrailing* with the hand or cane followed by the visually impaired to maintain a straight line of travel [67]. The purpose of this data collection methodology is two fold: 1) sensing/collecting magnetic disturbances caused by

---

The content in this chapter is reproduced from Kalyan Pathapati Subbu, Brandon Gozick and Ram Dantu, "Indoor Localization through Dynamic Time Warping," to appear, IEEE Systems, Man and Cybernetics 2011, with permission from IEEE.

pillars that may be significant in the signatures and 2) the proposed system could be used by the visually impaired following their mobility skills.

First, two subjects collected data to be fingerprinted and stored in the database. Then, four different subjects  $s_1, s_2, s_3$ , and  $s_4$  participated in the evaluation of the proposed technique by walking along the same set of hallways at different times of a day and repeated the experiment based on their availability and willingness. Fig. 8.1 depicts some hallways where the data collection and experiments were performed. Before implementing the proposed



FIGURE 8.1. Hallways in two buildings: Chemistry (a) and (b), College of Engineering (c) and (d), with clearly visible steel pillars.

system, we performed uncertainty analysis over a 2000 measurement set collected altogether over a period of 9 months using a number of phones with different built-in magnetic field sensors. This process confirmed the reliability of the collected data and repeatability of the methodology. A detailed analysis can be found in [68].

### 8.1.2. Fingerprinting

Classifying an unknown signature to a set of stored signatures and thereby inferring the location, involves developing fingerprints of different hallways. A 1D magnetic map was created by computing the average of the magnetic field data along a particular hallway obtained from the two subjects. Another form of magnetic map which is the spatial distribution of magnetic signatures along the hallways can be obtained by collecting data at equally spaced points on both sides of the hallway and also the center to obtain a grid like formation of data collection. This data was further interpolated to obtain the 2D magnetic map shown in Fig. 8.2. Since this form of map creation consumes a lot of time, we stick to the 1D map as the reference signature.

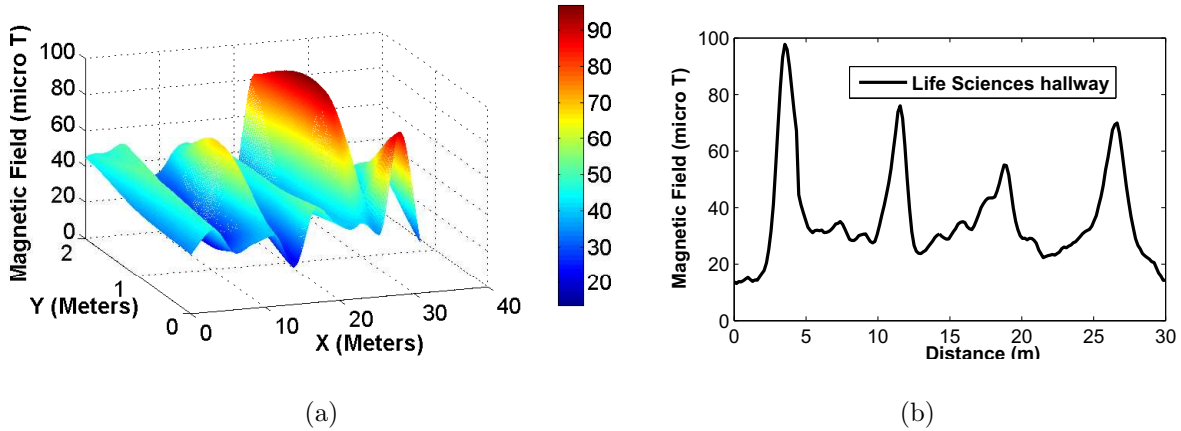


FIGURE 8.2. Magnetic maps: (a) The high intensities indicate high magnetic fields on one side of the hallway. (b) The peaks in the 1D signature support the high intensities in (a).

## 8.2. Performance Evaluation

In this section, I present the performance of the DTW classifier on the measurement data and the classification accuracies obtained for different hallways.

### 8.2.1. Alignment Evaluation

Fig. 8.3 shows the performance of DTW on the stored and test signatures obtained from the same hallway (CSE)

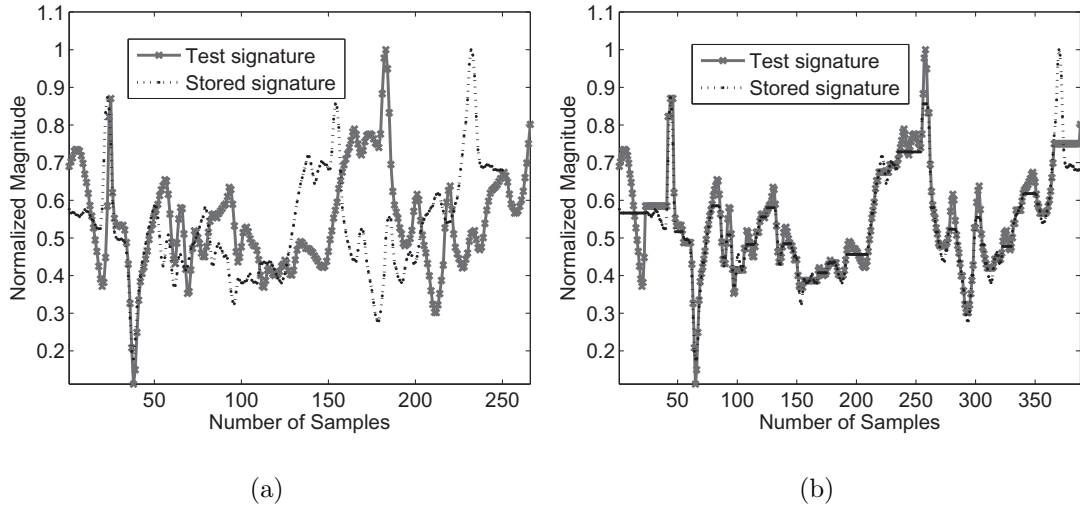


FIGURE 8.3. Correct classification: (a) Two subjects walking with different speeds in the same hallway obtaining similar signatures but with magnitude and time shifts. (b) DTW warps one signature with the other obtaining a close match.

Fig. 8.4 shows the alignment between two dissimilar signatures (test signature from EE hallway and stored signature of CSE hallway).

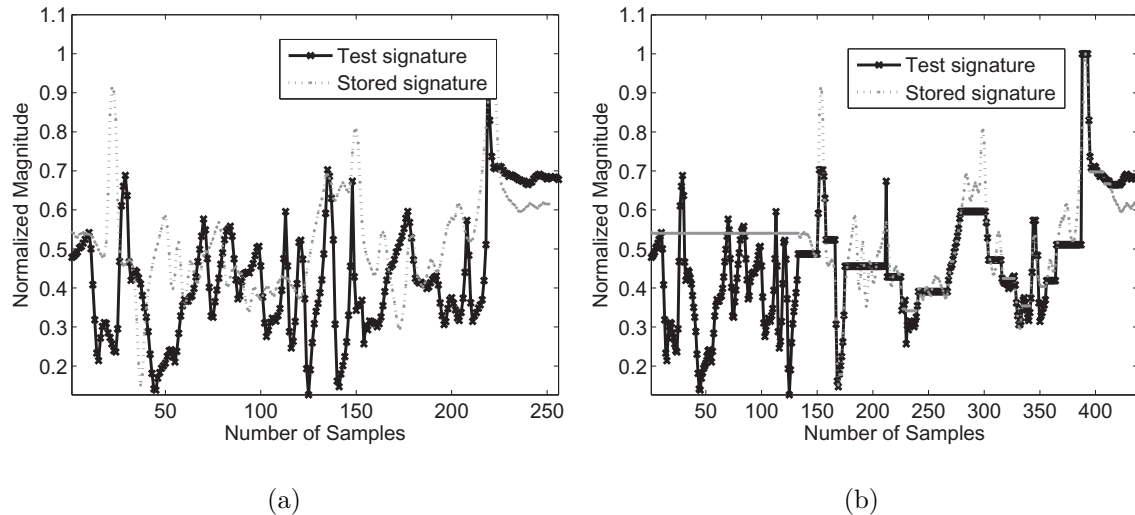


FIGURE 8.4. Misclassification: (a) Dissimilar signatures before alignment. (b) Alignment of one signature with the other by DTW, resulting in a mismatch between the two signatures.

We conclude that Fig. 8.4 results in a larger distance value as compared to Fig. 8.3, signifying two dissimilar signatures.

Fig. 8.5 shows the performance of DTW with a test signature obtained from a blindfolded individual. The individual walked at a slower speed (following the walltrailing principle) as compared to a sighted individual.

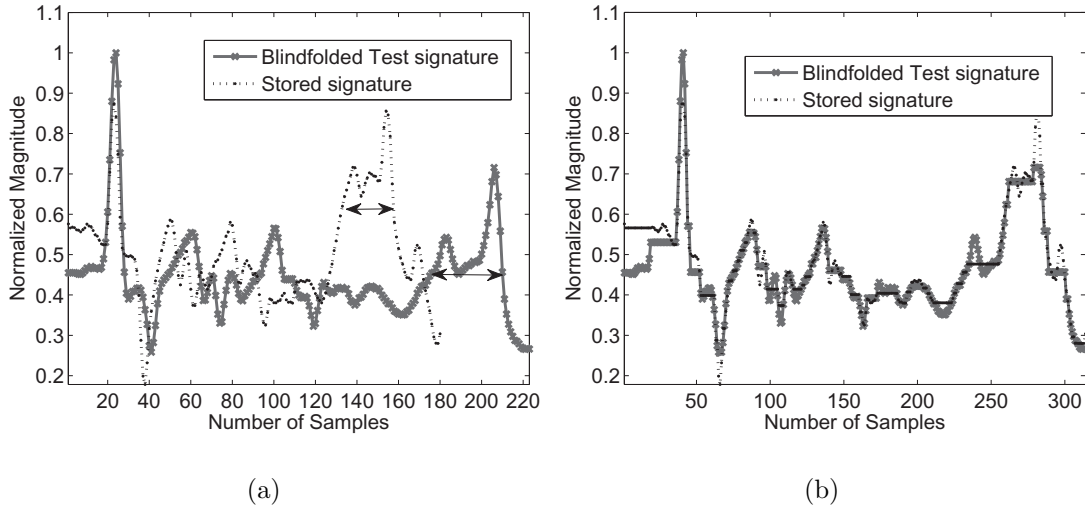


FIGURE 8.5. Classification of walking patterns: (a) Signatures showing a large time difference. (b) DTW warps the signature and obtains a close match.

We can see that with the signature obtained from a blindfolded being essentially a delayed version of the stored signature, DTW stretches the signature to align and obtains a close match.

### 8.2.2. Distance metric

We illustrate the distances computed by DTW between a test signature and the stored signatures of Computer Science and Engineering (CSE), Electrical Engineering (EE), General Access Lab (GAL), Electrical Technology (ET) and Material Sciences (MS) hallways. The experiment involved four subjects to walk along the CSE hallway recording data to obtain a signature. Each subject's signature subsequently matched to the stored CSE signature producing a correct result on all four accounts.

Fig. 8.6 infers the correct classification of the hallway by the time warping technique.

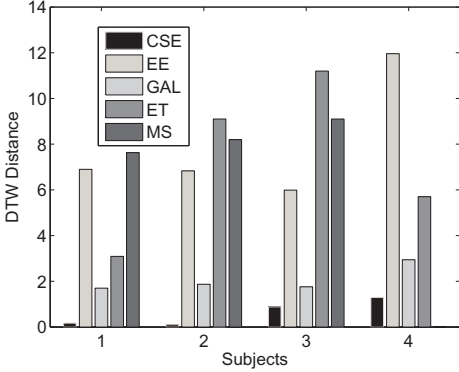


FIGURE 8.6. Distances between CSE and other hallways in the COE building:  
As can be seen, for all subjects, the lowest distance was obtained between the stored and the test CSE hallways, i.e. the hallway in which a subject walked.

### 8.2.3. Classification Accuracy

8.2.3.1. Accuracy per Hallway. The accuracy of every hallway for every subject was calculated as follows:

$$(40) \quad A_H = \frac{\sum_{s \in S} (C(s))}{\sum_{s \in S} (E(s))}$$

where  $A_H$  is the accuracy for individual hallway,  $C(S_i)$  is the number of times a correct match was obtained along the hallway for subject  $s_i$  and  $E(s_i)$  is the total number of times  $s(i)$  performed the experiment in a hallway. Table 8.1 lists the classification accuracies computed.

TABLE 8.1. Overall hallway accuracy(%).

Subj/Hall	CSE	EE	GAL	ET	MS
S1	9/10	8/10	9/10	9/10	10/10
S2	5/5	5/5	5/5	5/5	5/5
S3	9/10	8/10	9/10	9/10	9/10
S4	5/5	4/5	4/5	4/5	5/5
Accuracy	93.3	83.3	86.6	90.0	96.6

As we can see, a total of 30 experiments were performed in each hallway. Expanding this to 26 and 15 hallways of two buildings, accounted for 780 ( $30*26$ ) and 450 ( $30*15$ ) experiments in the COE and Chemistry buildings respectively. Translating the accuracy computation for an entire building, we present the accuracies in Table 8.2.

TABLE 8.2. Accuracy for entire building (%).

$T_E$	$H_C$	Accuracy(%)
780	722	92.6
450	410	91.1

where  $T_E$  denotes total number of experiments performed in each building and  $H_C$  denotes number of experiments that yielded a correct match.

#### 8.2.4. Implementation on the phone

The entire classification system was implemented on the smartphone. Fig. 8.7 depicts the system on the Nexus One.

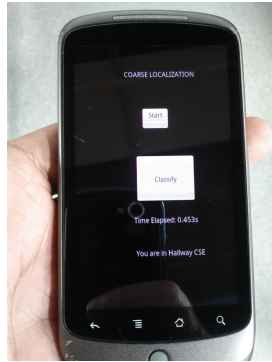


FIGURE 8.7. Resulting localization program on the phone presenting the matched hallway and the computational response time of the phone.

The subjects started the application and performed the experiments. The application first performs sensing. The stored signatures are downloaded onto the phone. The time taken to download a database of size 300kb (consisting of 26 signatures) on a WiFi network with a speed of 6Mbps was 2 secs and on a 3G network with a speed of 2Mbps was 5 secs. This is a very meager burden on the smartphone's memory and also the wait time of the

user. Next, the classification process was performed and the location of the subject was inferred.

### 8.3. Summary

In this chapter, I presented a localization application that works irrespective of variations in human walking or commuting speeds. By employing the smartphone as a magnetometer, I proposed a novel and convenient classification system capable of distinguishing hallways based on their magnetic signatures. A smartphone based system requires a minimal learning curve since mobile phones are virtually used by people of all ages and physical abilities. I also showed that the system is applicable to a variety of users while maintaining independence from the user's means of travel. By obtaining encouraging accuracies with low sampling rates, I confirmed that dynamic time warping technique can be implemented on a resource limited smartphone.

The next chapter involves performing fine localization whereby the user will be required to walk only a short distance instead of the entire hallway.

## CHAPTER 9

### FINE LOCALIZATION

The previous chapter proposed a classification framework for a coarse localization application. The work enabled to identify a person's location in terms of the hallway he/she was present. However, it lacked the capability of providing accurate location information like the distance estimates in meters in that particular hallway.

In this chapter, I propose a modified classification framework for estimating the location of a person in terms of the distance. The solution involves employing a windowed dynamic time warping on the magnetic signatures. This approach resulted in localization distances of approximately 2m-6m with accuracies between 81-99% implying that it is sufficient to walk short distances across hallways to be located by the smartphone. I also implemented the application on different smartphones which yielded response times of less than 5 secs thereby validating the feasibility of this approach and making it a viable solution.

#### 9.1. Introduction

Envision a scenario where a user walks a few meters in an unknown hallway, then uses his smartphone to identify the position in that hallway using magnetic signatures. To brief up the idea, we first fingerprint each hallway using its magnetic signature. Then, by classifying the test signature of an unknown hallway to one of the fingerprints, we obtain the person's position in meters, thereby providing fine grained localization. However, differences in human walking speeds cause variations in the time and magnitude of signatures, even if they retain the same pattern. Therefore, we incorporate the dynamic time warping (DTW) classifier

---

The content in this chapter is reproduced from Kalyan Pathapati Subbu, Brandon Gozick and Ram Dantu, "LocateMe: Magnetic Fields Based Indoor Localization Using Smartphones," ACM Transactions on Intelligent Systems and Technology (under review), with permission from ACM.

which is known to account for these differences and perform alignment by stretching or compressing the signals.

The proposed localization application has the following properties:

- (1) Encapsulated in a single sensing unit; requires no external device or infrastructure.
- (2) Position and orientation invariant.
- (3) Ability to work over a variety of users.

## 9.2. Challenges

In this section we briefly explain the challenges faced and our approaches in addressing them. A detailed analysis of all these factors is provided in [68].

- Long term variation: It is the change in the magnetic fields over a certain period of time. To observe this phenomenon, we computed the variance of the magnetic signature collected over a period of one year for a particular hallway. Fig. 9.1 depicts this observation.

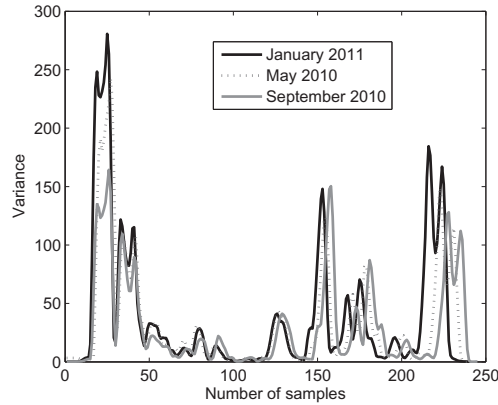


FIGURE 9.1. Variance of magnetic signatures: As can be seen, there is no major variation in the signatures that could render it ineffective for our solution.

- Sensor Accuracy: We performed measurement uncertainty treatment of multiple data sets collected at each hallway. Measurement uncertainty [49] is a statistical test to find the range of values for the variation of a measured quantity. Summarizing the results, for one hallway, the maximum and minimum values of the magnitude

ranged between  $110 \mu\text{T}$  and  $22 \mu\text{T}$ . The results reflect that the variation was not large enough to affect the signature.

- Effect of distance on signature: Magnetic field magnitudes are known to be inversely proportional to the square of the distance. In other words, the farther the distance from an object, the lower the magnitude of magnetic field. To observe this phenomenon, we walked at different distances from walls and pillars. From the measurements we found that although the magnitude decreased, the signature still held a similar pattern. Fig. 9.2 illustrates this observation.

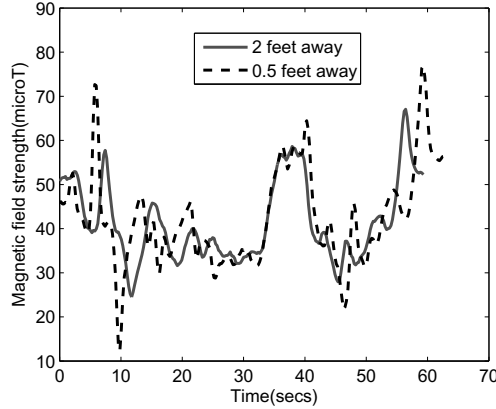


FIGURE 9.2. Distance relation: Signatures measured at 2 feet have a reduced magnitude when compared to that from 0.5 feet but the patterns are retained.

- Device placement: Since we are only considering the magnitude of the magnetic field, the placement of the phone should not cause any problems in our work. To verify this, we collected data with the phone at different locations. Fig. 9.3 illustrates the findings.
- Built-in sensor variation: We used Samsung Captivate smartphone with a built-in Yamaha MS-3C magnetic field sensor different from Nexus One which has a AK8973 sensor. Fig. 9.4 shows the signature of Computer Science hallway recorded using the two phones.
- Demagnetization: Work in [69] discussed preliminary experiments involving permanent magnets and increasing temperature to obtain the demagnetization point, the

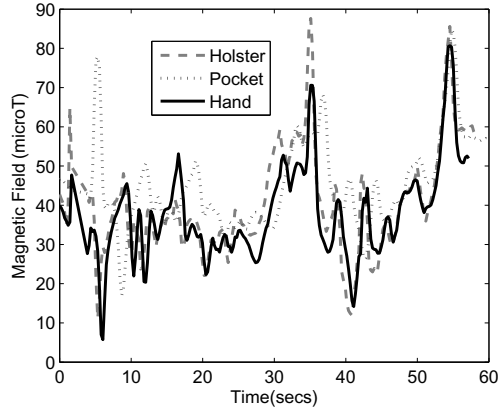


FIGURE 9.3. Device placement: Signatures obtained by placing the smartphone in a holster, pocket, and holding in the hand.

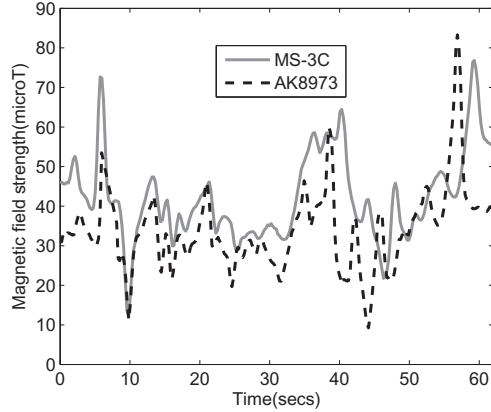


FIGURE 9.4. Signatures captured using two devices are similar showing that the measurement procedure is independent of devices.

point at which iron and other ferrous materials begin to lose their magnetization. They obtained a total of 16% loss in magnetization of the magnet at 110°C after 30 years. Similarly, after 30 years, a constant temperature of 80°C produced only less than 1% loss in magnetization. Correlating this to the pillars indoors and the environment where our system will be applicable, at room temperature or even a maximum temperature sustainable by a person, the percent loss produced by the demagnetization process would yield a time that would most likely outlast the average life of most buildings.

### 9.3. Data Collection and Classification Framework

In this section, I briefly discuss the data collection process and explain the classification set up. The procedure for collecting magnetic signatures was the same with the only difference being the locations. The idea was collect data and test the application on different hallway signatures.

#### 9.3.1. Data collection

The fingerprints were collected in different hallways of two campus buildings, University Union and College of Engineering (COE). The floor maps in Figs.9.5(a) and 9.5(b) illustrate the different hallways. A closer look at two of the hallways can obtained from the images shown below.

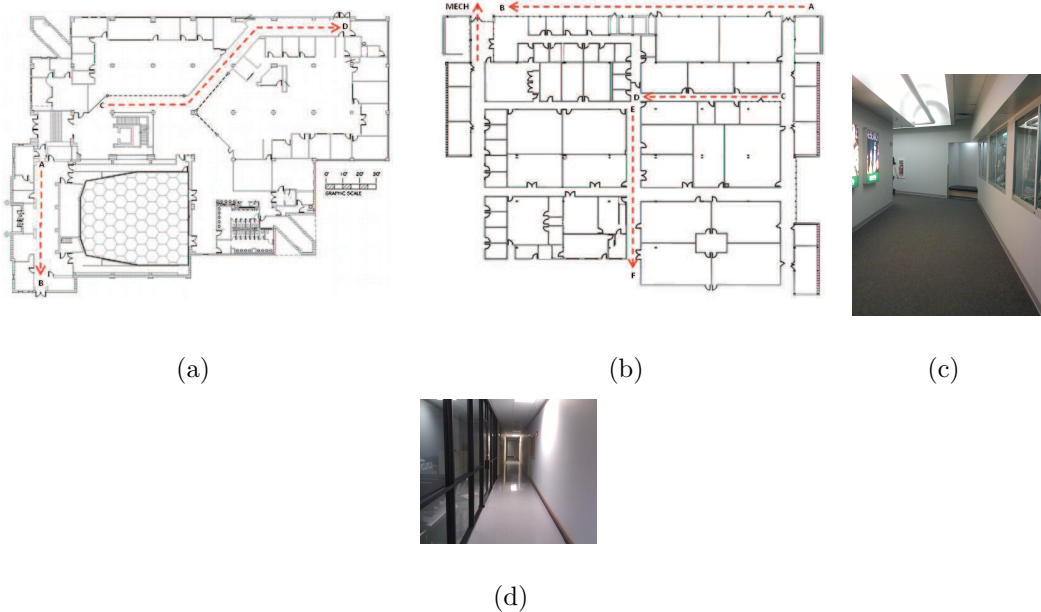


FIGURE 9.5. The paths AB, CD, EF and Mech, show the hallways where data collection and system evaluation were performed. Hallway in (c) corresponds to path CD in (a) and that in (d) corresponds to path EF in (b).

As we can see, one of the hallways is narrow and the other has a curved structure. To make our evaluation unique I chose a curved hallway and not just straight and narrow ones. Table 9.1 summarizes some experimental specifications for both buildings.

TABLE 9.1. Data collection statistics showing the number of hallways ( $N_{hwys}$ ), number of fingerprint repetitions ( $F_r$ ), average hallway length ( $HL_{avg}$ ) and total training file size ( $Tr_{fs}$ ) for each of the buildings.

	Union	COE
$N_{hwys}$	6	4
$F_r$	10	15
$HL_{avg}$	38m	51m
$Tr_{fs}$	12Kb	8Kb

Both the subjects walked with an average speed of 1.5m/s along the wall rather than the center of the hallway as in [38]. This was done for three main reasons 1) to obtain a dominant signature that could arise due to walls and ferromagnetic pillars 2) mimic usual walking patterns of people 3) make the application useful for visually impaired people who follow a wall trailing [67] procedure where they walk past walls holding or sensing the touch of pillars, doors, walls etc.

We computed an average fingerprint for each hallway from both the subjects and considered the fingerprint from subject1 as a test and subject2 as stored signature for evaluation.

### 9.3.2. Windowed Dynamic Time Warping

The classical dynamic time warping was explained in Chapter 7. Here, instead of classifying the test signature of an entire hallway, I performed DTW between a short test signature and running a sliding window on the stored signatures. Fig. 9.6 depicts this process.

The program picked 100 random positions from each test signature and performed classification for each of those positions. This was mimicking the procedure of obtaining a signature when a person walks for a short distance. The randomly picked segments were of length equal to  $W_l$  which ranged between 5 and 35. In simple terms,  $W_l$  is nothing but the resolution or shortest distance required to walk in a particular hallway to get localized. We basically tested different resolutions to see which one was the best for each hallway. The

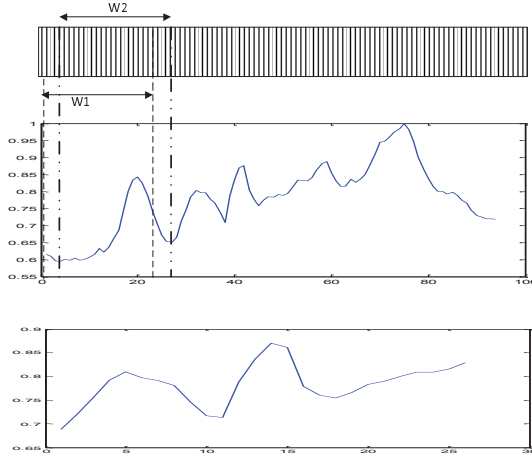


FIGURE 9.6. A test signature (below) and map (above) denoted by  $T_e = \{te_1, te_2, \dots, te_n\}$ , and  $M = \{m_1, m_2, \dots, m_m\}$ , respectively. Using a sliding window on  $M$ ,  $T_e$  is compared with segments of the map,  $\{M_a \dots M_m\}$ ,  $\{M_{a+1} \dots M_{m+1}\}$  corresponding to  $W_1$  and  $W_2$ , of width equal to  $W_l$ , the window length in samples.

DTW was performed between each short test segment and sliding windowed segments of the maps.

The classification accuracy was calculated as

$$(41) \quad A = \# \text{Correct matches} / 100$$

Then using the sampling rate  $s_r$  and  $W_l$ , the time taken to walk a certain distance  $t$  was calculated as  $W_l / s_r$ . The distance for the stored maps was calculated using  $\delta = v * t$ , where  $v$  is the velocity. The localized or estimated distance was obtained from the section of the stored maps where DTW correctly matched the test signature. The estimation error for every  $W_l$  was calculated as  $E = \delta_M - \delta_E$ , where  $\delta_M$  is the distance measured manually using a surveyor's wheel. Finally, the average estimation error  $\sigma_e$  over all positions for a particular  $W_l$  was calculated. Fig. 9.7 depicts the entire classification system.

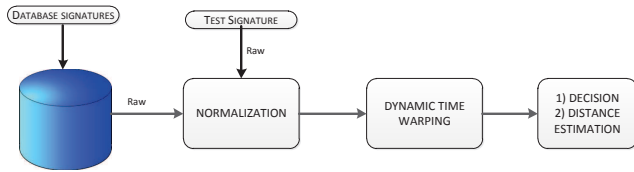


FIGURE 9.7. A short test signature and the maps in the database are normalized and fed to the DTW module which finds the best possible match between them. The localization distance and estimation error are computed from the matched signature.

#### 9.4. LocateMe Implementation

LocateMe is the localization application that runs on an Android smartphone to determine a user's location in a particular building. The application was written in Java using Android APIs and initially tested on the HTC Nexus One but was then easily installed on other smartphones which contained a built-in magnetometer. LocateMe has three components: sensor sampling rate identifier, test signature collector, and hallway classifier.

The sampling rate identifier calculates the frequency of the magnetic field sensor in the Android phone being used. During our preliminary data collection, we noticed that different smartphones had different sampling rates. For this application to function properly, it is required to find the sampling rates in the phones. This process is performed automatically once the application is opened and requires no user interaction to complete (no user requirements). The splash screen shown in Fig. 9.8(a) performs this analysis. Finding this rate allows consistency in functionality and an accurate hallway match. Fig. 9.8(b) shows the home screen for the LocateMe application. This screen contains the building selection drop down list. The user, assuming he/she knows which building they are in (can also be obtained using GPS just before entering), picks the building from the list. This list is shown in Fig. 9.8(c). Magnetic maps for the corresponding building are then downloaded onto the phone. The localization results will reflect the comparison of these stored maps with the test signature collected by the user. The test signature collector obtains the sensor data



FIGURE 9.8. User Interface: (a) splash screen (sensor frequency analysis), (b) home screen, (c) building selection, and (d) capture live data.

when the user pushes the Start/Stop toggle button shown in Fig. 9.8(b) and walks a certain distance. An example of test signature collection is shown in Fig. 9.8(d).

After collecting the test signature, the user pushes the Classify button located at the bottom right corner shown in Fig. 9.8(b). This is when the hallway classifier is activated which in turn activates the classification system block explained in Section 9.3.2.

## 9.5. Results

In this section, we present both the Matlab and smartphone based evaluation results. We first discuss the performance of the sliding windowed DTW algorithm, then the classification accuracies, estimation errors and localization distances obtained for each of the evaluations. Next, we compare these results with a particle filter based approach proposed in [38]. We also discuss the response or result computation times, memory and power consumption of the algorithm when run on different smartphones.

### 9.5.1. Alignment evaluation

Fig. 9.9 illustrates the sliding windowed DTW on the measurement data. Short segments of a test signature were randomly picked as explained in Section 9.3 and DTW aligned these segments with an appropriate windowed segment of the map, thereby matching the test signatures correctly to the respective map or hallway.

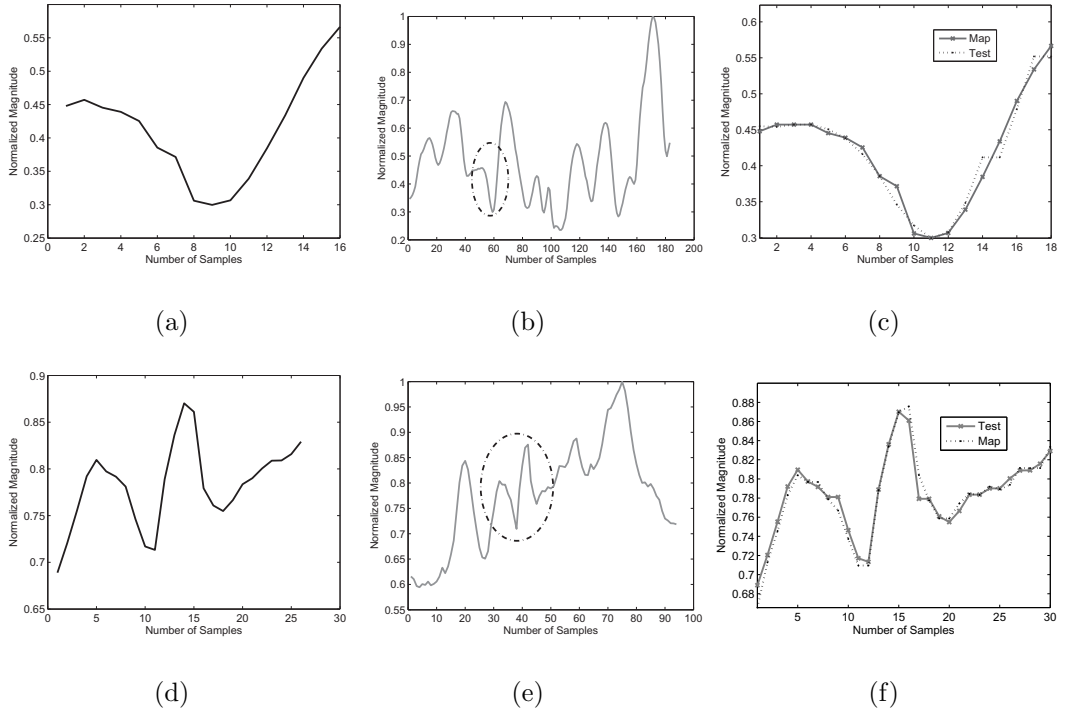


FIGURE 9.9. Alignment by DTW: Short test signatures (a) and (d) are compared with windowed segments from maps (b) and (e) to obtain correct matches as (c) and (f) respectively. (The correctly matched segments are marked by an ellipse in the maps. Finally, the distance walked is estimated by using the sample number at which the match was obtained).

### 9.5.2. Estimation error and Localization distance

The estimation error was computed for each random position and averaged. Fig. 9.10 depicts the average estimation errors over all the positions chosen for every window size (resolution) in the University Union building.

We can see that for five out of the six hallways, the error is between 0 and 3.5m approximately. There are some outliers at 25.2m for a  $W_l$  of five samples in the ESSCLvL2 and 17m for 15 samples in the Bookstore hallways. The reason for this is very low resolution in those particular hallways for which DTW was unable to obtain a correct match. Moreover, there could have been segments of signatures that had a similar pattern as that of the test

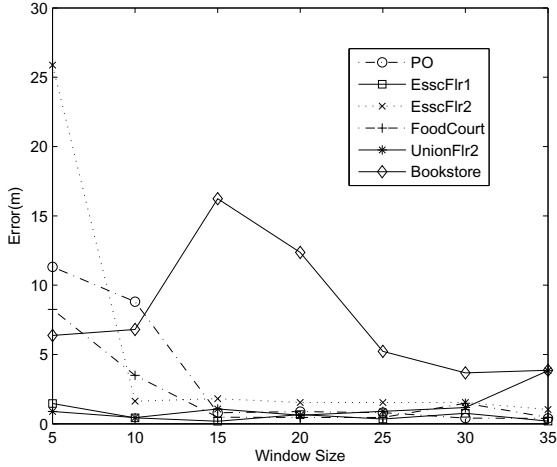


FIGURE 9.10. Estimation errors for University Union as a function of window length or resolution.

TABLE 9.2. Accuracy (A), Avg estimation error ( $\sigma_e$  (m)) and Avg localization distances ( $\delta_l$  (m)) for College of Engineering.

	Hallway			Matlab			Smartphone		
	A	$\sigma_e$	$\delta_l$	A	$\sigma_e$	$\delta_l$	A	$\sigma_e$	$\delta_l$
Corr2	90	3.05	2.32	96	3.2	3.4			
Corr4	99	3.50	3.43	93	3.6	4.0			
Mech	86	3.37	4.57	83	3.7	5.3			
CSE	96	0.66	4.57	92	1.2	4.7			

which resulted in the DTW performing a wrong match. However, for the remaining window sizes, the error reduced to within 2m and 5m respectively for the two hallways.

From these error plots, we analyzed which particular window size resulted in a high accuracy and low estimation error for a particular hallway. In other words, we picked the lowest resolution that was obtained with a high accuracy and low estimation error. We list these statistics in Tables 9.2 and 9.3.

The tables indicate the resolution (distance required to walk) within certain meters with a certain accuracy obtained from offline (Matlab) and online (smartphone) evaluations. The procedure for offline evaluation was explained in Section 9.3. For the online version, the

TABLE 9.3. Accuracy (A), Avg estimation error ( $\sigma_e$  (m)) and Avg localization distances ( $\delta_l$  (m)) for University Union.

	Hallway			Matlab			Smartphone		
	A	$\sigma_e$	$\delta_l$	A	$\sigma_e$	$\delta_l$	A	$\sigma_e$	$\delta_l$
Post Office	90	0.79	2.2	88	1.5	3.0			
ESSCLvL1	100	0.33	4.57	94	1.1	5.1			
ESSCLvL2	80	1.62	1.83	81	1.9	2.1			
Foodcourt	100	0.45	3.5	93	0.7	4.2			
UnionLvL2	90	1.17	5.5	90	1.3	5.9			
Bookstore	90	3.67	6.3	87	4.0	6.5			

application was implemented and tested on Nexus One, Droid, Nexus S, and HTC Hero smartphones. We chose 10 users for 10 hallways, one user per hallway. Based on the user willingness and availability, they were instructed to walk 10 different positions in each hallway using different phones. They used the options provided in the user interface explained in Section 9.4.

The numbers in the tables should be read as for instance, in Corr2 hallway, it is required to walk 2.32m to be localized within 3m with a 90% accuracy. The smartphone based results were close to the Matlab results thereby validating the evaluation procedure. The slight differences in the results between the two evaluations were due to minor variations in the sensor data collected while experimenting which did not affect the outcome in a major way.

Now, we compare our results with those obtained (tabulated in Table 9.5) from a particle filter based approach followed in [38]. This is the only existing work related to magnetic field based localization with humans. The authors in [38] conducted their experiment in main corridors of a floor of total length 278 m. The particle filter simulation program incremented the position of the human by 1m thereby obtaining 278 positions for the entire hallway. Further, each experiment set was conducted using different values of standard deviation  $\sigma_r$

TABLE 9.4. Smartphones and their specifications.

Model	Processor Make	Processor Speed	RAM
Nexus One	Qualcomm QSD8250	1GHz	512 MB
Droid	TI OMAP3430	600MHz	256 MB
Nexus S	Cortex A8	1GHz	16GB iNAND flash memory
HTC Hero	Qualcomm MSM7200A	528MHz	288 MB

of the measurement model between  $[1 \mu\text{T}, 5 \mu\text{T}]$ . The measurement model used was a single variable Gaussian probability density function given by

$$(42) \quad p(z|x) = \frac{1}{\sigma_r \sqrt{2\pi}} \exp\left(-\frac{(z - |h(x)|^2)}{2\sigma_r^2}\right)$$

where  $x$  is the state of the system. The magnetic field data captured by a user using a wireless magnetometer was the observation  $z$  and function  $h(x)$  was used to map  $x$  to the observation. In other words, the particle filter compared the  $z$  at every instant to the map data (collected by a robot).

 TABLE 9.5. Avg estimation error( $\sigma_e$  (m)) and Avg localization distances ( $\delta_l$  (m))for different  $\sigma_r$  using particle filters.

$\sigma_r$ ( $\mu$ T)	$\sigma_e$ (m)	$\delta_l$ (m)
1.0	3.47	9.98
3.0	3.46	23.98
5.0	3.43	45.02

From Tables 9.2 and 9.3, we can see that the minimum and maximum localization distance required to walk are 1.83m and 6.3m respectively. Although 6.3m is a large distance, for most of the hallways, it was less than 5m. This is a significant improvement over values between 9m and 45m shown in Table 9.5. The cause for large localization distances obtained using particle filters can be attributed to the fact that particles take a longer time or distances to converge at a point where there is a minimal deviation between the map and the test

signatures. In contrast, the DTW algorithm handles these deviations very well by either stretching or compressing the signatures.

### 9.5.3. Response Times on different phones

Response time is the time spent by the user waiting from initially pushing the classify button to the time he/she receives a classification and position estimates. Average response times were calculated for each hallway and summed to obtain a total response time for the building. The response times in seconds, obtained from each smartphone are illustrated in Fig. 9.11.

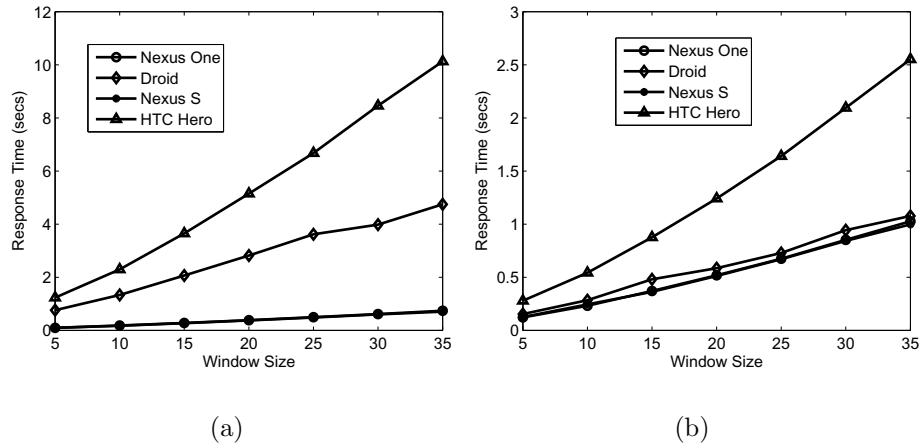


FIGURE 9.11. A linear relationship between response times and window length for COE (a) and University Union (b) buildings.

The following observations can be made from the above figure:

- (1) There was a linear increase in the response times for both buildings. This was due to the inverse proportionality between window length and number of sliding windows. A shorter window length resulted in more windows. This made the DTW perform faster with since it had less number of samples to classify as compared to a longer one, thereby resulting in faster response times.
- (2) The hallways in the University Union had shorter response times when compared to COE. This was because the average length of hallways in COE was greater than University Union as listed in Table 9.1.

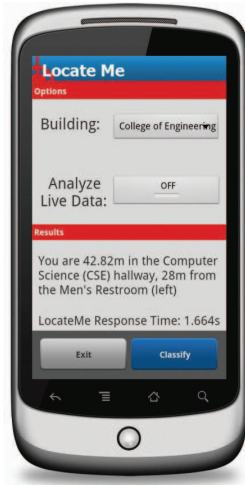


FIGURE 9.12. The screen shows the classified hallway, position of the user in that hallway and from a nearby landmark. The response time of the algorithm is also shown.

- (3) Both Nexus One and Nexus S had faster response times when compared to Droid and Hero. This can be correlated with the information from Table 9.4, which means faster the processor, faster the computation time.

A screenshot of the results showing the classification result, distance and response time is illustrated in Fig. 9.12.

In [68], the authors showed how magnetic signatures can be used as landmarks. Using this information, the position of a user near certain landmarks as shown in Fig. 9.12 can be given. There are also other means of extracting landmarks [70] and integrating them with the fine localization results presented in this work.

#### 9.5.4. Memory and Power Consumption

Android allows external storage up to 32GB which is more than sufficient for storing a set of magnetic maps for each building since the size of the database is very small as listed in Table 9.1.

The amount of resources taken by the LocateMe application is of primary interest. From the response times shown earlier, it is clear that LocateMe does not require more than 2 minutes for all the three components explained in Section 9.4 to run. So we compared the

memory usage of RAM in mega bytes and power consumed in mill Watts by our application to other activities that normally run on a smartphone for a duration of 2 minutes.

TABLE 9.6. Performance - memory and power consumption on Nexus One.

Application	Memory (MB)	Power (mW)
Active Call	1.14	327
Game	4.70	556
<b>LocateMe</b>	<b>6.63</b>	<b>480</b>
Music	13.66	250
Navigation	24.13	600
System	31.78	74

The table shows that LocateMe does not consume much resources and can be run without affecting the functioning of other applications or burdening the CPU.

## 9.6. Discussion

From the results obtained, we showed the applicability of DTW to match signatures collected by different people and provide localization independent of the *user and the hallway*. The proposed application was also validated with subjects completely new to the buildings. This makes it practically feasible and usable by anyone owning a smartphone (regardless of the position and orientation).

Creating and building a database of fingerprints is not a cumbersome task. As mentioned in [71], the time spent in fingerprinting hallways can be very much less than that for following maintenance procedures like elevator servicing, emergency exit lighting etc. Crowdsourcing is the concept that describes a distributed problem solving and product model, in which small tasks are broadcasted to a crowd in the form of open calls for solutions [72]. Everyday users engage in activities that help in solving or providing information for a larger context [73]. As part of future work, we plan on integrating this concept to our data collection process around different hallways. In other words, the occupants of the building can collect magnetic signatures of different hallways since they usually move around the same set of locations

daily, following routine paths and most of them carry smartphones. The data collected can be uploaded onto a server. This form of data collection and sharing can be also categorized as participatory sensing [74] where users can passively participate in the sensing process since all that is required is to walk and collect data. A crucial question that can be asked here is the effect of metal objects that can be moved, added or changed, on the magnetic field as time progresses. The authors suggest referring to [68] where some analysis regarding this scenario is provided. But following the crowdsourcing concept, a database can be easily built and continuously updated providing accurate maps of the building.

## 9.7. Related Work

Many indoor localization systems or solutions exist. They can be grouped based on the types of systems used to provide location estimates: 1) wearable sensors, 2) infrastructure, 3) ambient sensing, 4) probabilistic, and 5) smartphones. For each category, we highlight the well-known solutions and also list some of the areas where DTW has been applied.

### 9.7.1. Wearable sensors

Golding et al. [75] use wearable accelerometer, magnetometer, light and audio sensors to provide indoor localization and navigation. Collin [76] propose an indoor positioning system using accelerometers and compasses. Lee [77] develop a dead reckoning based activity and location recognition system. Elena [78] propose a location estimation system by combining data from wearable sensors and a map. Although pioneering, these solutions require all kinds of electronic circuitry in order to be usable.

### 9.7.2. Infrastructure

Cricket [25] functions through a combination of RF and ultrasound beaconing systems. Active Badge[23] provides location information using infra red based transmission and reception. Bat system [79] used ultrasonic location estimation to provide more accurate position data. Another system for location tracking, PlaceLab [80] uses signal strength of GSM (Global System for Mobile Communications), Bluetooth, and WiFi. Randall [81] use solar cells combined with an RFID based localization system to determine the user's location.

Although these works achieved very fine localization accuracies, they carry with them high installation costs and are not practically feasible for daily use.

### 9.7.3. Ambient sensing

Ravi et al. [82] perform room level localization using light sensors assuming uniform lighting conditions. This assumption may not be valid every time and users' movement is constrained to very slow speeds in order to obtain match. Also the position of the sensor is fixed. Bucur et al. [83] propose indoor localization system by sensing indoor radioactivity. This work requires specialized sensors not available in smartphones, for both fingerprinting and using as an application. Location fingerprinting based systems surveyed in [84] use pattern recognition techniques like k-nearest neighbor, neural networks, probabilistic methods and support vector machines. SkyLoc [71] performs floor level localization of different buildings using GSM fingerprinting. RADAR [24] uses WiFi fingerprints but requires calibration of signal strengths at many physical locations in the building. Kemppi et al. [85] generate synthetic anomalies for pedestrian localization. However, a practical implementation of this work is questionable. Suksakulchai et al. [44] utilize the compass deviations caused by magnetic anomalies as distinct sources of location recognition. Despite the presence of a number of compensating mechanisms for compass deviations, electronic compasses cannot be used as the only source for indoor applications due to inconsistent dependencies on anomaly present locations. William et al. [86] propose a kalman filter based approach for localization of robots and vehicles in a hallway.

### 9.7.4. Probabilistic

Probabilistic techniques based particle filters [28] have been employed for location estimation using foot mounted inertial sensors [14, 12], fusing information from multiple sensors [11] and using infrared laser range finders, ultrasound sensors [15, 21]. But these are not classification based systems where the location information is available in a database. Instead they have to be integrated with floor plan information or have to be used with map matching techniques [87] to obtain the position estimates.

### 9.7.5. Smartphones

With the proliferation of mobile phones embedded with sensors, various solutions for indoor localization have been on the rise such as those based on activity recognition using accelerometers [88]. However, this work relies on initial GPS and Google Maps for path trails. Accelerometers have also been used for human localization in that a human's daily walking trial is used to locate him. This involves monitoring, collecting and storing every user's movement. Avinash et al. [89] perform coarse localization using a mobile phone's built-in accelerometer by recognizing the walking type. Their idea of using the time taken to walk a particular staircase as a means for localization may not be valid for people walking with different speeds or implementation in all possible buildings. WiFi based fingerprinting and localization using mobile phones has also been attempted [90]. However, fluctuations in signal strengths, temporary disconnections, maintaining accurate distances from access points during training and testing phases are some of the issues. Ravi et al. [91] propose a solution by capturing images with a mobile phone camera. The camera has to be worn as a pendant thereby imposing a placement constraint. Also, building a database of images for all possible locations is cumbersome and may even raise privacy concerns.

### 9.7.6. Dynamic Time Warping

DTW has been employed as a classifier in some of the existing work. We highlight a few here. Authors in [63] perform activity recognition by considering variability in speeds and perform classification of motor activities using DTW and derivative DTW. Avinash et al. [89] perform DTW based classification of user activities, however, they do not build upon the classification to provide fine grained location estimates. Grzonka et al. [92] classify motion templates using DTW to perform simultaneous localization and mapping (SLAM). SLAM techniques may not be useful for a common man since a simple localization application should have prior knowledge about the locations in order to accurately locate him indoors. Work in [93], estimates vehicular speeds through classification of RSS signal strengths of similar looking but time or magnitude varying GSM signals obtained while traveling in a car at

different speeds. DTW has also been utilized in power disturbance classification [94], chromosome classification [95], recognition of ECG changes [96]. Tuzcu [96] use DTW algorithm to account for time fluctuations and classify footsteps using the footstep sound.

Overall, the existing work requires sensors to be interfaced with laptops or base stations that have to be placed strategically or systems that pose constraints on the placement and orientation. There is also infrastructure, installation and maintenance cost associated with certain solutions. But most importantly, these works do not consider variations in human walking speeds, or other means of traveling indoors such as wheelchairs. This is important because these speed changes could alter the magnitudes or shift the time axis of the magnetic signatures rendering them unfit although they may retain the same pattern. These factors have to be addressed to develop a user centered localization system.

In contrast to all these existing systems, this work utilizes just a smartphone. It does not pose any placement or orientation constraints, is practically implementable on smartphones with different hardware and most importantly can perform localization independent of the subject and his/her walking speed.

## 9.8. Summary

In this chapter, extending the idea of exploiting the magnetic fields present indoors as a solution to the localization problem, I showed how windowed dynamic time warping could help in classifying a user's location by requiring him to walk only a short distance instead of the entire hallway as in Chapter 8. Hence the low resolution and estimation errors proved the feasibility of the proposed approach. The faster response times, low memory and power consumption indicate the successful implementation of dynamic time warping algorithm on resource limited smartphones.

This concludes the magnetic field based indoor localization. In the next chapter, I further extend the approach of identifying hallways to identify rooms and different objects inside a particular room.

## CHAPTER 10

### ROOM IDENTIFICATION

The indoor localization problem can be considered as an hierarchy which involves finding a particular hallway, room and even an object in that particular room. In this chapter, I use the same methodology of classifying hallways explained in Chapters 8 and 9 to classify different kinds of rooms. I show the similar uniqueness property of magnetic signatures of various rooms and then discuss the implementation of dynamic time warping on these signatures.

#### 10.1. Related Work

Ravi et al. [82] performed room level localization using light sensors assuming uniform lighting conditions. This assumption may not be valid every time and users' movement and position of the sensor are Walrus [97] provided room-level positioning by using wireless networking and microphones. The presence of a PC in each room and WiFi coverage are not realistic assumptions. Similarly, audio location [98] determined user location by using microphones that listen to sounds made by the users. Microphones may not work properly in a noisy environment. In contrast, the work in this chapter requires a single mobile phone without any additional infrastructure.

#### 10.2. Methodology

From the results and analysis presented in the previous chapters, it is understood that every hallway had different levels of magnetic fields that differentiated one from the other. In a similar way, I proceeded onto performing classification of classrooms, laboratories, conference rooms etc. Intuitively we can say that the magnetic field intensity would be different in different rooms due to the presence of servers, printers, computers, etc in these rooms which mainly create electromagnetic fields. The problem of identifying which room the user is in,

based on the different levels of magnetic field intensities can be formulated as a classification problem for which fingerprints of rooms have to be created.

#### 10.2.1. Data Collection

By holding the smart phone at waist high, I measured magnetic fields in three research laboratories in the Computer Science and Engineering department, one laboratory from the Electrical Engineering department and several classrooms with and without computers installed at the desks. Fig. 10.1 shows the images of some of the rooms.

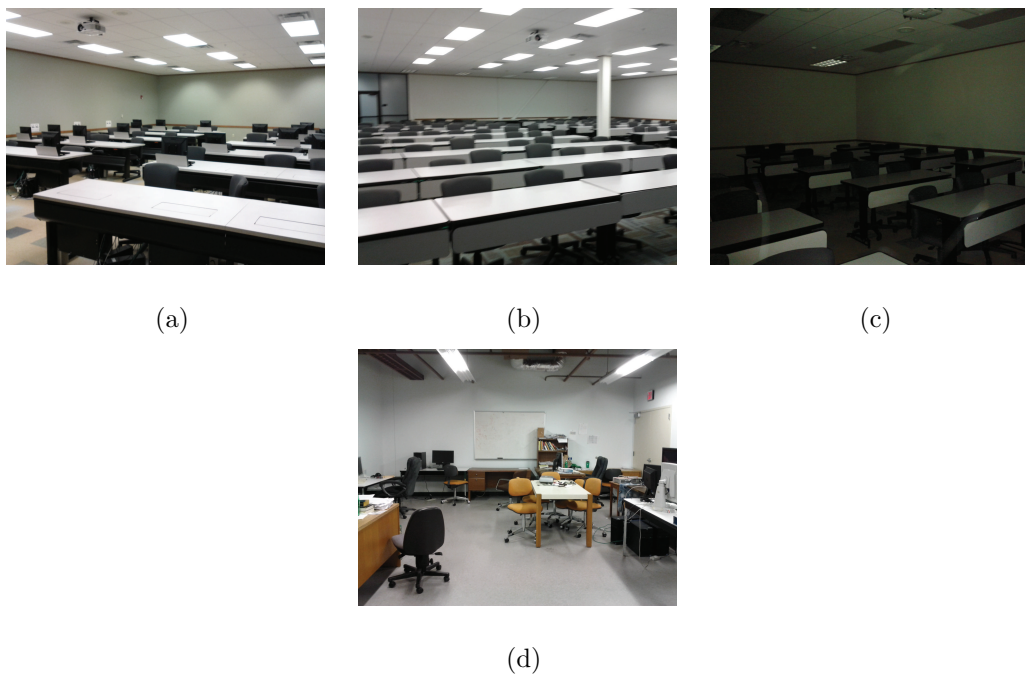


FIGURE 10.1. Different classrooms: (a) classroom with computers, (b) classroom without computers, (c) room without PCs, (d) a research laboratory.

The measurements were taken on different days at different times of the day. The data collection involved walking along the perimeter of the rooms or along a walkable path. The experiments were repeated to check for reliable data. Table 10.1 lists the different rooms and the number of measurements taken.

TABLE 10.1. Measurement statistics.

Test/Training	# Measurements	Type
F237	20	lab
F238	20	lab
F236	20	lab
B219	20	classroom with PC
B190	20	classroom with PC
B150	20	classroom without PC
B192	20	classroom without PC
B140	20	lab

#### 10.2.2. Preliminary Evaluation

Initially, the similarity of the signatures was studied using a Pearson's correlation coefficient. I used one set of data from each room as a template and computed the correlation coefficient between these templates and a newly collected signature (from same and different rooms). The results are tabulated below in Table 10.2 where the rooms in column 1 are the reference templates and the rooms in row 1 are the test templates. Table 10.2 shows that

TABLE 10.2. Correlation coefficients for different rooms.

Location	F238	F237	F236	B219
F238	1	-0.54	0.58	0.06
F237	-0.54	1	-0.49	-0.15
F236	0.58	-0.49	1	0.01
B219	0.06	-0.15	-0.01	1

similar signatures were strongly correlated as compared to different signatures that had a weak correlation. However, correlation is valid only for equal length sequences and signatures without any time delay.

### 10.2.3. Performance Evaluation of DTW on room signatures

By employing DTW, I obtained the results depicted in Fig. 10.2 for rooms F237 and F238.

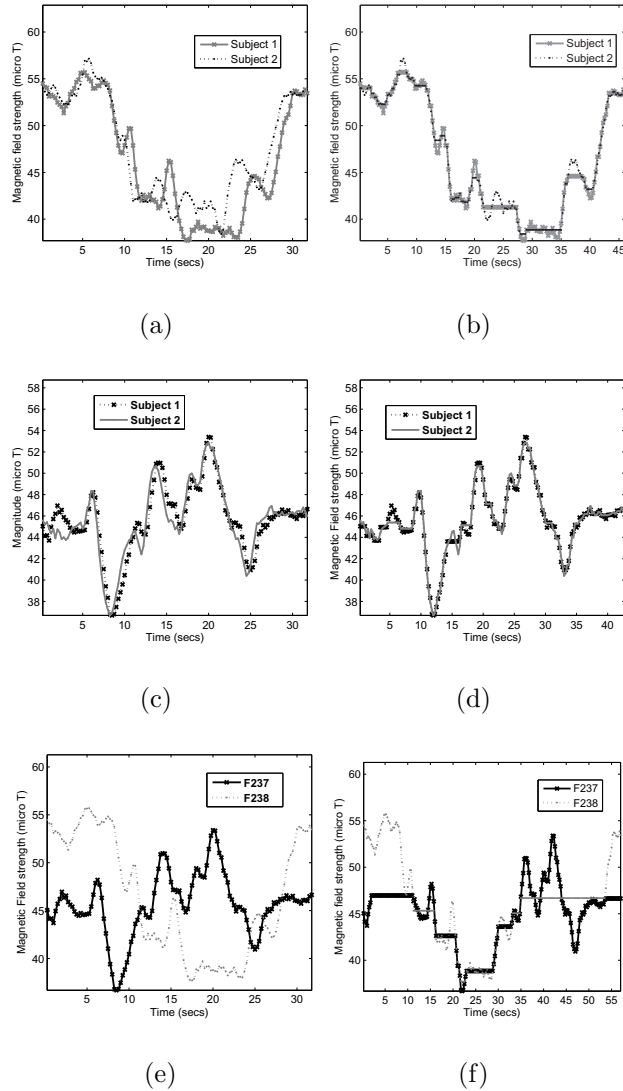


FIGURE 10.2. Research labs signature alignment: (a) original signature of F238 from two different subjects, (b) aligned signatures, (c) original signature of F237 from two different subjects, (d) aligned signatures (e) original signature of F238 and F237 from a single subject, (f) a mismatch of signatures.

Similar DTW alignment can be seen in Figure 10.3 for two classrooms which were empty but still differed in their signatures.

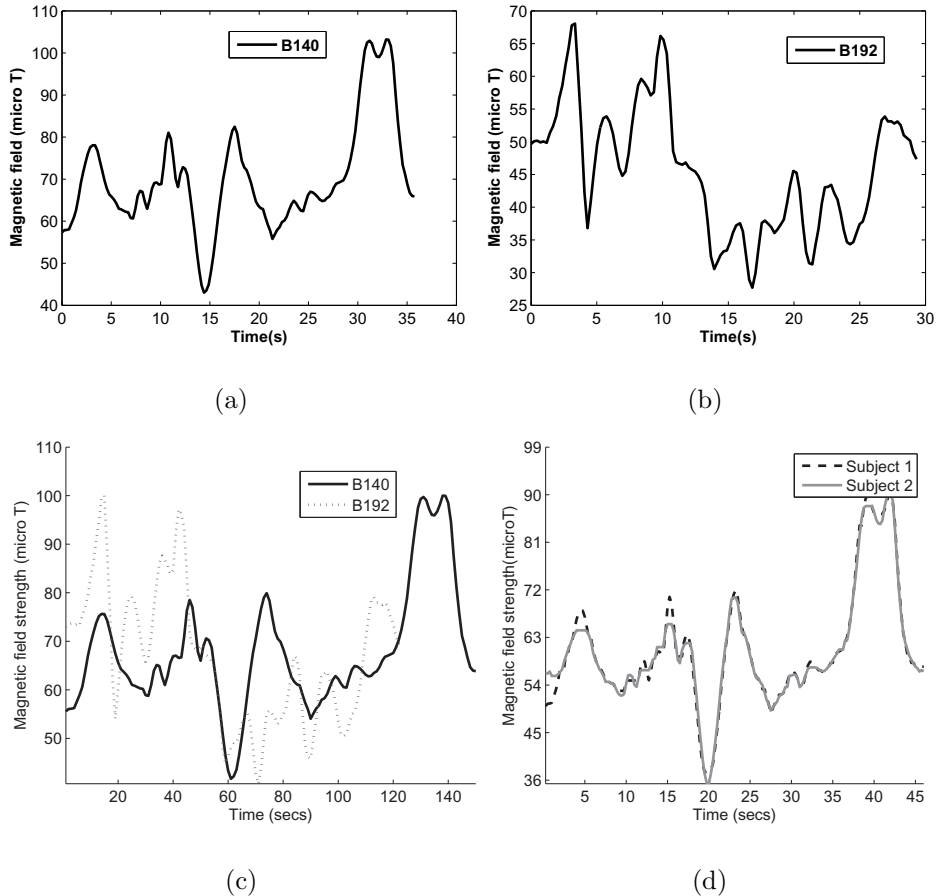


FIGURE 10.3. Classroom signature alignment: (a) B140. (b) B192. (c) Improper match of B140 and B192. (d) Correct match of B140 signatures.

We can also understand the above depicted results quantitatively from the distances computed by the DTW algorithm between the two signatures. Table 10.3 lists how the signature of F237 collected from 10 subjects was matched to the other signatures.

From the results, it can be inferred that it is feasible to differentiate rooms using their magnetic signatures as long as the equipments are not moved on a regular basis. The possibility of this may be low since once set up, research labs remain the same unless a malfunctioning equipment needs to be replaced. Similarly for classrooms with computers, the set up remains the same. So, this idea will work as long as the infrastructure in the rooms remains static. Consistent data collection over a period of time can aid in database maintenance for every room so that necessary update can be done if and when necessary.

TABLE 10.3. Time warping distances between test and training signatures of labs.

Test/Training	$F237_{S5}$	$F238_{S5}$	$B219_{S5}$
$F237_{S1}$	0.23	0.25	0.22
$F237_{S2}$	0.44	0.36	0.45
$F237_{S3}$	0.35	0.24	0.17
$F237_{S4}$	0.25	0.31	0.33
$F237_{S5}$	0	0.55	0.28
$F237_{S6}$	0.21	0.19	0.21
$F237_{S7}$	0.38	0.41	0.15
$F237_{S8}$	0.14	0.26	0.35
$F237_{S9}$	0.12	0.41	0.29
$F237_{S10}$	0.16	0.18	0.32

### 10.3. Summary

The idea behind this chapter was to show the uniqueness of electromagnetic signatures of different rooms. This is in one way extending the hallway classification idea to rooms. The ideal application or scenario can be identifying which room a person is in. The set up of different research labs, classrooms with and without computers was shown through pictures and their signatures were successfully differentiated by adopting dynamic time warping. More exhaustive measurement process needs to be performed to collect signatures from more rooms and a thorough validation also needs to done.

## CHAPTER 11

### SIMULATION BASED VALIDATION OF CLASSIFICATION FRAMEWORK

This chapter presents a simulation based validation of the proposed classification framework for fine localization. By incorporating the analytical model explained in Chapter 6, I generate magnetic signatures and use the time warping technique to perform pattern classification. From the correctly matched signatures, I calculate the classification accuracy, estimation error and the shortest distance required to walk in a hallway for a correct classification.

#### 11.1. Generation of Magnetic Signatures

##### 11.1.1. Need for Simulation

From Chapter 6, it was understood that the measured magnetic signatures consisted predominantly of anomalies in the Earth's magnetic field caused by ferromagnetism in pillars. A detailed discussion was provided through an analytical model. Next in Chapters 8 and 9, I showed how coarse and fine location estimates could be obtained from the measured magnetic signatures. As evident from the results, the evaluation could be performed only for a few hallway signatures since it is practically cumbersome to collect data from all possible hallways.

So, for wide scale validation, first an analytical model is required to generate different kinds of magnetic signatures. The model must mainly incorporate the ferromagnetic behavior of pillars, doors and elevators that are commonly present in hallways. Then, the time warping algorithm can be used to perform classification of the generated signatures.

##### 11.1.2. Uniqueness of magnetic signatures

From the measurement process which resulted in collection of magnetic signatures from hallways in different buildings, the following observations were made:

- The magnitude of the magnetic field at every pillar was different
- The signatures comprised of the Earth's magnetic field, the field from a ferromagnetic object and noise.
- The magnetic fields of steel reinforced concrete pillars, both cylindrical and rectangular were higher than solid steel pillars

A detailed explanation was provided in Chapter 6. Summarizing the causes for each of the observations:

Variation in the ferromagnetic fields: As explained in Sections 6.1.1 and 6.1.2, the strength and direction of the field depends on the following:

- (1) The relation between the strength of magnetization and electron spins
- (2) The relation between electron spins, atoms and magnetic moment
- (3) Number of atoms present in the material,  $N_{atoms}$
- (4) Number of atoms that are aligned when induced by an external magnetic field,  $N_{aligned}$
- (5) Magnetic behavior/distribution of the material

Disturbances in Earth's magnetic field: As explained in Section 6.2.3, the components of the ferromagnetic fields interact with those of the Earth's magnetic field creating disturbances in the Earth's field. It was shown how the interaction results in a low field at certain pillar and high at another.

Steel reinforced Vs solid Steel: Section 6.3 clearly explained how the presence of multiple steel rods or ferromagnetic objects inside a structure caused stronger magnetic fields than solid structures.

Combining all the above mentioned causes, the answer to the question What is the reason behind the uniqueness of magnetic signatures? was provided.

#### 11.1.3. Analytical Model

The point magnetic dipole field model explained in Chapter 6 is given by

$$(43) \quad B(\vec{m}, \vec{r}) = \frac{\mu}{4 * pi} \left[ 3 \frac{(\vec{m} \cdot \vec{r}) \vec{r}}{|\vec{r}|^5} - \frac{\vec{m}}{|\vec{r}|^3} \right]$$

where  $\vec{m}$  is the magnetic moment,  $\vec{r}$  is the unit vector in the direction of  $r$  which is the distance at which the magnetic field is calculated and  $\mu_o$  is the permeability of air.

A simplified model of the above equation is given as

$$(44) \quad B_x = \frac{\mu_o m}{4 * pi} \left[ \frac{\sqrt{3 \cos^2 \theta - 1}}{r^3} \right]$$

where  $B_x$  the magnetic field component which is aligned with the x-axis.  $r$  is the distance from the dipole to the field measurement point, in meters.  $\theta$  is angle between the dipole axis, and the position vector of the field measurement point. The magnetic dipole moment ( $m$ ) is given by

$$(45) \quad \frac{B_i V}{\mu_o}$$

Where  $V$  is the volume of the magnet.  $B_i$  is the intrinsic magnetic induction. Equation 44 is obtained from Equation 43 from the following derivation:

$$\begin{aligned}
 v &= \left( \frac{\vec{m}}{r^2} \cdot \vec{r} \right) \\
 &= \left( \frac{m \cos \theta}{r^2} \right) \\
 H &= (-\Delta v) \\
 &= -\frac{\delta}{\delta r} \left( \frac{m \cos \theta}{r^2} \right) - \frac{1}{r} \frac{\delta}{\delta \theta} \hat{\theta} \left( \frac{m \cos \theta}{r^2} \right) \\
 &= \left( -\frac{2m \cos \theta}{r^3} \hat{r} \right) + \left( \frac{m \sin \theta}{r^2} \hat{\theta} \right) \\
 H &= \left( H_r \hat{r} + H_\theta \hat{\theta} \right) \\
 H &= \left( \sqrt{\left( \frac{m \sin \theta}{r^3} \right)^2 + \left( \frac{2m \cos \theta}{r^2} \right)^2} \right) \\
 &= \left( \sqrt{\frac{m^2 \sin^2 \theta}{r^5} + \frac{4m^2 \cos^2 \theta}{r^5}} \right) \\
 &= \left( \frac{m}{r^3} \sqrt{(1 - \cos^2 \theta) + 4 \cos^2 \theta} \right) \\
 &= \left( \frac{\mu_o}{4 * pi} \frac{m}{r^3} \sqrt{3 \cos^2 \theta - 1} \right)
 \end{aligned} \tag{46}$$

#### 11.1.4. Problem Formulation

In simple mathematical terms, consider a set of buildings,  $B_i$ ,  $i = 1, 2...N$ . Every building has a set of hallways  $H_j$ ,  $j = 1, 2...M$ . Every hallway in turn consists of pillars, doors and elevators with steel or iron frames. The magnetic field from these objects can be computed using Equation 46 and represented as

$$\begin{aligned}
 \vec{Bx}_1 &= \left( \frac{\mu_o}{4 * pi} \frac{m}{r^3} \sqrt{3 \cos^2 \theta - 1} + \vec{B}_E \right) \\
 \vec{Bx}_2 &= \left( \frac{\mu_o}{4 * pi} \frac{m}{r^3} \sqrt{3 \cos^2 \theta - 1} + \vec{B}_E \right) \\
 \vec{Bx}_3 &= \left( \frac{\mu_o}{4 * pi} \frac{m}{r^3} \sqrt{3 \cos^2 \theta - 1} + \vec{B}_E \right) \\
 &\dots \\
 (47) \quad \vec{Bx}_n &= \left( \frac{\mu_o}{4 * pi} \frac{m}{r^3} \sqrt{3 \cos^2 \theta - 1} + \vec{B}_E \right)
 \end{aligned}$$

where  $Bx_n$  could be magnetic fields from different ferromagnetic objects along a hallway. The magnetic signature obtained for a hypothetical hallway using the above equations is given by  $M = \{\vec{Bx}_k, k = 1, 2...n\}$ . A set of these signatures forms a database  $\{M_1, M_2, M_3...M_l\}$ .

The problem can be stated as that of classifying a section of the generated signature  $S = \{s_1, s_2, ..., s_n\}$  correctly to one of the simulated signatures in the database  $M$ . The approach to this problem is similar to that explained in Section 9.3.2 where the program picked 100 random positions from each test signature and performed classification for each of those positions comprising of short signatures. The next section first explains the methodology for generating signatures and then the classification results obtained using the time warping algorithm.

#### 11.1.5. Simulation Methodology

Based on the discussions in Chapter 6, each of the steps below were followed for first computing the magnetic field of different ferromagnetic objects and then obtaining a signature from those fields.

- (1) Consider a geometrical shape, for instance, a cube for a solid pillar as seen in the College of Engineering building with dimensions given in the table below.

TABLE 11.1. Different pillars: Dimensions in cm.

Type	a	b	h
Solid(corner)	20	20	500
Solid(middle)	20	20	500
H-Shape	10	11	500
Solid(small)	15	15	500

- (2) The magnetic moment is the strength of a dipole when a current flows in a loop of area A. In ferromagnetic objects, the flow of electrons causes a current flow and the interaction of these electron spins in the material cause ferromagnetism. The atomic magnetic moment was computed as

$$(48) \quad \vec{\mu} = -\left(\frac{e}{m}\right)\vec{S}$$

where  $e$  and  $m$  are the charge and mass of an electron given by  $1.6 \times 10^{-9}$  coulombs and  $9.11 \times 10^{-31}$  respectively.  $\vec{S}$  is the angular momentum due to the electrons spin. It has units  $kg.m^2/s$ .  $\mu$  has units of  $Am^2$  - current times area since magnetic dipole moment is current times the area of loop.

$$(49) \quad \mu_z = \pm \frac{eh}{4 * pi * m}$$

the  $\pm$  corresponds to the two values of the electron spin quantum number  $+1/2$  and  $-1/2$ . The above quantity is called the Bohr magneton and is equal to:

$$(50) \quad \mu_B = \mu_z = \frac{eh}{4 * pi * m} = 9.27 \times 10^{-24} Am^2$$

According to Pauli's Exclusion principle, only two electrons with parallel spins may be present in an atom for a ferromagnetic object. Taking this into account, the total magnetic moment of an atom  $\mu_{atom}$  can be taken as that of two Bohr

magnetrons with a value of  $2.1 \times 10^{-23}$  J/T. Next, the  $N_{atoms}$  in a pillar given the dimensions was computed as

$$(51) \quad N_{atoms} = \frac{(Fe_{den})(V)}{(L)(A_{mass})}$$

where  $Fe_{den}$  is the density of  $1m^3$  of iron given as  $7.87 \times 10^3 \text{ kgm}^{-3}$  and  $A_{mass}$  is the atomic mass given as  $92.711 \times 10^{-27} \text{ kg}$  and  $L$  is the Avagadro's number given by  $6.22 \times 10^{23}$ .

Next, the magnetic moment of the pillars was calculated as

$$(52) \quad \mu_{pillar} = (\mu_{atom})(N_{atoms})$$

- (3) The magnetic moment in the pillar varies depending upon the number of atoms aligned. Using the formula below, the moment was varied as

$$(53) \quad \mu_{pillar} = (N_{aligned})(\mu_{pillar})$$

- (4) Finally using the dipole model, the magnetic field of a ferromagnetic object at a certain distance  $r$  from the user was calculated using

$$(54) \quad B_x = \frac{\mu_o m}{4 * \pi r^3} [\frac{\sqrt{3 \cos^2 \theta - 1}}{r^3}]$$

- (5) Using the IGRF model, the individual components of the Earth's magnetic field were obtained and a vector addition of the fields from the pillar was performed.

## 11.2. Results

### 11.2.1. Signature Generation

The amplitude of a magnetic anomaly depends on the distance to an object and the distribution of the magnetic material. This was clearly depicted in Section 6.2. To summarize, in the absence of a magnetic object, the number of flux lines would remain the same, and all of the lines would be parallel. In other words, the Earth's magnetic field is not affected if the ferromagnetic object is far away. This can be seen again in Fig. 11.1.

Fig. 11.2 shows a resultant signature.

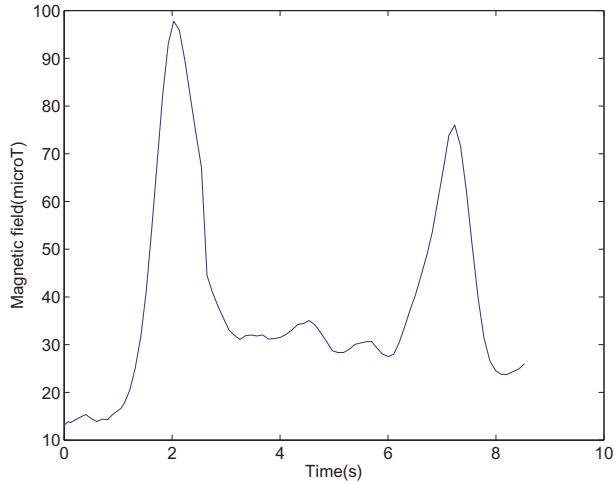


FIGURE 11.1. Magnetic field distribution in measured data: The magnitude is high near the first pillar. As the distance increases, the magnitude reduces and then increases when approaching the next pillar. The amplitude of the field at the two pillars depends on the magnetization intensity of each pillar.

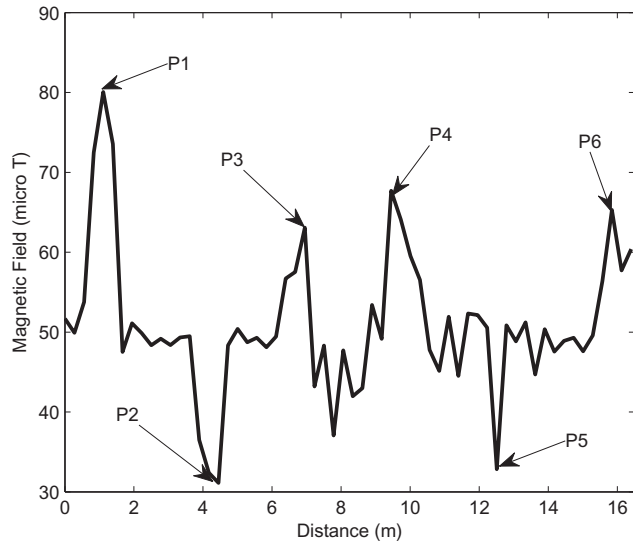
This methodology was followed for generating magnetic signatures assuming hallways of lengths 40-80m since most of the hallways at which measurements were taken were normally between this range. For each hallway length, 100 different hallway signatures were obtained and the classification algorithm was evaluated on each of those 100 signatures.

### 11.2.2. Time warping of simulated signatures

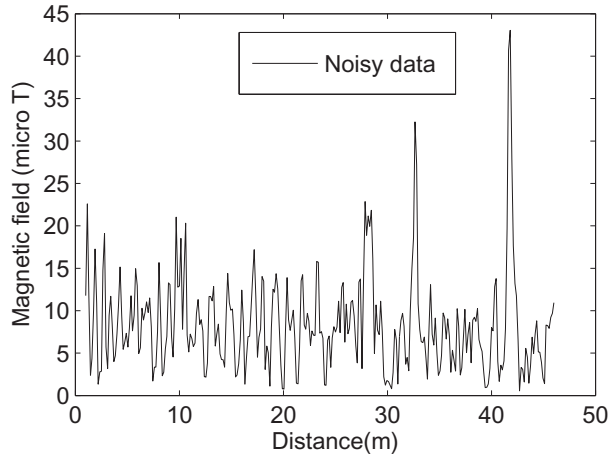
Using the sliding window DTW algorithm explained in Section 9.3.2, I evaluated the fine localization technique on the simulated signatures. Let us revisit the procedure here:

- (1) The algorithm randomly selects a segment from the signature: This is equivalent to walking a short distance from any random position
- (2) A sliding window is passed over the signature of the entire hallway and a close match with the short signature is obtained

I performed 100 repetitions of simulation i.e for 100 signatures, with varying number of pillars and dimensions. I considered 20 samples between two pillars which again was the usual number in the real data. So, a new signature was generated for every simulation run assuming a new hallway and the sliding window time warping was evaluated on each of those



(a)



(b)

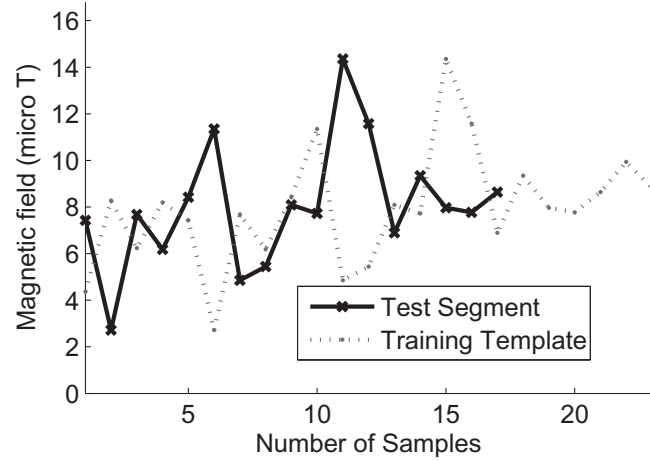
FIGURE 11.2. Generated magnetic signatures: The highs and lows of magnetic fields that were observed in the measured signatures can be seen at each of the pillars.

different signatures. By checking if the closest match was equal to the expected, I calculated the classification accuracy as

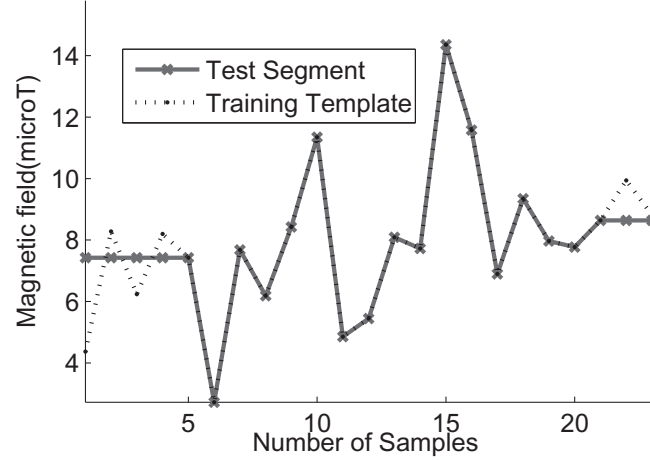
$$(55) \quad Accuracy_{simulated} = \frac{N_{close}}{H}$$

where  $H$  is the total number of hallways and  $N_{close}$  is number of times the closest match was same as the expected match. Once a close match was verified, the distance walked was estimated from the signature.

Fig. 11.3 illustrates the above explained procedure.



(a)



(b)

FIGURE 11.3. DTW on synthetic signatures: (a) Training and test signatures. (b) Aligned signatures.

Table 11.2 lists the average error and average localization distances obtained for hallways of different lengths generated assuming the presence of pillars, doors and elevators. The

distance between each of these objects was assumed to be 4.75m similar to the distances measured in the College of Engineering.

TABLE 11.2. Avg estimation error( $\sigma_e$  (m)) and Avg localization distances ( $\delta_l$  (m))for different length hallways.

$H_l$	A	$\sigma_e$ (m)	$\delta_l$ (m)
40	93	3.47	3.68
50	92	3.46	3.9
60	91.6	3.7	5.02
70	91	4.43	5.6
80	90	5.5	6.2

### 11.3. Summary

In this chapter, I presented a simulation based validation of the dynamic time warping technique. By incorporating a simulation model that considers the magnetic field due to a dipole moment, I generated magnetic signatures and used the time warping technique to perform pattern classification. From the correctly matched signatures, I calculated the classification accuracy, distance walked in a particular hallway, and distance estimation error.

Hence, this chapter essentially validated my idea of using dynamic time warping on magnetic signatures for localization. Instead of just evaluating the technique on only measured data, I evaluated it on numerous kinds of signatures that may pertain to a hallway in a building.

## CHAPTER 12

### CONCLUSIONS

This dissertation provided different solutions to the problem of indoor localization. By capturing physical quantities such as environmental noise, accelerations of human motions, heading or azimuth using microphone, accelerometer and orientation sensor respectively, I looked at providing the best possible solution.

Analyzing the disturbance for the compass revealed the source as indoor magnetic fields. This prompted to utilize the orientation sensor as a magnetometer and collect these fields. Initial analysis of the data indicated uniqueness in the signatures. An exhaustive data collection with statistical analysis proved the uniqueness of the signatures and paved a way for using them as solution for the problem being addressed. Hence magnetic fields based indoor localization forms the core part of this dissertation.

Below, I list the contributions of each chapter again.

#### 12.1. Summary of Contributions

- Chapter 2 (Architecture): In this chapter, I provided a brief description on smartphones and the characteristics of each of the built-in sensor used in this work followed by a description of an architecture consisting of different modules such as data acquisition, data analysis.
- Chapter 3 (Indoor tracking): In this chapter, I presented a stochastic filter based indoor tracking application developed using the built-in accelerometer and compass. The application was able to estimate the distance walked by a person and the turns taken by fusing the accelerometer and the compass data. The fluctuation of the compass due to magnetic interferences prevented a consistent working of the application.

- Chapter 4 (Ambient Sound Based Localization): In this chapter, I showed how different background sounds or noise can be collected using the built-in microphone and then proposed a classification methodology using vector quantization and clustering for a sound based context aware application. This was a very low level coarse localization scheme. The classification results obtained were encouraging and motivated for exploitation of the other built-in sensors for indoor localization.
- Chapter 5 (Magnetic Maps for Indoor Localization): In this chapter, I presented a data collection technique using the built-in magnetic field sensor as a magnetometer. With the magnetic signatures of different hallways collected using the smartphone, I discussed identification of landmarks, guideposts and also development of magnetic maps, followed by some theoretical results of magnetic field distributions that validated the measured data.
- Chapter 6 (Ferromagnetism): In this chapter, I discussed the ferromagnetism phenomenon and a detailed analytical discussion on the causes of magnetic anomalies present indoors. I also discussed how the magnetic signatures in different hallways were created and how ferromagnetic objects such as pillars, doors and elevators caused uniqueness in the magnetic signatures.
- Chapter 7 (Dynamic Time Warping): In this chapter, I provided an introduction to the classification technique employed and its applicability to this work. I also provided a justification for the use of this technique by comparing its advantages with another classification technique namely the hidden markov model.
- Chapter 8 (Coarse Localization): This chapter built upon the findings from Chapter 5. I discussed the applicability of ambient magnetic signatures of different hallways for indoor localization. By employing the dynamic time warping classification framework, I presented an easy to use application that could differentiate signatures and identify a person's location.
- Chapter 9 (Fine Localization): In this chapter, which is an extension of the previous chapter, I performed classification using the windowed dynamic time warping

on short test signatures obtained by walking short distances in various hallways. The localization distances or distance required to walk in a certain hallway were computed thereby presenting a solution to the problem of indoor localization that requires the user to walk only a few meters in a hallway to find his position. I also discussed other metrics such as response times and memory consumption of the application on the phone. The results in this chapter comprise the core part of this dissertation which is using the mobile phone as a platform for the indoor localization issue.

- Chapter 10 (Room Identification): In this chapter, by employing the same DTW classification framework, I extended the indoor localization to rooms and showed that it is possible identify different kinds of rooms such as classrooms, laboratories etc based on their magnetic signatures. This work can be extended to more number of rooms and also varying the configuration of the rooms like position of furniture, equipment.
- Chapter 11 (Simulation Based Validation of Classification Framework): In this chapter, by utilizing the theoretical analysis presented in Chapter 6, I generated magnetic signatures of hallways assuming different pillars, doors and elevators. I then validated the proposed classification framework on these signatures and proved the usability of DTW for classifying different signatures.

To conclude, this dissertation has evolved from interdisciplinary research involving data mining, machine learning, mobile computing, signal processing, multisensor fusion, physics, and material sciences.

## 12.2. Limitations

The localization application developed is purely smart phone based. Hence a user must have access to a smartphone to leverage the application for his/her location identification needs. But this may not be considered as a limitation since the proliferation of mobile or

smartphones in the market is rising and an estimated 25% of American population adopting these devices for purposes beyond voice communication.

A major variation in the magnetic signature will hinder the application since the classification algorithm requires a closely matching signature to perform alignment and compute the localization metrics. Causes for variations can be improper walking or sudden disturbances while walking or a major change in the intensity of magnetic fields in that particular hallway. The possibility of the last factor is very low as evident from [69]. Hence a minor limitation of this work is the requirement for users to walk as close as possible to walls and pillars and maintain a straight trajectory.

### 12.3. Potential Applications and Future Work

#### 12.3.1. Applications

There are different domains in which the magnetic field based localization application can be used. The most important one is in an emergency situation involving a 911 call. By asking a person to walk a few feet in a particular hallway, it would become easier for 911 personnel to locate the person instead of surveying an entire building. This would drastically reduce the search time in a tall building.

One of the future works would be to collect magnetic field data from different floors in very tall buildings and first confirm the uniqueness of magnetic signatures. Then a floor level accuracy would be obtained.

The background sound in that particular location can also be recorded and used in conjunction with the magnetic field data. This would involve multisensor fusion as explained in Chapter 3. Sometimes background sound could become a valuable tool in analyzing a crime or emergency situation.

#### 12.3.2. Crowdsourcing

Crowdsourcing is the process of presenting a task to the crowd such as performing a survey or reporting an event etc. With the usage of sensor rich mobile phones by people,

crowdsourcing could be a cost effective, time saving and powerful mechanism to collect data about the ambient environment.

There are certain issues such as designing robust applications, handling human subjects, privacy etc pertaining to collecting data and utilizing them. Hence this section just presents the idea of using the concept of crowdsourcing to collect magnetic field data inside different buildings and perform some data processing to fingerprint a hallway using that data.

One of the limitations of the proposed localization application is its inability to work in buildings for which there is no magnetic map. It would be convenient to obtain magnetic field data from new buildings by asking people working or regularly going to those buildings to be involved in a passive sensing task. They can download the simple data collection application and walk along different hallways which they usually do and then transfer the collected data to a centralized server. They can also label the data which is nothing but naming the excel file to which the data has been written. In this way, multiple files of the same label can be obtained and a measurement uncertainty as explained in Section 5.3.2 would be performed to first analyze the sensor accuracy and then confirm the reliability of the data. This would help in implementing a comprehensive data quality assessment, filtering, cleaning, and validation framework that combines sophisticated computational data processing in conjunction with human computation.

## REFERENCES

- [1] B. Kobben, A. Bunningen, and K. Muthukrishnan, “Wireless campus lbs: Building campus-wide location based services based on wifi technology,” *Geographic Hypermedia*, pp. 399–408, 2006.
- [2] Q. Ladetto and B. Merminod, “In Step with INS Navigation for the Blind, Tracking Emergency Crews,” *GPS World*, vol. 13, no. 10, pp. 30–38, 2002.
- [3] C. Fischer and H. Gellersen, “Location and navigation support for emergency responders: A survey,” *Pervasive Computing, IEEE*, vol. 9, no. 1, pp. 38 –47, jan.-march 2010.
- [4] H. Huang and G. Gartner, “A survey of indoor navigation systems.”
- [5] “Non-voice usage,” <http://www.pewinternet.org>.
- [6] “Asahi-kasei,” <http://www.asahi-kasei.co.jp/asahi/en/news/2006/e070313.html>.
- [7] “Android audio capture,” <http://developer.android.com/guide/topics/media/index.html>.
- [8] D. Hall and J. Llinas, “An introduction to multisensor data fusion,” *Proceedings of the IEEE*, vol. 85, no. 1, pp. 6–23, Jan 1997.
- [9] H. B. Mitchell, *Multi-Sensor Data Fusion*. Springer, 2007.
- [10] B. Dasarathy, “Sensor fusion potential exploitation-innovative architectures and illustrative applications,” *Proceedings of the IEEE*, vol. 85, no. 1, pp. 24–38, Jan 1997.
- [11] K. Wendlandt, M. Khider, M. Angermann, and P. Robertson, “Continuous location and direction estimation with multiple sensors using particle filtering,” in *Multisensor Fusion and Integration for Intelligent Systems, 2006 IEEE International Conference on*, Sept. 2006, pp. 92–97.
- [12] O. Woodman and R. Harle, “Pedestrian localisation for indoor environments,” in *Ubicomp '08: Proceedings of the 10th international conference on Ubiquitous computing*. New York, NY, USA: ACM, 2008, pp. 114–123.
- [13] B. Krach and P. Roberston, “Cascaded estimation architecture for integration of foot-mounted inertial sensors,” pp. 112–119, 2008.

- [14] ——, “Integration of foot-mounted inertial sensors into a bayesian location estimation framework,” pp. 55–61, 2008.
- [15] V. Fox, J. Hightower, L. Liao, D. Schulz, and G. Borriello, “Bayesian filtering for location estimation,” *Pervasive Computing, IEEE*, vol. 2, no. 3, pp. 24–33, July-Sept. 2003.
- [16] T. Brezmes, J.-L. Gorricho, and J. Cotrina, “Activity recognition from accelerometer data on a mobile phone,” in *IWANN '09: Proceedings of the 10th International Work-Conference on Artificial Neural Networks*. Berlin, Heidelberg: Springer-Verlag, 2009, pp. 796–799.
- [17] A. L. Liu, H. Hile, H. Kautz, G. Borriello, P. A. Brown, M. Harniss, and K. Johnson, “Indoor wayfinding:: developing a functional interface for individuals with cognitive impairments,” in *Assets '06: Proceedings of the 8th international ACM SIGACCESS conference on Computers and accessibility*. New York, NY, USA: ACM, 2006, pp. 95–102.
- [18] S. Ram and J. Sharf, “The people sensor: A mobility aid for the visually impaired,” in *ISWC '98: Proceedings of the 2nd IEEE International Symposium on Wearable Computers*. Washington, DC, USA: IEEE Computer Society, 1998, p. 166.
- [19] L. Ojeda and J. Borenstein, “Non-gps navigation with the personal dead-reckoning system,” G. R. Gerhart, D. W. Gage, and C. M. Shoemaker, Eds., vol. 6561, no. 1. SPIE, 2007.
- [20] D. A. Ross and B. B. Blasch, “Wearable interfaces for orientation and wayfinding,” in *Proceedings of the fourth international ACM conference on Assistive technologies*, ser. Assets '00. New York, NY, USA: ACM, 2000, pp. 193–200.
- [21] J. Hightower and G. Borriello, in *Particle Filters for Location Estimation in Ubiquitous Computing: A Case Study*, September 2004.
- [22] J. Raper, G. Gartner, H. Karimi, and C. Rizos, “Applications of location based services: a selected review,” *Journal of Location Based Services*, vol. 1, 2007.
- [23] R. Want, A. Hopper, V. Falcão, and J. Gibbons, “The active badge location system,” *ACM Trans. Inf. Syst.*, vol. 10, pp. 91–102, January 1992.

- [24] P. Bahl and V. N. Padmanabhan, “Radar: An in-building rf-based user location and tracking system,” in *IEEE INFOCOM*, 2000, pp. 775–784.
- [25] P. B. Nissanka, A. Chakraborty, and H. Balakrishnan, “The cricket location-support system,” in *MobiCom '00: Proceedings of the 6th annual international conference on Mobile computing and networking*. New York, NY, USA: ACM Press, 2000, pp. 32–43.
- [26] P. B. Nissanka, K. L. M. Allen, H. Balakrishnan, and S. Teller, “The cricket compass for context-aware mobile applications,” in *MobiCom '01: Proceedings of the 7th annual international conference on Mobile computing and networking*. New York, NY, USA: ACM, 2001, pp. 1–14.
- [27] J. Hightower and G. Borriello, “A survey and taxonomy of location systems for ubiquitous computing,” *IEEE Computer*, Tech. Rep., 2001.
- [28] M. S. Arulampalam, S. Maskell, N. Gordon, and T. Clapp, “A tutorial on particle filters for on-line non-linear/non-gaussian bayesian tracking,” *IEEE Transactions on Signal Processing*, vol. 50, pp. 174–188, 2001.
- [29] A. Doucet, S. Godsill, and C. Andrieu, “On sequential monte carlo sampling methods for bayesian filtering,” *STATISTICS AND COMPUTING*, vol. 10, no. 3, pp. 197–208, 2000.
- [30] B. Saha, “Introduction to particle filters.” [Online]. Available: <https://dashlink.arc.nasa.gov/algoritm/particle-filter-tutorial>
- [31] V. Peltonen, J. Tuomi, and A. Klapuri, “Computational Auditory Scene Recognition,” in *IEEE Intl Conf. on Acoustics, Speech, and Signal Processing*, 2002, pp. 1941–1944.
- [32] N. Sawhney and P. M., “Situational awareness from environmental sounds,” Tech. Rep., 1997, [http://web.media.mit.edu/~nitin/papers/Env\\_Snds/EnvSnds.html](http://web.media.mit.edu/~nitin/papers/Env_Snds/EnvSnds.html).
- [33] L. Ma, D. Smith, and M. Ben, “Environmental Noise Classification for Context-Aware Applications,” in *Proceedings of the International Conference on Database and Expert Systems Applications (DEXA)*, 2003, pp. 360–370.
- [34] B. Clarkson, N. Sawhney, and A. Pentland, “Auditory context awareness via wearable computing,” in *1998 Workshop on Perceptual User Interfaces (PUI98)*, 1998.

- [35] N. Sawhney and C. Schmandt, “Nomadic radio: speech and audio interaction for contextual messaging in nomadic environments,” *ACM Trans. Comput.-Hum. Interact.*, vol. 7, no. 3, pp. 353–383, 2000.
- [36] J. Makhoul, S. Roucos, and H. Gish, “Vector quantization in speech coding,” *Proceedings of the IEEE*, vol. 73, no. 11, pp. 1551–1588, Nov. 1985.
- [37] Y. Linde, A. Buzo, and R. Gray, “An algorithm for vector quantizer design,” *Communications, IEEE Transactions on*, vol. 28, no. 1, pp. 84–95, Jan 1980.
- [38] J. Haverinen and A. Kemppainen, “Global indoor self-localization based on the ambient magnetic field,” *Robotics and Autonomous Systems*, July 2009.
- [39] D. Navarro and G. Benet, “Magnetic map building for mobile robot localization purpose,” in *Emerging Technologies Factory Automation, 2009. ETFA 2009. IEEE Conference on*, Sept 2009, pp. 1 –4.
- [40] J. Burnett and P. D. Yaping, “Mitigation of extremely low frequency magnetic fields from electrical installations in high-rise buildings,” *Building and Environment*, vol. 37, no. 8-9, pp. 769 – 775, 2002.
- [41] K. Yamazaki, K. Kato, K. Ono, H. Saegusa, K. Tokunaga, Y. Iida, S. Yamamoto, K. Ashiho, K. Fujiwara, and N. Takahashi, “Analysis of magnetic disturbance due to buildings,” *Magnetics, IEEE Transactions on*, vol. 39, no. 5, pp. 3226 – 3228, Sept 2003.
- [42] M. A. Fuentes, A. Trakic, S. J. Wilson, and S. Crozier, “Analysis and measurements of magnetic field exposures for healthcare workers in selectedmr environments,” *Biomedical Engineering, IEEE Transactions on*, vol. 55, no. 4, pp. 1355 –1364, April 2008.
- [43] Serway and Jewett, *Physics for Scientists and Engineers*, 6th ed., 2004, pp. 894–916.
- [44] S. Suksakulchai, S. Thongchai, D. Wilkes, and K. Kawamura, “Mobile robot localization using an electronic compass for corridor environment,” in *Systems, Man, and Cybernetics, 2000 IEEE International Conference on*, vol. 5, 2000, pp. 3354 –3359 vol.5.
- [45] S. A. Rahok and O. Koichi, “Odometry correction with localization based on landmarkless magnetic map for navigation system of indoor mobile robot,” in *Autonomous Robots and Agents, 2009. ICARA 2009. 4th International Conference on*, Feb 2009, pp.

572 –577.

- [46] K. Soeda, S. Aoki, K. Yanashima, and K. Magatani, “Development of the visually impaired person guidance system using gps,” in *Engineering in Medicine and Biology Society, 2004. IEMBS '04. 26th Annual International Conference of the IEEE*, vol. 2, Sept 2004, pp. 4870 –4873.
- [47] B. Ando and S. Graziani, “Multisensor strategies to assist blind people: A clear-path indicator,” *Instrumentation and Measurement, IEEE Transactions on*, vol. 58, no. 8, pp. 2488 –2494, Aug 2009.
- [48] Z. Hunaiti, V. Garaj, and W. Balachandran, “An assessment of a mobile communication link for a system to navigate visually impaired people,” *Instrumentation and Measurement, IEEE Transactions on*, vol. 58, no. 9, pp. 3263 –3268, Sept 2009.
- [49] S. Bell, “A beginner’s guide to uncertainty of measurement,” National Physical Laboratory, Tech. Rep., 1999.
- [50] M. McCaig and A. G. Clegg, *Permanent Magnets in Theory and Practice*, 2nd ed. Cambridge University Press, 1987.
- [51] “Asahi-kasei,” <http://www.asahi-kasei.co.jp/ake/en/technology/magnet/magnet.html>.
- [52] C. Oldenburg and G. Moridis, “Ferrofluid flow for tough2,” Lawrence Berkeley Laboratory, Berkeley, Tech. Rep. LBL-41608, 1998.
- [53] N. A. Spaldin., *Magnetic Materials: Fundamentals and Device Applications*. Halsted Press, Div of J. Wiley and Sons.
- [54] “Ising model,” <http://farside.ph.utexas.edu/teaching/329/lectures/node110.html>.
- [55] “Introduction to magnetism,” <http://fds.oup.com/www.oup.com/pdf/13/9780198570752.pdf>.
- [56] “Introduction to geomagnetism,” [http://web.\linebreak\[0\]mit.\linebreak\[0\]edu/worldmap/www/teiabm/Geomagnetism\%20Intro.\linebreak\[0\]pdf](http://web.\linebreak[0]mit.\linebreak[0]edu/worldmap/www/teiabm/Geomagnetism\%20Intro.\linebreak[0]pdf).
- [57] “The geomagnetic reference model,” <http://www.ngdc.noaa.gov/IAGA/vmod/igrf.html>.
- [58] G. L. Muhammad Haris Afzal, Valérie Renaudin, “Assessment of indoor magnetic field anomalies using multiple magnetometers,” in *ION GNSS*, Sept 2010.

- [59] J. D. Jackson, *Classical electrodynamics*, 3rd ed. New York, NY: Wiley, 1999.
- [60] E. Čermáková, “Magnetization of steel building materials and structures in the natural geomagnetic field,” *Acta Polytechnica*, vol. 45, no. 6, 2005.
- [61] M. O. E. Craig M. Newtonson, “Two dimensional magnetic algorithm to detect reinforcing steel,” in *Journal of Materials in Civil Engineering*, vol. 7, no. 3, Aug 1995.
- [62] H. Sakoe and S. Chiba, “Dynamic programming algorithm optimization for spoken word recognition,” *Acoustics, Speech and Signal Processing, IEEE Transactions on*, vol. 26, no. 1, pp. 43 – 49, feb 1978.
- [63] R. Muscillo, S. Conforto, M. Schmid, P. Caselli, and T. D’Alessio, “Classification of motor activities through derivative dynamic time warping applied on accelerometer data,” in *Engineering in Medicine and Biology Society, EMBS 2007, 29th Annual International Conference of the IEEE*, Aug. 2007, pp. 4930 –4933.
- [64] V. Niennattrakul and C. Ratanamahatana, “On clustering multimedia time series data using k-means and dynamic time warping,” in *Multimedia and Ubiquitous Engineering, 2007. MUE ’07. International Conference on*, april 2007, pp. 733 –738.
- [65] E. J. Keogh and M. J. Pazzani, “Scaling up dynamic time warping for datamining applications,” in *Proceedings of the sixth ACM SIGKDD international conference on Knowledge discovery and data mining*, ser. KDD ’00. New York, NY, USA: ACM, 2000, pp. 285–289.
- [66] B. Zhang, K. Yan, S. Jiang, Y. Mao, and D. Wei, “Feature selection methods in walking stability analysis,” in *Computer and Information Technology, 2009. CIT ’09. Ninth IEEE International Conference on*, vol. 1, Oct 2009, pp. 258 –262.
- [67] E. W. Hill and P. Punder, *Orientation and Mobility Techniques:A Guide for the Practitioner*, 1st ed. American Foundation for the Blind, 1976, p. 119.
- [68] B. Gozick, K. P. Subbu, R. Dantu, and T. Maeshiro, “Magnetic maps for indoor navigation,” *Instrumentation and Measurement, IEEE Transactions on*, vol. PP, no. 99, pp. 1 –9, 2011.

- [69] M. Haavisto, S. Tuominen, H. Kankaanpää andä and, and M. Paju, “Time dependence of demagnetization and flux losses occurring in sintered nd-fe-b permanent magnets,” *Magnetics, IEEE Transactions on*, vol. 46, no. 9, pp. 3582 –3584, Sept 2010.
- [70] A. Millonig and K. Schechtner, “Developing landmark-based pedestrian navigation systems,” in *Intelligent Transportation Systems, 2005. Proceedings. 2005 IEEE*, 2005, pp. 197–202.
- [71] A. Varshavsky, A. LaMarca, J. Hightower, and E. de Lara, “The skyloc floor localization system,” in *Pervasive Computing and Communications, 2007. PerCom '07. Fifth Annual IEEE International Conference on*, march 2007, pp. 125 –134.
- [72] F. Alt, A. S. Shirazi, A. Schmidt, U. Kramer, and Z. Nawaz, “Location-based crowdsourcing: extending crowdsourcing to the real world,” in *Proceedings of the 6th Nordic Conference on Human-Computer Interaction: Extending Boundaries*, ser. NordiCHI '10. New York, NY, USA: ACM, 2010, pp. 13–22.
- [73] N. Eagle, “txteagle: Mobile crowdsourcing,” in *Internationalization, Design and Global Development*, ser. Lecture Notes in Computer Science, N. Aykin, Ed. Springer Berlin / Heidelberg, 2009, vol. 5623, pp. 447–456.
- [74] J. Burke, D. Estrin, M. Hansen, A. Parker, N. Ramanathan, S. Reddy, and M. B. Srivastava, “Participatory sensing,” in *In: Workshop on World-Sensor-Web (WSW06): Mobile Device Centric Sensor Networks and Applications*, 2006, pp. 117–134.
- [75] A. R. Golding and N. Lesh, “Indoor navigation using a diverse set of cheap, wearable sensors,” *Wearable Computers, The Third International Symposium on*, pp. 29–36, 1999.
- [76] J. Collin, O. Mezentsve, and G. Lachapelle, “Indoor positioning system using accelerometry and high accuracy heading sensors,” in *Proceedings of the 16th International Technical Meeting of the Satellite Division of the Institute of Navigation ION GPS/GNSS*, 2003, pp. 796–799.
- [77] S.-W. Lee and K. Mase, “Activity and location recognition using wearable sensors,” *Pervasive Computing, IEEE*, vol. 1; 1, no. 3, pp. 24–32, 2002.

- [78] E. Vildjiounaite, E.-J. Malm, J. Kaartinen, and P. Alahuhta, “Location estimation indoore by means of small computing power devices, accelerometers, magnetic sensors, and map knowledge,” in *Pervasive Computing*, ser. Lecture Notes in Computer Science, F. Mattern and M. Naghshineh, Eds. Springer Berlin / Heidelberg, 2002, vol. 2414, pp. 5–12.
- [79] M. Addlesee, R. Curwen, S. Hodges, J. Newman, P. Steggles, A. Ward, and A. Hopper, “Implementing a sentient computing system,” *Computer*, vol. 34, no. 8, pp. 50 –56, aug 2001.
- [80] V. Otsason, A. Varshavsky, A. LaMarca, and E. de Lara, “Accurate gsm indoor localization,” in *In The Proc. of Ubicomp 2005*, 2005, pp. 141–158.
- [81] J. Randall, O. Amft, J. Bohn, and M. Burri, “Luxtrace: indoor positioning using building illumination,” pp. 417–428, 2007.
- [82] N. Ravi and L. Iftode, “Fiatlux: Fingerprinting rooms using light intensity,” 2007.
- [83] D. Bucur and M. Kjrgaard, *GammaSense: Infrastructureless Positioning Using Background Radioactivity*, ser. Smart Sensing and Context. Springer Berlin / Heidelberg, 2008, vol. 5279, pp. 69–82.
- [84] H. Liu, H. Darabi, P. Banerjee, and J. Liu, “Survey of wireless indoor positioning techniques and systems,” *Systems, Man, and Cybernetics, Part C: Applications and Reviews, IEEE Transactions on*, vol. 37, no. 6, pp. 1067 –1080, nov. 2007.
- [85] P. Kemppi, J. Pajunen, and T. Rautiainen, “Use of artificial magnetic anomalies in indoor pedestrian navigation,” in *Vehicular Technology Conference Fall (VTC 2010-Fall), 2010 IEEE 72nd*, sept 2010, pp. 1 –5.
- [86] W. F. Storms and J. F. Raquet, “Magnetic field aided indoor navigation,” in *Proceedings of the 13th European Navigation Conference GNSS*, 2009.
- [87] D. Bernstein and A. Kornhauser, “An introduction to map matching for personal navigation assistants,” Tech. Rep.
- [88] I. Constandache, X. Bao, M. Azizyan, and R. R. Choudhury, “Did you see bob?: human localization using mobile phones,” in *Proceedings of the sixteenth annual international*

- conference on Mobile computing and networking*, ser. MobiCom. New York, NY, USA: ACM, 2010, pp. 149–160.
- [89] A. Parnandi, K. Le, P. Vaghela, A. Kolli, K. Dantu, S. Poduri, and G. S. Sukhatme, “Coarse in-building localization with smartphones,” in *Mobile Computing, Applications, and Services*, ser. Lecture Notes of the Institute for Computer Sciences, Social Informatics and Telecommunications Engineering. Springer Berlin Heidelberg, 2010, vol. 35, pp. 343–354.
- [90] M. Azizyan and R. R. Choudhury, “Surroundsense: Mobile phone localization using ambient sound and light,” *SIGMOBILE Mob. Comput. Commun. Rev.*, vol. 13, pp. 69–72, June 2009.
- [91] N. Ravi, P. Shankar, A. Frankel, A. Elgammal, and L. Iftode, “Indoor localization using camera phones,” in *Mobile Computing Systems and Applications, 2006. WMCSA '06. Proceedings. 7th IEEE Workshop on*, aug. 2006, p. 19.
- [92] S. Grzonka, F. Dijoux, A. Karwath, and W. Burgard, “Mapping indoor environments based on human activity,” in *Robotics and Automation (ICRA), 2010 IEEE International Conference on*, May 2010, pp. 476 –481.
- [93] C. Gayathri, V. Tam, V. Alexander, G. Marco, M. Rich, Y. Jie, and C. Yingying, “Tracking vehicular speed variations by warping mobile phone signal strengths,” in *IEEE International Conference on Pervasive Computing and Communications (PERCOM), 2011*, March 2011.
- [94] A. Youssef, T. Abdel-Galil, E. El-Saadany, and M. Salama, “Disturbance classification utilizing dynamic time warping classifier,” *Power Delivery, IEEE Transactions on*, vol. 19, no. 1, pp. 272 – 278, Jan 2004.
- [95] B. Legrand, C. S. Chang, S. H. Ong, S.-Y. Neo, and N. Palanisamy, “Chromosome classification using dynamic time warping,” *Pattern Recogn. Lett.*, vol. 29, pp. 215–222, February 2008.
- [96] V. Tuzcu and S. Nas, “Dynamic time warping as a novel tool in pattern recognition of ecg changes in heart rhythm disturbances,” in *Systems, Man and Cybernetics, 2005*

*IEEE International Conference on*, vol. 1, Oct 2005, pp. 182 – 186 Vol. 1.

- [97] G. Borriello, A. Liu, T. Offer, C. Palistrant, and R. Sharp, “Walrus: wireless acoustic location with room-level resolution using ultrasound,” in *Proceedings of the 3rd international conference on Mobile systems, applications, and services*, ser. MobiSys ’05. New York, NY, USA: ACM, 2005, pp. 191–203.
- [98] J. Scott and B. Dragovic, “Audio location: accurate low-cost location sensing,” in *In Proceedings of the Third International Conference on Pervasive Computing*, 2005, pp. 1–18.